Universidad de Concepción

Facultad de Ingeniería

Departamento de Ingeniería Química

DEVELOPMENT AND VALIDATION OF A NEW HEMOSTATIC DEVICE BASED ON A GELATIN – GRAPHENE OXIDE AEROGEL REINFORCED WITH GRAPE SKIN EXTRACTS FOR USE AS A WOUND DRESSING MATERIAL

POR

JESSICA BORGES VILCHES

Tesis para optar al grado de Doctor en Ciencias de la Ingeniería con mención en Ingeniería Química

TUTOR: Prof. Katherina Fernández Elgueta, PhD
Departamento de Ingeniería Química
Universidad de Concepción

CO-TUTOR: Prof. Claudio Aguayo Tapia, PhD
Departamento de Farmacia
Universidad de Concepción

CONCEPCIÓN, CHILE 2022

DEDICATORIA

A mi mamá, Josefa Emilia Vilches Lescaille, por guiarme en todo momento desde el cielo.

A mi abuela Alvarina, mi papá Jorge y a mis tías Daisy e Ileana por acompañarme en este largo camino, darme ánimos y fuerzas.

AGRADECIMIENTOS

Mis más sinceros agradecimientos quiero darlos:

A toda mi familia, especialmente a mi abuela Alvarina, a mi papá Jorge, a mis tías Daysi e Ileana y a mi tío Santiago por su apoyo constante, por sus palabras de aliento y por su infinita dedicación para conmigo.

A mis amigas de toda la vida Claudia, Laura y Patricia y su esposo por acompañarme siempre en los momentos difíciles, por tener siempre una palabra de aliento para animarme a pesar de la distancia.

A mis tutores Dra. Katherina Fernández Elgueta y Dr. Claudio Aguayo Tapia por haberme guiado en este arduo camino del doctorado, tanto en mi trabajo académico como en mi formación como doctora.

A mi nueva familia cubana en Chile, con la cual he compartido bellos momentos durante estos casi 5 años, en especial a mis siempre amigos Oscar y Amaidy, por haberme ofrecido desde el primer día su casa, su amistad y ayuda desinteresada, por haber sido mi familia en Chile, por simplemente haber estado siempre ahí. Agradecer además a mis amigos Daviel, Maray, Anamary, Maidelys, Yenisleidy, Pedro Pablo y Raydel, por los lindos momentos compartidos.

A Paulina, Karen, Carla, Isidora, José Luis, Álvaro, quienes han sido mi familia chilena acá y con quienes he compartido hermosos momentos.

A mis también amigos Cristian, Diego y Andrés, con quienes tengo lindos momentos compartidos.

A todos mis compañeros de doctorado, quienes me ayudaron tanto en las actividades docentes como investigativas, en especial a Toribio por su gran ayuda desde mis comienzos en el programa, a Sebastián y a todos los chicos con los que he compartido en el Laboratorio de Biomateriales del DIQ. Agradecer también a Gregory y Sebastián Godoy por su ayuda con los ramos.

A todos los profesores del DIQ, quienes han aportado un granito de arena más en mi formación como profesional y como persona. En especial agradecer al profe Romel y al profe Luis Ernesto, por toda su ayuda, tanto en el proceso para llegar a Chile como en mi estancia acá.

Un infinito agradecimiento a todo el personal del DIQ, de quienes siempre he recibido hermosas atenciones y ayuda desinteresada, especialmente agradecer a la Sra. Erika, una de las personas más bellas que he conocido y quien ha estado al pendiente mío todo este tiempo.

Al profesor Dr. Aldo Boccaccini por haberme guiado durante mi pasantía en el Institute of Biomaterials, FAU University Erlangen-Nuremberg, Germany.

Todo el sacrificio que implicó para mi dejar a mi familia, mis amigos y mi país ha sido remunerado con esta hermosa experiencia en Chile, tanto personal como profesional. Por ello, una y mil veces gracias a todos.

CONTENT

List of Abbreviations

ACGS: N-alkylated chitosan/graphene oxide sponge

ADP: adenosine diphosphate

$AgNO_3$: silver nitrate

aMW: average molecular weight

ANOVA: One-way analysis of variance

aPTT: activated partial thromboplastin time

ATR: attenuated total reflectance

A549: human lung cancer cells

BEAS-2B: normal human lung cells

BGCS: *Bletilla striata* (Bsp) polysaccharide/ graphene oxide composite sponge

C: (+)-catechin

$CaCl_2$: calcium chloride

CGS: cross-linked graphene sponge

CH_3COOH: acetic acid

ClO_2: chlorine dioxide

CIN: contrast-induced nephropathy

CO_2: carbon dioxide

C-P: (+)-catechin-phloroglucinol

CS: chitosan

c.v.: cell viability

C_2H_5OH: ethanol

$C_5H_8O_2$: glutaraldehyde

C_3H_6O: acetone

C_6H_{14}: n-hexane

CH_3COOH: acetic acid

DapA: 2,3-diaminopropionic acid

DCGO: polydopamine cross-linked graphene oxide sponge

DCGS: DapA cross-linked graphene sponge

DDS: drug delivery system

DMEM: Dulbecco’s modified Eagles medium

DMSO: dimethyl sulfoxide

DNA: deoxyribonucleic acid

DW: deionized water

EC: (-)-epicatechin

ECM: extracellular matrix

ECG: epigallocatechin

ECG-P: epicatechin gallate-phloroglucinol

EC-P: (-)-epicatechin-phloroglucinol

EGC-P: epigallocatechin-phloroglucinol

FBS: fetal bovine serum

FTIR: Fourier-Transform Infrared Spectroscopy

GEL: gelatin

GKCS: graphene-kaolin composite sponge

GMCS: graphene-montmorillonite composite sponge

GO: graphene oxide

GPC: gel permeation chromatography

GpO: graphite oxide

GSE: grape skin extracts

GSPE: grape seed proanthocyanidin extracts

HaCaT: Human keratinocyte cells

HCl: hydrochloric acid

HDF: human dermal fibroblast

HeLa: human tumor

HepG2: hepatocarcinoma human

HFF1: human foreskin fibroblast

HPLC: High Performance Liquid Chromatography

HUVEC: umbilical vein endothelial

H_2O_2: oxygenated water

H_2SO_4: sulfuric acid

H_3PO_4: phosphoric acid

IUPAC: International Union of Pure and Applied Chemistry

$KMnO_4$: potassium permanganate

L-929: mouse dermal fibroblast

MCF-7: human cancer

mDP: degree of polymerization

MRC5: human fibroblast

MTT: 3-(4,5-dimethylthiazol-2-yl)-2,5-diphenyltetrazolium bromide

MW: microwave

Na^+: sodium ions

NaCl: sodium chloride

NIH-3T3: mouse embryonic fibroblasts

NMR: nuclear magnetic resonance

NO^{3-}: nitrate ions

NO_2: nitrous oxide

N_2O_4: dinitrogen tetraoxide

NO_x: ‘nitrogen oxides’

O_2: oxygen

PAs: proanthocyanidins

PBS: phosphate saline solution

PCL: poly (ε-Caprolactone)

PE: *Pinus radiata* bark extracts

PEG: polyethylene glycol

PEO: polyethylene oxide

PhIP: 2-Amino-1-methyl-6-phenylimidazo[4,5-b] pyridine

pI: isoelectric point

PLA: polylactic acid

PPP: platelet-poor plasma

PRP: platelet-rich plasma

PT: prothrombin time

PVA: polyvinyl alcohol

RBCs: red blood cells

rGO: reduced graphene oxide

SA: sodium alginate

SD: Sprague-Dawley

SEM: Scanning electron microscopy

SR: swelling ratio

TCGS: thrombin/cross-linked graphene sponge

TGA: Thermogravimetric analysis

UV: ultraviolet

XPS: X-ray photoelectron spectroscopy

XRD: X-ray diffraction

vWF: von Willebrand factor

List of Figures

List of Tables

Abstract

Rapid profuse bleeding control is increasingly important in current civilian and military emergency medicine due to the high number of caused deaths. Although many materials have been explored as effective hemostats, their different mechanisms for hemostasis cause them to fail their function under certain circumstances. Therefore, the development of new hemostats to achieve efficient hemorrhage control remains a major challenge. Hence, this study aims to develop new hemostatic materials based on gelatin (GEL)-graphene oxide (GO) aerogels reinforced with *País* grape skin extracts (GSE) for the control of profuse bleedings. These aerogels were developed by a new microwave-assisted synthesis method, which significantly reduced the reaction time by 97% compared to traditional synthesis methods. The effects of loading GSE into aerogels were investigated in terms of their hemostatic performance both *in vitro* and *in vivo.* The aerogels showed highly resistant porous structures with the ability to absorb more than 50 times their own weight in contact with fresh human blood. All aerogels coagulated more than 60% of the blood content added to their structures after 240 seconds in the *in vitro* dynamic whole-blood clotting assay. In addition, the GEL-GO aerogels showed a high hemocompatibility, with hemolysis rates lower than 5%. The non-toxic effects of aerogels on human dermal fibroblast cells and their ability to act as carriers in the release of GSE were confirmed. GSE-loaded aerogels exhibited higher negative surface charge, blood absorption capacity, and clotting ability compared to GEL-GO aerogels, which was beneficial for hemostasis. According to their hemostatic action mechanism, none of the aerogels promoted coagulation by either the extrinsic or intrinsic pathway. However, their surfaces showed suitable characteristics for accelerating hemostasis by promoting coagulation alternative routes. Furthermore, *in vivo* rat-tail amputation assays revealed that all aerogels significantly shortened the hemostatic times and reduced the amount of blood loss compared to the two commercial hemostats evaluated (Spongostan™ and ChitoGauze®XR) and the control gauze sponge. Therefore, GSE-loaded aerogels and GEL-GO aerogels could be used as wound-dressing materials for hemostatic applications, thus enlarging the family of engineered aerogels-based biomaterials containing phytotherapeutic agents.

Resumen

El control rápido de las hemorragias profusas es cada vez más importante en la medicina de urgencias civil y militar actual debido al elevado número de muertes que se producen. Aunque se han explorado muchos materiales como hemostáticos eficaces, sus diferentes mecanismos de hemostasia hacen que ellos fallen en su función bajo determinadas circunstancias. Por lo tanto, el desarrollo de nuevos hemostatos para lograr un control eficaz de las hemorragias sigue siendo un reto importante. Por ello, este estudio tiene como objetivo desarrollar nuevos materiales hemostáticos basados en aerogeles de gelatina (GEL) y óxido de grafeno (*GO*) reforzados con extractos de piel de uva (*GSE*) para el control de sangramientos profusos. Estos aerogeles fueron desarrollaron mediante un nuevo método de síntesis asistido por microondas, el cual redujo significativamente el tiempo de reacción en un 97% en comparación con los métodos de síntesis tradicionales. Los efectos de incorporar *GSE* en los aerogeles fueron investigados en términos de su rendimiento hemostático tanto *in vitro* como *in vivo*. Los aerogeles mostraron estructuras porosas altamente resistentes con capacidad para absorber más de 50 veces su propio peso en contacto con sangre humana fresca. Todos los aerogeles coagularon más del 60% del contenido de sangre añadido a sus estructuras después de 240 segundos en el ensayo de coagulación dinámica *in vitro* de sangre total. Además, los aerogeles de GEL-GO mostraron una alta hemocompatibilidad, con tasas de hemólisis inferiores al 5%. Los efectos no tóxicos de los aerogeles en células de fibroblastos dérmicos humanos y su capacidad para actuar como transportadores (*carriers*) en la liberación de *GSE* fueron confirmados. Los aerogeles cargados con *GSE* mostraron una mayor carga superficial negativa, capacidad de absorción de sangre y capacidad de coagulación en comparación con los aerogeles de GEL-GO, lo cual fue favorable para la hemostasia. De acuerdo a su mecanismo de acción hemostática, ninguno de los aerogeles promovió la coagulación por la vía extrínseca o intrínseca. Sin embargo, sus superficies mostraron características adecuadas para acelerar la hemostasia mediante la promoción de rutas alternativas de coagulación. Además, los ensayos *in vivo* de amputación de cola de rata revelaron que todos los aerogeles acortaron significativamente los tiempos hemostáticos y redujeron la pérdida de sangre en comparación con los dos hemostatos comerciales evaluados (Spongostan™ y ChitoGauze®XR) y con la esponja de gasa control. Por lo tanto, los aerogeles cargados con *GSE* y los aerogeles de GEL-GO podrían utilizarse como materiales de curación de heridas en aplicaciones hemostáticas, ampliando así la familia de biomateriales de ingeniería basados en aerogeles que contienen agentes fitoterapéuticos.

Introduction

Uncontrolled hemorrhages are one of the major causes of deaths in battlefields, surgeries, traffic accidents, and emergencies [1–5]. In these situations, bleeding accounts for 30-40% of trauma mortality, and approximately 33-56% of these deaths occur during the prehospital period [6,7]. The cost of wound care is also a major economic burden worldwide, with an estimated cost over $22 billion in 2020 and an upward trend in the coming years [3,8]. Despite the enormous progress made over the last decades to improve trauma treatments, significant challenges remain to be addressed, especially in relation to the search of new effective hemostats. Consequently, the development of rapid, safer, and more effective hemostatic materials is an urgent issue and also of clinical and socioeconomic importance.

To this end, new hemostatic materials or modifications of existing ones have been intensively developed using different active components (inorganic and organic materials or a combination of both) [2,7,9]. Among their main functions, hemostatic materials must be biocompatible, biodegradable, easy to handle, non-toxic, and inexpensive [2,10]. They must also have a good affinity for blood cell components, rapidly absorb large amounts of blood, prevent bacterial infection, and promote wound healing and tissue regeneration [3,11]. Because of their multiple functions, it is of increasing interest to develop new hemostatic materials that provide other supportive functions and increased efficiency [3]. To date, many hemostatic materials are being fabricated in various forms, such as gauze, dressing, sprays, granules, scaffolds, nanofibers, powders, adhesives, aerogels, hydrogels, physical devices, and so on [1,3,5,12–18]. Among them, aerogels have emerged as an interesting class of engineered biomaterials for hemostasis due to their excellent properties.

Aerogels are highly porous materials with a structure similar to the solid networks of a gel with gas or vacuum between the skeleton [19,20]. Among their properties, aerogels exhibit high porosity, low density, high specific surface area, and micro- and mesoporous structures [21,22]. Their porous structures are extremely favorable for the absorption and preservation of biological fluids such as blood plasma [13] and also for the transport of fluids and molecules [19]. Aerogels are also being used to promote blood clotting in wounds after blood cell accumulation on their surfaces [5,14,17].

In particular, carbon-derived materials, such as graphene oxide (GO), have been widely used to develop aerogels for a wide range of applications. GO-based materials have shown remarkable potential for trauma treatments due to their ability to rapidly absorb plasma and their capacity to

accumulate blood cells on their surfaces, thus promoting blood coagulation [1,5,9,14–18]. In this context, Singh *et al.* [23] demonstrated for the first time that GO sheets can elicit a strong aggregatory response in platelets due to the presence of oxygenated functional groups in the GO structure, which was corroborated by other authors [12,24,25]. Despite their advantages, GO-containing materials have shown certain shortcomings as hemostats in terms of their high hemolysis rate, cytotoxic effects, and potential thrombosis, thus limiting their use in such applications [1,23,26]. To overcome these drawbacks, several authors have proposed different functionalization strategies to crosslink the GO with other materials, mainly polymers, in order to bring new functionalities to the GO and improve its properties [1,4,27,28].

In order to develop new composites with improved both hemostatic as well as biological performance, many materials have been crosslinked with GO, including chitosan (CS) [29], alginate [30], gelatin (GEL) [16], polyvinyl alcohol (PVA) [5], polyethylene glycol (PEG) [17], kaolin [7], and thrombin [9]. In particular, GEL has emerged as a promising material for biomedical applications due to its outstanding properties [31]. GEL, as a natural polymer, is hydrophilic, biocompatible, biodegradable, non-toxic, and has a good affinity for proteins [10,31]. GEL also possesses remarkable capability for potential modifications [31] and has been used to promote cell adhesion and proliferation in wound dressing applications [32,33]. Its hemostatic activity is directly related to its active role in platelet activation [34]. However, GEL has shown poor mechanical strength [35,36], high solubility and high rate of degradability in aqueous solutions [31], which limits its use as a wound-dressing material. To overcome these drawbacks, GEL has been crosslinked before usage with materials such as GO to develop new composites for biomedical applications [37–39].

The use of natural compounds combined with engineered biomaterials has been continuously growing. Numerous investigations have focused on the search for new therapeutic properties of these compounds. Among them are the grape extracts obtained from the skin and seed of grapes, other fruits, and vegetables. These extracts are a mixture of polyphenols with a high proanthocyanidins (PAs) content and antioxidant, antimicrobial, cardioprotective, and anti-inflammatory bioactivities [40]. Their high PAs content has favored cell adhesion and proliferation of human fibroblast cells [41], suggesting their potential for wound healing. However, certain properties of phenolic compounds, such as their low solubility, high sensitivity against environmental changes, instability in the physiological medium, and volatility, have limited their use in biomedical applications [41,42]. Aerogels, as engineered biomaterials, could be used as robust carriers of this phytotherapeutic agent to overcome these drawbacks.

Taking into consideration the above premises, the following hypotheses and objectives are proposed.

Hypotheses

- The physicochemical properties of the gelatin-graphene oxide aerogels and their ability to adhere blood cells to their surfaces make them suitable materials for controlling profuse bleeding.
- The incorporation of *País* grape skin extracts into gelatin-graphene oxide aerogels improves the hemostatic performance of these materials.

General Objective

- To develop hemostatic materials based on gelatin-graphene oxide aerogels reinforced with *País* grape skin extracts, evaluating the effects of loading extracts on their physicochemical properties and hemostatic performance.

Specific objectives

- To develop gelatin-graphene oxide aerogels by a microwave-assisted synthesis method, evaluating the influence of different synthesis conditions on their physicochemical properties.
- To incorporate *País* grape skin extracts into gelatin-graphene oxide aerogels and to investigate the physicochemical and hemostatic properties of the new materials.
- To evaluate the hemostatic efficiency of gelatin-graphene oxide aerogels both *in vitro* and *in vivo*, comparing their properties with the ones of other materials (graphene oxide-based aerogels, gauze sponge, and commercial hemostats).
- To investigate the hemostatic potential of *País* grape skin extracts in *in vitro* and *in vivo* models.

Chapter 1: Background

1.1. General aspects of GO

1.1.1. Synthesis methods of GO

The history of the GO extends back to the 19th century, involving many studies regarding the chemistry of graphite [43,44]. Since then, many efforts have been devoted to finding safer synthetic routes to produce GO, with the use of strong oxidizing agents being one of the most common approaches [45]. The pioneering work in the synthesis of GO was reported by Brodie in 1859 [46]. In his work, Brodie mixed one equal weight of graphite with three equal weights of potassium chloride and then the mixture was reacted in fuming nitric acid at 60°C for 4 days to produce GO. Brodie determined that the resulting material was composed of carbon, hydrogen, and oxygen, which resulted in an increase in the total mass of the flake graphite. In addition, his material was dispersible in water, but not in acidic media, leading him to name the material “graphic acid” [43].

Nearly 60 years after Brodie, Staudenmaier improved Brodie’s method by replacing about two-thirds of fuming nitric acid with concentrated sulfuric acid and adding potassium chloride in multiple portions [43,47]. This slight change allowed the overall reaction in a single vessel, thus simplifying the synthesis method. Although the degree of oxidation of Staudenmaier’s material was similar to the one of Brodie (C:O~2:1), the reaction to produce GO still required 4 days.

Later, Hummers and Offeman developed an alternative synthesis method (Hummers method) based on the oxidation of graphite using potassium permanganate and sodium nitrate in concentrated sulfuric acid [48]. This new method showed important advantages compared to the above-mentioned procedures. First of all, the potassium chloride was replaced by sulfuric acid, thus improving the safety of the reaction and avoiding the evolution of the explosive ClO_2. Secondly, the reaction time was reduced from days to a few hours, and, finally, the replacement of sodium nitrate by fuming nitric acid eliminated the formation of acid fog during the synthesis reaction [43]. Despite these improvements, the Na^+ and NO^{3-} ions contained in the residual water of the synthesis were not removed. In addition, toxic gasses such as NO_2 and N_2O_4 were released during the oxidation process.

After the Hummers method, many attempts were developed to improve the GO’s synthesis, until 2010, when Marcano *et al.* proposed an improved synthesis to produce GO, which became known as the “improved Hummers method” [45]. Marcano’s synthesis protocol is based on the incorporation of H_3PO_4 and in the increase of the amount of $KMnO_4$ during the reaction, according to the proportions

shown in **Figure 1.1**. Among its main advantages, the Marcano's method provided a higher amount of hydrophilic oxidized graphene material compared to Hummer's method, without including toxic gases such as NO_x. This synthesis method also allowed the formation of a material with a more regular structure than the above materials [45]. Due to its advantages, this method is being the most widely used to produce GO. In this study, the GO was produced according to the protocol described by Marcano *et al* [45], with a slight modification in the reaction time based on Wang's results [49].

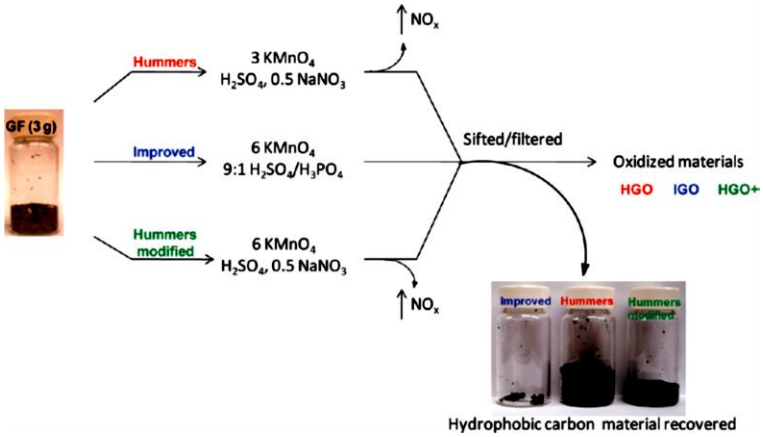

Figure 1.1. Graphic representation of some synthesis methods followed to produce GO from graphite flakes. The route marked with blue color corresponds to the method proposed by Marcano. Source: Marcano *et al.* [45].

1.1.2. Chemical composition of GO

GO is a material obtained from the oxidative processes of graphite, consisting of chemically exfoliated graphene sheets with a flat two-dimensional honeycomb sheet structure [44,45]. GO is composed of oxygenated functional groups, including epoxy (>O), hydroxyl (-OH), carbonyls (C=O), and carboxyl (-COOH) groups (**Figure 1.2**) [5,12,28,29]. The functional groups of the GO are attached on both or either side of its sheets, which allows the stabilization of this material in water [50]. Depending on its distribution, GO can be obtained in the form of mono-, bi- or tri-layers, few layers (2-5 sheets), multilayers (2-10 sheets) or graphite nanoplates (two-dimensional graphite material, with thicknesses and/or lateral dimensions less than 100 nm) [51,52].

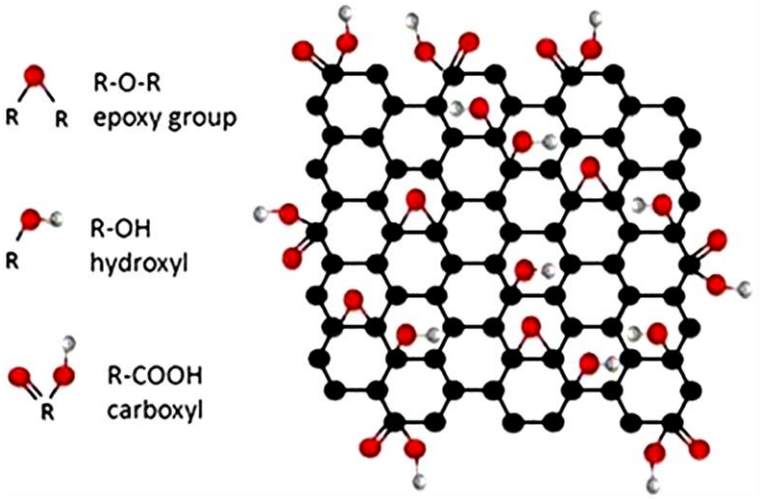

Figure 1.2. The chemical structure of the GO containing various functional groups on its edges and surfaces. Source: Singh *et al.* [50].

1.1.3. Properties and applications of GO

GO has shown interesting properties for a wide range of applications, mainly due to its chemical structure. GO exhibits interesting mechanical, thermal, and optical properties [28,53,54] that support its use in applications such as electronics, catalysis, energy storage, and so on [50]. GO also has remarkable potential for biomedical applications, being widely used as a loading platform for small molecules such as antibodies, DNA, and proteins [55], in tissue engineering [56], as a *'nanocarrier'* for drug delivery [57,58], in the synthesis of functional materials [9,14,59], and others, as shown in **Figure 1.3**.

In addition, GO exhibits suitable biological properties in terms of its biocompatibility, non-toxicity at low concentrations [28] and functionalization capacity [57]. These properties support the use of the GO as a support material for the formation of composites, porous materials, and other structures. Moreover, the hydrophilic nature of GO favors the formation of strong bonds between the basal and interlaminar planes of the GO with water molecules, mainly through the hydroxyl and epoxide groups present in the GO structure [60,61]. In particular, the affinity for water endows GO with excellent liquid absorption capacity, which is similar to that of passive hemostats [4]. Thus, GO has been widely used for hemostatic applications due to its capacity to absorb plasma, enrich blood cells, platelets, coagulation factors, and other components on its surface that accelerate coagulation [1,4,9,14]. In this context, Singh *et al.* [23] first reported that GO sheets elicited a strong aggregatory response in platelets, which has been corroborated in later studies [12,24,25]. Despite its suitable properties for hemostasis, GO has shown certain shortcomings as a hemostat, such as its high hemolysis rate,

cytotoxicity and potential thrombosis, which limits its use in such application [1]. A widely used alternative to overcome these drawbacks has been the crosslinking of GO with other molecules, mainly polymers, to improve its properties [27,28,62]. In this study, different crosslinking strategies of GO with polymers were evaluated to improve the properties of the resulting materials.

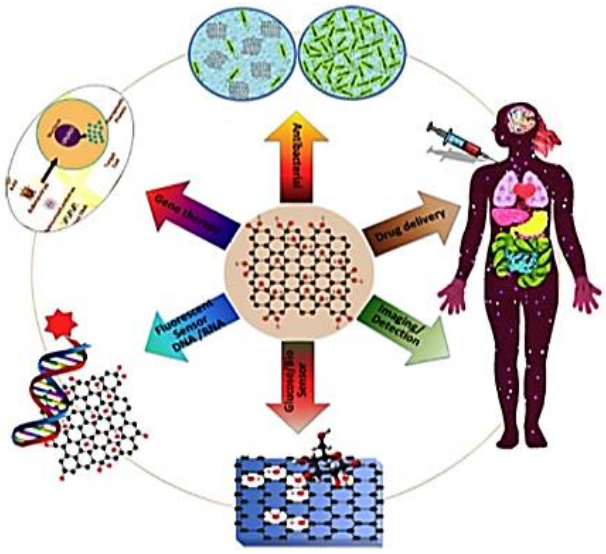

Figure 1.3. Biomedical applications of GO. Source: Singh *et al.* [50]

1.2. Functionalization of GO

The functionalization of the GO has typically been studied by covalent and non-covalent interactions. Both methods modify the original structure of the GO, either by alterations in its chemical structure or by the addition of new specific characteristics to other materials, mainly polymers.

1.2.1. Covalent functionalization

GO is covalently crosslinked with new molecules via chemical bonding, which is possible due to the presence of defects in the basal structure of GO and the existence of oxygenated groups in the GO's chemical structure [43]. In particular, the covalent functionalization of GO with polymers has been developed mainly by applying 'grafting to' and 'grafting from' techniques [27]. The first technique is based on a synthesis process involving the formation of bonds between polymer chains and GO functional groups. In contrast, the 'grafting from' technique involves the polymerization of the monomers derived from the surfaces of graphene, which are subsequently bonded to the hydroxyl and carboxyl groups of the GO [27]. In general, both techniques focus on producing a direct bond between the GO's functional groups and polymers via amidation, esterification, and nitration reactions [27].

This type of functionalization mainly involves the carboxylic and epoxy functional groups of GO. In this context, the carboxylic functional groups promote the formation of ethers and amines, while the

epoxy groups are modified by nucleophilic attacks of the amino groups of the polymers to the *α*-carbons of the GO [43]. In the least proportion, covalent functionalization could arise by reactions with the hydroxyl functional groups of GO.

1.2.2. Noncovalent functionalization

The non-covalent functionalization of GO occurs mostly by Van der Waals forces, hydrogen bonds, *π−π* interactions, and electrostatic interactions [27,43]. Typically, Van der Waals forces develop between GO and organic molecules or polymers with a high hydrophobic character. In contrast, the *π−π* interactions commonly occur between GO and molecules with short to highly extended *π*- systems [63]. Due to the presence of oxygenated groups on the surface and edges of the GO, ionic interactions and hydrogen bonds are often involved in non-covalent syntheses [63].

On the other hand, there are pros and cons related to the application of both functionalization methods. In particular, for biological applications, the non-covalent syntheses produce weaker bonds than covalent functionalization, being more vulnerable to changes caused by the external environment. In addition, the non-covalently functionalized materials are less stable when interacting with biological systems and have a lower drug loading and release capacity compared to covalently-bonded materials [64]. The low capacity of non-covalent materials to act as a drug delivery system (DDS) could be explained by the polymers coating the conjugated areas of graphene [64]. In addition, the non-covalent functionalization gives the possibility to re-adsorb molecules on the surface of graphene without altering the electronic structure, which also allows important properties such as electric conductivity or mechanical strength of the resulting materials to remain unaffected [63].

As mentioned above, GO has been functionalized mainly with polymeric materials to produce composites for a wide range of applications. Among their characteristics, polymers containing amino groups could be suitable to form covalent interactions with GO by the “grafting to” technique. In this study, the chemical nature of such interactions, in particular between GO and GEL will be investigated.

1.3. Characterization techniques of GO

GO-based materials are usually characterized by various spectroscopic and microscopic techniques, which provide valuable information regarding the qualitative and quantitative characteristics of both the GO and the transformations it undergoes after exfoliation and functionalization processes. Some of the most commonly used techniques to characterize GO and its derivatives are mentioned below:

Scanning electron microscopy (SEM): This technique is used to observe the morphology, surface, and cross-sections of a sample. In this technique, the images are produced due to electron scattering,

which consists of making an electron beam on the sample, normally covered with a thin layer of gold or carbon (by "sputtering"), which confers conductive properties to the sample and allows observing from 5-10 nm with high quality.

Raman spectroscopy: This is a non-destructive technique that provides structural information on carbon materials. Typically, the Raman spectrum of GO is characterized by the presence of two significant bands called D and G, which are located at ~1350 cm^{-1} and ~1588 cm^{-1}, respectively. The D band is related to the structural defects of the material caused as a consequence of the bonding of the oxygenated groups present in plane basal of the carbon. The G band is associated with sp^2 carbon hybridization. In addition, the Raman spectrum of GO shows a region of lower intensity called 2D (located between 2400-3250 cm^{-1}), which is associated with the number of layers of GO. The shape of this region is also related to the GO defects.

Fourier-Transform Infrared Spectroscopy (FT-IR): This is one of the most widely used techniques to characterize carbon-derived materials. FTIR is based on striking an electromagnetic ray of a known wavelength (in this case infrared) and measuring the energy absorption of a sample. These absorptions are referred to specific wavelengths that are also associated with the bonds of the molecules. Thus, it is possible to detect the presence of functional groups in a sample and even quantify the intensity of the peaks.

X-ray diffraction (XRD): This technique is based on the coherent scattering of the X-ray beam in the material and on the constructive interference of the waves that are in phase and scattered in certain directions in space. This phenomenon is described by Bragg's Law according to **Equation 1.1:**

$$n\lambda = 2 * d * sen\,\theta \qquad (1.1)$$

This law predicts the direction in which constructive interference occurs between the X-ray beams coherently scattered by crystalline material at an angle θ, where d represents the distance between crystal planes, n corresponds to the diffraction order, and λ is the wavelength.

Thermogravimetric analysis (TGA): TGA is a thermal analysis method used to evaluate the thermal stability of materials and the fraction of volatile components. With this technique, the weight of a sample (placed under a controlled atmosphere of purified air or an inert gas such as helium or argon) is continuously recorded as a function of increasing temperature. In particular, for graphitic materials, the weight loss may be due to the oxidation of carbon in gaseous CO_2 and the increase of weight could be due to the oxidation of catalytic metal residues in solid oxides. The graphic representation of mass or weight percent as a function of temperature is called a "thermogram or thermal decomposition curve".

X-ray photoelectron spectroscopy (XPS): The XPS technique consists of the excitation of the innermost levels of atoms by an X-ray beam, causing the emission of photoelectrons that provide information on the energy of each level and, therefore, on the nature of each emitting atom. This technique provides qualitative and quantitative information about the chemical elements present in a sample and allows to determine the chemical state of the elements on the surface of the material. XPS is a complementary technique, which must be analyzed together with other spectroscopic techniques such as nuclear magnetic resonance (NMR).

1.4. General aspects of GEL

1.4.1. Chemical composition of GEL

GEL is a natural polymer composed of a mixture of water-soluble proteins derived from collagen by partial hydrolysis [65,66]. Based on its method of production and isoelectric point (pI), it is possible to distinguish two types of GEL. Type A GEL (pH between 3.8-6.0 and pI 6-9) is obtained by acidic treatment of collagen and provides plasticity and elasticity to the mixtures, however, type B GEL (pH between 5.0-7.4 and pI~5) is obtained by alkaline hydrolysis of collagen, providing high gel strength to the mixture [65,66]. According to its chemical composition, the protein fraction of GEL consists almost entirely of amino acids (**Figure 1.4**), the most abundant being glycine (~27%), proline and hydroxyproline (~25%), followed by glutamic acid (~10%), alanine (~9%), arginine (~8%), aspartic acid (~6%), and other amino acids (~15%) [65,67]. Due to its triple-helical structure, GEL can be arranged in a tridimensional conformation that provides an ideal geometry for hydrogen chain crosslinking [68].

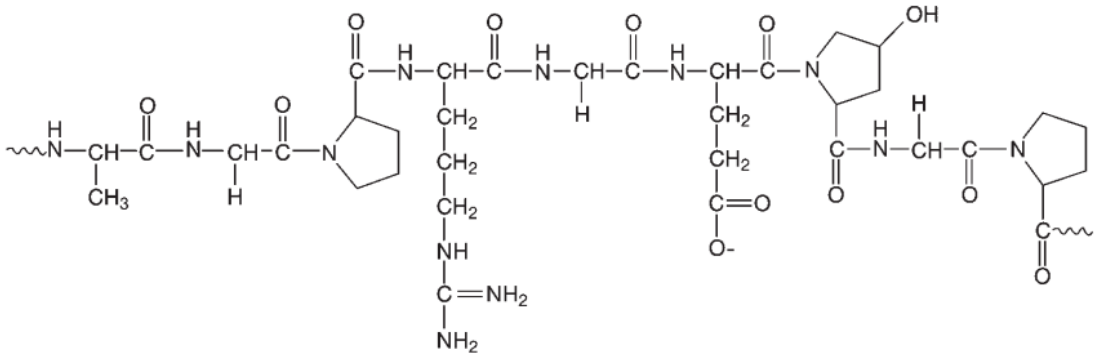

Figure 1.4. Chemical structure of GEL, showing its main chemical groups. Source: Kommareddy *et al.* [67].

1.4.2. Properties and applications of GEL

As a natural polymer, GEL has a hydrophilic nature, an amphoteric character and a high affinity to proteins, including its biocompatible, biodegradable, and non-toxic properties. In particular, the

amphoteric character of GEL is given by the presence of amino acid functional groups and by the amino and carboxyl-terminal groups originating during hydrolysis. In addition, GEL has a positive charge in acidic media, which allows it to migrate as a cation in an electric field. In contrast, GEL is negatively charged under alkaline conditions [65].

Due to its characteristics, GEL is being widely used in many biomedical applications. GEL is considered a promising DDS for a variety of drugs [31]. In addition, GEL-containing materials provide a structural composition similar to the extracellular matrix (ECM), which enables them to activate platelet aggregation on the surface of the material [16,69]. GEL also promotes cell adhesion and proliferation of human dermal fibroblast cells when it is used in wound dressing applications [32,33], and mesenchymal stem cell differentiation in tissue engineering applications [66,70]. Furthermore, GEL has been used to produce different commercial hemostats such as FloSeal®®, Gelfoam®®, and Spongostan™, which are being used in the international market. Despite its advantages, GEL has some drawbacks related to its low mechanical strength and high degradation rates [31,35,36], which limits its use in biomedical applications. To overcome these disadvantages, GEL is being crosslinked with other materials prior to use to improve the properties of the resulting materials. This crosslinking is made possible by the ability of GEL for potential modifications [31]. Therefore, GEL has been previously crosslinked with GO to form various functional materials such as hydrogels, aerogels, nanosheets and others for a wide range of biomedical applications [38,39,54,71].

1.4.3. GO-GEL composites formation

To date, several materials based on GO and GEL have been developed through covalent and non-covalent interactions for biomedical applications. For example, Chen *et al.* [38] developed biocompatible GEL-functionalized graphene nanosheets by evaluating the influence of different synthesis conditions (GEL:GO ratio, pH, temperature) on the properties of the composites to establish the optimal reaction conditions for the synthesis of these materials. Their main results showed that such nanosheets have properties suitable for use as a DDS for controlled and targeted drug delivery. In a similar study, Piao and Chen [39] synthesized GO-GEL nanocomposite hydrogels by a simple self-assembling approach, demonstrating the potential of these materials for pH-controlled drug delivery applications. Similarly, Piao *et al.* [71] demonstrated that reduced graphene oxide (rGO)-GEL nanocomposite hydrogels developed via a covalent synthesis process have great potential for both tissue engineering and drug delivery applications. In addition to these studies, many functional materials for biomedical applications based on GO and GEL such as foams, films, microspheres,

porous scaffolds, nanofibers, hydrogels, aerogels, and so on are being developed. In this study, the hemostatic potential of GO and GEL incorporated in aerogel-based biomaterials is investigated.

1.5. General aspects of aerogels

1.5.1. Aerogels: definition, properties, and applications

Aerogels were produced for the first time by Kistler in the early 1930s by a supercritical drying method [19], in which the resulting material was not referred to as a specific material, but a group of materials with extraordinary characteristics [19]. In his study, Kistler produced highly porous materials by removing the liquid part in a gel, whose process avoided shrinkage and solid network deformations during drying, keeping porosity open and preserving the gel structure. In this way, a solid was obtained, in which the dispersed phase was air, i.e., an aerogel [21,72]. According to the IUPAC definition, an aerogel is a “gel composed of a microporous solid in which the dispersed phase is a gas” [19]. Therefore, aerogels can be considered a state of matter with a porous structure similar to the solid networks of a gel with gas or vacuum between the skeletons [20].

In recent years, research on the production of aerogels has intensified extensively due to the interesting physical and chemical properties of these materials, such as their high porosity (80–99.8%), ultralight weight, thermal conductivity (from 0.005 to 0.1 W m K^{-1}), high specific surface area (between 500-1200 m^2 g^{-1}), low dielectric constant (κ value range from 1.0 to 2.0), low refractive index (≈1.05), and micro- and mesoporous structures (2-50 nm in the pore diameter) [20–22,72]. Therefore, many aerogel-based materials have been developed and recognized as promising candidates for applications such as thermal insulation, photocatalysts, sensor, supercapacitor, water treatment, and so on [73,74]. In addition, aerogels show remarkable potential for biomedical applications due to their ability to absorb liquids such as blood plasma, which makes them suitable for hemostatic applications [13]. Aerogel-based biomaterials are also very favorable for the absorption and preservation of biological fluids and exhibit fluid and molecule transport properties [19].

1.5.2. GO-based aerogels

A large number of studies have been developed to produce GO-based aerogels with properties suitable for use in many applications. In particular, there is a growing interest in developing GO-based aerogels for biomedical applications, as shown in **Figure 1.5**.

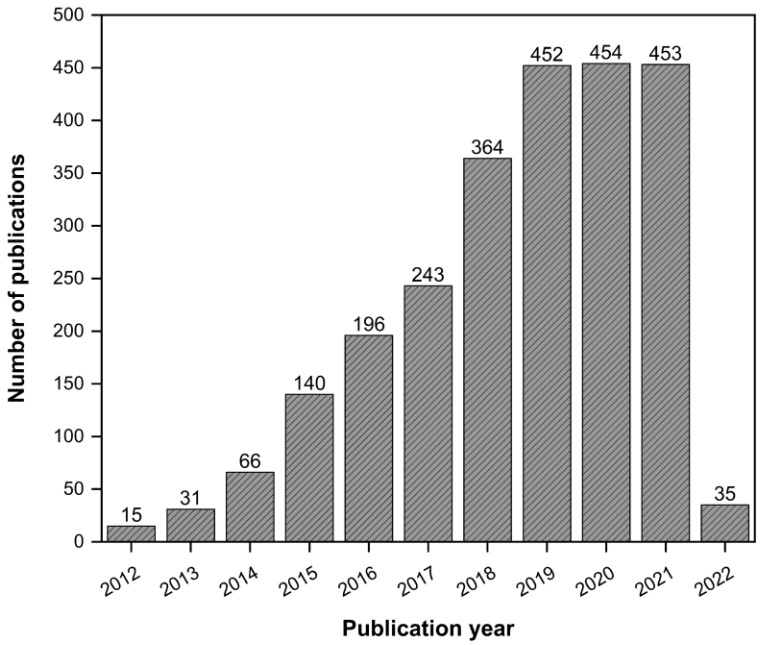

Figure 1.5. The number of scientific publications contributing in the last 10 years to the topics "aerogels" and "graphene oxide". Data were collected from *Web of Science* on January 6th, 2022. Source: Own elaboration.

Targeting biomedical applications, GO has been widely used to produce composite aerogels through covalent and non-covalent interactions with polymeric materials. Previous studies demonstrated that GO/polymer composites have both improved mechanical properties compared to GO [75] and enhanced responses against pH changes [76]. In addition, GO-based aerogels have shown great potential for hemostatic applications. Quan *et al.* [13] first demonstrated the outstanding hemostatic performance *in vitro* and *in vivo* of a cross-linked graphene sponge (CGS). Similarly, Quan *et al.* [14] produced 2,3-Diaminopropionic acid cross-linked graphene sponges (DCGS) with the ability to absorb plasma, stimulate RBCs and platelets on their surfaces, and promote hemostasis by enhancing cell/graphene interface interaction, thus demonstrating the great potential of these materials for the treatment of traumas. In another study, Li *et al.* [9] also evaluated the hemostatic potential of thrombin/cross-linked graphene sponges (TCGS) produced by a facile spray method. Their results showed that such materials exhibited remarkable hemostatic performance based on their ability to absorb plasma, stimulate thrombin, and prevent bleeding within 100 seconds. Zhang *et al.* [29] demonstrated that N-alkylated chitosan/graphene oxide sponges (ACGS) could be used as emergency hemostats due to their excellent absorption capacity, mechanical stability, biocompatibility, and their capacity to accelerate RBCs and platelet adhesion. According to Li *et al.* [12], GO sponges reinforced

with polydopamine promote hemostasis through enhanced platelet stimulation, allowing to increased negative surface charge and shortened hemostasis time by 165 seconds compared to a non-crosslinked GO aerogel.

Based on these studies, it is possible to conclude that: *(1)* GO-based aerogels have extraordinary potential for hemostasis, *(2)* crosslinked GO aerogels improve their hemostatic efficiency compared to a GO aerogel alone, *(3)* interfacial stimulation could be considered as an effective strategy to improve hemostasis in materials. To achieve these purposes, the combination of natural compounds with engineered biomaterials has emerged as a promising approach. In this context, the hemostatic potential of *País* grape extracts - rich in PAs - loaded into GEL-GO composite aerogels will be investigated in this study.

1.6. General aspects of *País* grape extracts

1.6.1. Chemical structure of grape extracts

Polyphenols belong to a variety of natural compounds obtained as a product of the secondary metabolism of plants such as cocoa (*Theobroma cacao*), grapes (*Vitis vinífera*), tea (*Camelia sinensis*), and apples (*Malus domestica*) [77]. Polyphenols present hydroxylated structures composed of one or more hydroxyl groups attached to a benzoic ring [78]. Depending on their number of phenolic rings and the structural elements of these rings, polyphenols can be divided into flavonoid and non-flavonoid compounds, flavonoids being the most abundant in the vegetal kingdom [40,78]. Among them are the PAs, also called condensed tannins, which are found in the solid parts of the grape, mainly in the skin and seed. PAs are a type of high molecular weight flavonoid formed by catechin, epicatechin, and their galloylated derivatives [79,80]. They are flavan-3-ols polymers composed of C-C bonds and occasionally C-O-C bonds with chemical structures corresponding to C_6-C_3-C_6 flavonoids (**Figure 1.6**). The major flavan-3-ols monomers in grape comprise (+)-catechin, (−)-epicatechin, and (−)-epicatechin 3-gallate, (−)-epigallocatechin, and traces of (+)-gallocatechin [81]. Most flavonoids are found primarily in the outer epidermal cells (grape skin), whereas about 60-70% of total polyphenols are stored in grape seeds [40]. PAs present in the seed and skin of grapes also differ in their composition, quantity, and mean degree of polymerization (mDP) [79,80], with skin PAs showing a higher mDP than seed PAs [82].

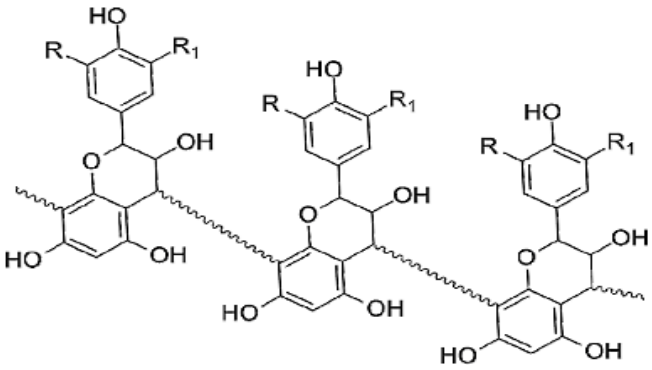

Figure 1.6. Chemical structure of PAs, showing hydroxyl groups attached to their benzoic rings. Source: Georgiev *et al.* [40].

1.6.2. Properties and applications of grape extracts

Grape seed and skin extracts have interesting properties for many applications, such as antioxidants, antimicrobial, cardioprotective, anticancer, antiviral, neuroprotective, and anti-inflammatory properties [40,83–85]. Among them, the antioxidant capacity of the extracts has been related to two main reasons, firstly, by the redox properties that allow them to act as reducing agents in oxidative reactions [85], and secondly, by the presence of a high amount of catechin, gallic acid, epicatechin, proanthocyanidin, and procyanidins in the chemical structure of the extracts [86]. On the other hand, the antimicrobial potential of these extracts has been associated with the high number of hydroxyl groups in their structures, which inhibit bacterial adhesion and coaggregation, reducing biofilm formation, and decreasing inflammation [81]. In this context, grape seed extracts have shown antibacterial effects against bacteria strains *E. coli, P. aeruginosa, M. luteus, S. aureus, A. niger*, and *F. oxysporum*, with a diameter of the growth zone of inhibition in a range between 15-20 mm [81,87]. Furthermore, grape flavonoids and PAs can target multiple pathways to overcome chronic inflammation, being potentially more effective compared to synthetic monodirected anti-inflammatory drugs [40].

Both extracts have also been used in hemostatic applications due to their physicochemical structure and properties. Mellado *et al.* [5] demonstrated that the incorporation of grape seed and skin extracts into GO/PVA aerogels improved both blood clotting and the material-blood cell interactions. Their results were attributed to an increase in the number of oxygenated functional groups in the aerogels after loading PAs and a charge-effect on the resulting material. In another study, Locilento *et al.* [41] demonstrated that grape seed extracts loaded into PLA/PEO nanofibrous membranes enhanced the activity of HFF1 cells due to the presence of PAs, which are contained in the chemical composition of this extract. Although these natural compounds have shown interesting biological activities, their

hemostatic potential has not been investigated. Therefore, the hemostatic performance *in vitro* and *in vivo* of the grape skin extracts (GSE) loaded into GEL-GO aerogels will be investigated.

1.6.3. PAs - polymers interactions

Numerous chemical reactions and physical interactions have been developed to design functional materials and modulate surface properties using polyphenols as starting materials. These reactions include hydrogen bonding, electrostatic, hydrophobic, covalent interactions, oxidative reactions, among others. Polyphenols contain abundant phenolic groups that could act as excellent hydrogen-bond donors by forming hydrogen bonds with molecules containing hydrogen-bond acceptors [85], such as PEG [88], PVA [89], and GEL [90]. In addition, these natural compounds can react through hydrophobic interactions, involving planar aromatics of polyphenols and hydrophobic sites of the substrate molecules, such as GEL [91]. On the other hand, the covalent interactions include esterification, etherification, amidation reactions, among others [85].

1.7. Blood - biomaterial interactions

Medical devices that come into contact with blood are widely used in clinical practice for many applications, from short-time treatments to long-term implants [92]. During these treatments, the occurrence of bleeding as a consequence of accidents, battlefield, and emergency settings is very common. This leads to the search for new hemostatic materials or a combination of the existing ones to control profuse bleeding.

1.7.1. Hemostasis mechanism

Hemostasis is the innate and multifaceted response of the organism to bleeding, involving the combined action of blood vessels, platelets, and the coagulation system to keep the circulatory system closed and protect the body from severe blood loss [3,93]. This process can be divided into three synergistic and orderly steps: *(i)* vascular spasm and stypsis; *(ii)* platelet plug formation; and *(iii)* coagulation cascade [3,92], as shown in **Figure 1.7**.

Once a blood vessel is ruptured, the hemostasis process begins immediately. First, in response to vascular damage, vasoconstriction of local and small arterioles is stimulated to restrict blood flow out of the vessel and reduce blood loss at injured sites. Meanwhile, exposure of the von Willebrand factor (vWF), collagen, and other thrombogenic molecules activate circulating platelets and cause them to adhere to the injured endothelium. Subsequently, the activated platelets release molecules such as adenosine diphosphate (ADP), thromboxane A_2, and serotonin, causing aggregation of more platelets at injured sites. This allows the initial formation of platelet plugs, which physically prevent the outflow of blood. This process is called primary hemostasis [3,93].

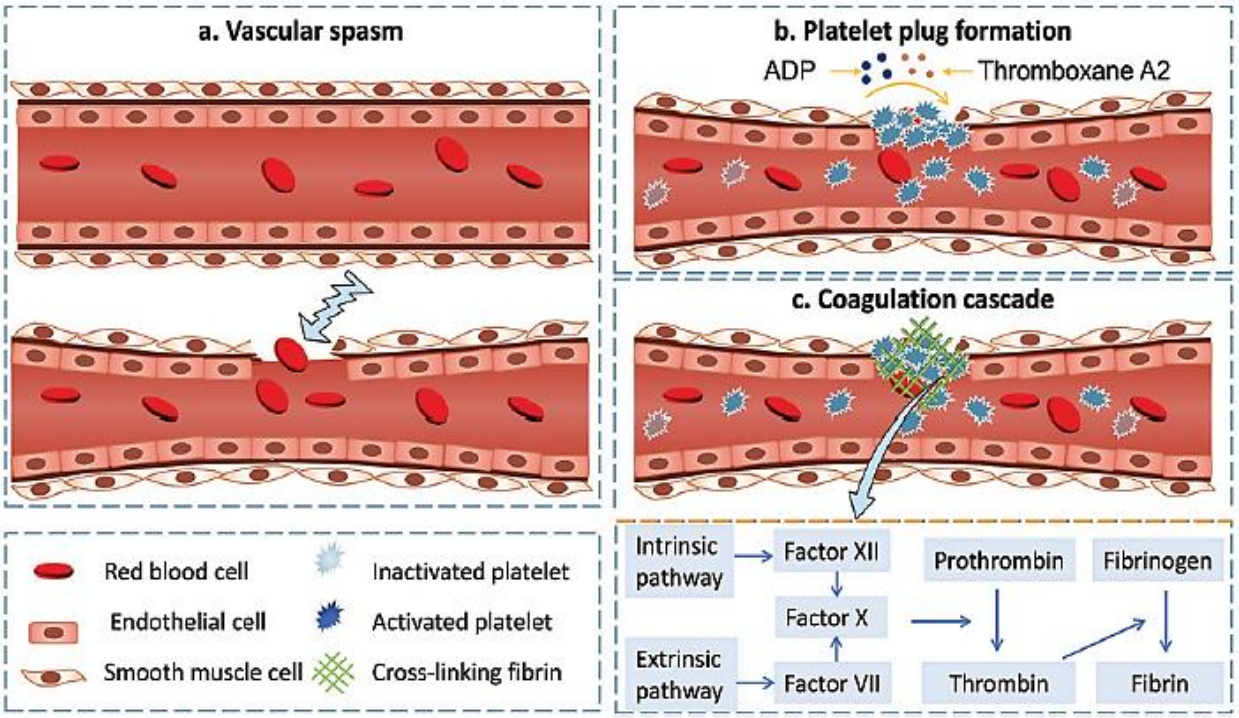

Figure 1.7. Illustration of the hemostasis process: (a) vascular spasm and stypsis, (b) platelet plug formation, and (c) coagulation cascade. Source: Wang *et al.* [3].

The coagulation cascade, which is also referred to as secondary hemostasis, begins at the time of primary hemostasis. This stage consists of two pathways: intrinsic and extrinsic, which converge to form a common pathway that converts fibrinogen into insoluble fibrin strands and reinforces weak platelet plugs [3]. The intrinsic pathway is associated with contact activation because it is triggered by contact between coagulation factors and the surface of the damaged blood vessel. This pathway activates Factor XII and at that time, exposure of the tissue factor to the blood triggers the extrinsic pathway, further activating Factor VII and amplifying the coagulation cascade in the presence of calcium ions [92,94]. This hemostatic pathway is also activated near or on negative surfaces in general through autoactivation of FXII to FXIIa factor [94]. Subsequently, the two hemostatic pathways converge to the common pathway to activate Factor X, which further converts prothrombin to thrombin. Thus, the generated thrombin activates Factor XIII, which can catalyze fibrinogen into cross-linked fibrin, thereby reinforcing the platelet plugs formed in the primary hemostasis stage [95]. **Figure 1.8** shows a schematic diagram of extrinsic and intrinsic pathways in the blood coagulation cascade, as well as endothelial injury and platelet adhesion. In contrast, when bleedings is light in small vessels,

the body's clotting process can induce hemostasis. However, it is very difficult to control bleeding naturally in situations of severe and uncontrolled bleeding, thus, external techniques and treatments must be applied to facilitate coagulation and achieve the hemostasis effect.

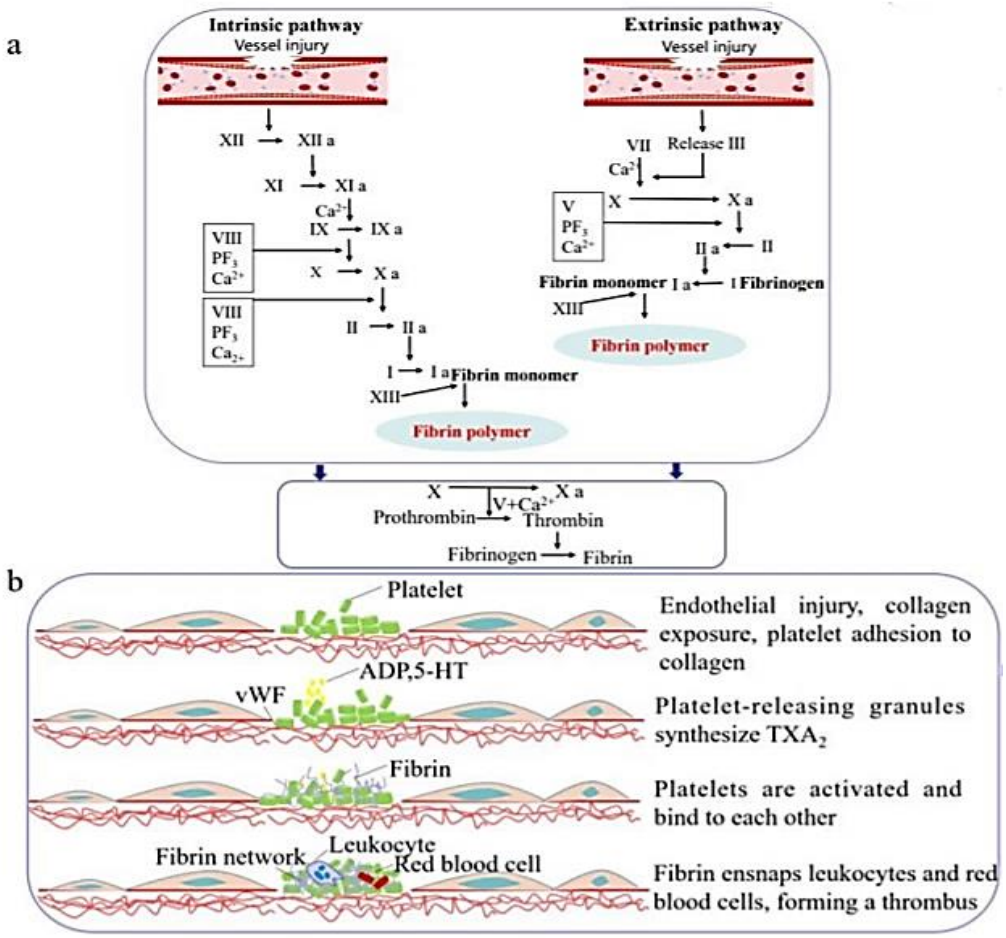

Figure 1.8. Schematic diagram of intrinsic and extrinsic hemostasis, (a) Process of blood clotting, (b) Schematic diagram of endothelial injury and platelet adhesion. Source: Zheng *et al.* [96].

1.7.2. Role of platelets and RBCs in the coagulation process

Blood cells represent approximately 99% of the total number of blood cells and their main function is to transport O_2 and CO_2 to the body, although they also play a key role in hemostasis and thrombosis [96]. Among blood cells, platelets and RBCs play an essential role in blood coagulation processes. Platelets are disc-shaped blood components with an average diameter of 2~4 μm, which can move and deform. Among their main functions, platelets are involved in the processes of coagulation and hemostasis, repairing damaged blood vessels, maintaining the integrity of blood vessel walls, and capillary permeability. On the other hand, RBCs are negatively-charged components with a volume of ~90 μm^3, a surface area of ~140 μm^2, and a hemostatic function is related to their physical

characteristics. They have the ability to accumulate rapidly on the surfaces of materials and can form blood clots quickly under the action of fibrin due to their relatively large volume and surface area [97,98].

Therefore, hemostatic materials could activate platelets and accumulate RBCs on their surfaces through the following pathways: *(1)* when the hemostatic material acts on the wound surface, the surface charge or composition of the material directly accumulates RBCs and activates platelets on its surface to participate in the coagulation system, *(2)* hemostatic materials can close or contract blood vessels through physical or chemical vias, increasing platelet adhesion and RBCs aggregation indirectly, *(3)* hemostatic materials participate in the coagulation system by mimicking the shape, structure, and function of platelets or RBCs [96]. Among these hemostatic mechanisms, we postulate that our aerogels promote hemostasis by the first pathway, which will be investigated in this thesis.

Similarly, other authors have also shown that surface charges, both negative and positive, play a key role in the material-blood interaction, activating different coagulation pathways to promote hemostasis [99,100]. Therefore, the understanding of these phenomena involves aspects of biocompatibility and hemocompatibility of materials, and as well their interactions with blood components, which will be investigated in this study.

1.7.3. Blood - GO interactions

Among all the proteins circulating in blood plasma, albumin and fibrinogen are the most important extracellular proteins related to blood-material interaction, especially in blood coagulation [94,101]. These plasmatic proteins can be incorporated into the GO structure due to the loading capacity of this material. This phenomenon is mainly governed by electrostatic interactions between GO and proteins and depends on factors related to the physicochemical properties of GO such as the size, O_2 content, surface charge, sonication time, C-O content, and amount of C=O [102]. In addition, the nature of proteins, platelet activation and aggregation, hemolysis after erythrocytes rupture, and the fibrinogen/albumin ratio adsorbed by GO are also involved in blood-GO interactions [101]. In this context, some authors have shown that GO-based materials have a greater hemolytic effect than rGO-containing materials due to their higher content of oxygenated functional groups. Similarly, a GO with longer sonication time exhibits more pronounced hemolytic effects compared to a GO with shorter sonication time [101,102]. Consequently, all these variables must be controlled during GO synthesis to achieve a material with suitable properties to interact with blood cell components.

In addition to plasma protein effects, GO-based materials have shown strong thrombus-inducing potential and considerable thrombogenicity, which allows triggering platelet activation and secondary

processes to accelerate blood coagulation [102]. This phenomenon is directly related to the hemocompatibility of the materials and to their anticoagulant activity; therefore, it should be evaluated in terms of the blood clotting time and the surface charge of the material.

1.7.4. Blood - PAs interactions

Polyphenol compounds have the ability to interact with different blood cell components through various mechanisms. Due to their antioxidant properties, these compounds can interact with plasma through albumin-quercetin interactions, which allows the formation of flavonoid-albumin complexes that help to maintain flavonoid concentrations in plasma, thus prolonging its antioxidant action [103]. In addition, the biological effects of polyphenols could be modulated through their interactions with lipids and membrane proteins. The existence of hydrophobic and hydrophilic chains in most polyphenol molecules also allows them to reach different levels in the membrane: on the surface of the adsorbed bilayer on lipids and/or insert into the bilayer and interact with hydrophobic lipid chains [78]. Their interactions with lipidic groups are directly related to the amount of hydroxyl groups of polyphenol and inversely related to the hydrophobicity of the molecules [78]. Consequently, a set of structural features determines the adsorption or penetration of polyphenols into the membrane lipid bilayer, thus governing their interactions with cell components.

In order to improve the understanding of PAs-blood interactions, protein-tannin interactions have been investigated. These interactions are essentially a dynamic surface phenomenon, generally reversible, involving mainly hydrophobic proteins. Furthermore, these interactions are enhanced by the formation of hydrogen bonds between the phenolic groups of the tannin (as proton donors) and the carbonyl groups of the binding peptide (as proton acceptors). The strength of these interactions depends on both the nature of the protein and the nature of the PAs molecule [104].

According to the premises discussed in this section, it is possible to conclude that: *(1)* crosslinked GO-based materials could have a higher capacity for rapid absorption of fluids compared to GO alone, *(2)* the incorporation of GSE, rich in PAs, into crosslinked GO materials could improve material-blood interactions due to the ability of PAs to form bonds with blood cells. These hypotheses will be investigated in this study.

1.8. GO - based materials cytocompatibility

The evaluation of the *in vitro* cytotoxicity is essential for developing materials with biomedical applications. GO-based materials have shown certain drawbacks related to their toxicity, demonstrating that GO toxicity is dose- and time-dependent [28]. Some authors have suggested that the cytotoxicity effects of GO-based materials are associated with the GO-cell membrane interactions

[57,105], while others have related it to GO-protein interactions governed by Van der Waals forces [106], which produces in both cases a physical damage to the cell membrane [64]. Most *in vitro* toxicity studies of GO-containing materials have been addressed in the literature through cell viability (*c.v.*) assays, which can be by direct or indirect contact of GO with cells.

1.8.1. *In vitro* cytotoxicity of GO - based materials

In vitro cytotoxicity of materials is defined as a modification of basic cellular functions that generates visible damage in primary culture models and/or in isolated organs. Among the *in vitro* studies developed on GO-based materials, the most performed ones use cell models under static conditions, which prevents extrapolating the hematological properties of the materials to dynamic *in vivo* environments [102]. Thus, *in vitro* assays provide relevant, but not conclusive, information on the biocompatibility of the material.

Graphitic materials induce obvious cytotoxicity effects, which depend on their concentration, incubation time with cells, surface chemistry [28,64], and other factors. Some authors have associated these dependencies to graphitic materials-membrane protein interactions, leading to cleavage of functional proteins that damage the phospholipid layer of cells, thus disrupting their metabolism and leading to cell death [107]. The cytotoxic effects of graphitic materials have also been related to the material properties, such as size, surface chemistry, morphology, and also to cell lines, route of administration [64], and so on.

As mentioned above, the cytotoxic of graphitic materials is dose- and time-dependent [28]. Numerous toxicity studies using different cell lines and doses have been addressed in the literature to evaluate the toxic effects of these materials at different incubation times. These studies have included the use of different cell lines, such as mouse dermal fibroblast cells (L-929), umbilical vein endothelial cells (HUVEC), human dermal fibroblast cells (HDF), normal human lung cells (BEAS-2B), human lung cancer cells (A549), hepatocarcinoma human cells (HepG2), HeLa cells, human cancer cells (MCF-7), among others. Due to the large number of *in vitro* cell viability studies performed to evaluate the toxicity of GO-based materials, only the most representative ones for the purpose of this study are presented in **Table 1.1**.

Table 1.1. Summary of different *in vitro* toxicity studies developed on GO-based materials.

Materials	Cell line	Dose	Incubation time (h)	Biological effects	Ref.

CGS	L-929	-	48	*c.v.* values of 95%, no cytotoxic effects observed	[13]
DCGS	L-929	-	48	Relative cell growth above 100% for all samples, no toxic effects	[14]
GMCS	L-929	62.5 – 250 µg/mL	24	Most of the cells showed death at 62.5 µg/mL and a complete collapse at 250 µg/mL	[108]
GKCS	L-929	62.5 – 250 µg/mL	36	Cell concentration greater for GKCS compared to a kaolin sponge alone	[7]
SA/GO/PVA	NIH-3T3	0.1 g dry sample	72	*c.v.* above 80%. Increasing GO content decreased the *c.v* values. Non-toxic materials	[30]
ACGS	MRC5	-	72	*c.v.* values close to 100% for ACGS. The GO incorporation reduced the *c.v.* values up to 81.8%	[29]
BGCS	L-929 mouse fibroblast cells	15.63 - 250 µg/mL	24	*c.v.* values between 78.4-98.8%. Bsp-loaded GCS reduced cell viability	[1]

All these studies agree that: *(1)* the cytotoxicity of graphitic materials is dose- and time-dependent, *(2)* the incorporation of new functional molecules into materials could favor cell adhesion and proliferation of the resulting composites. These considerations will be evaluated in this study.

1.9. *In vivo* performance of GO-based materials

Although *in vitro* studies can be considered a "good" approach to evaluate the hemostatic performance of materials for wound-dressing applications, the complexity of the toxic effects of graphitic materials leads to study them using *in vivo* animal models. Typically, rats are usually used as the primary model to evaluate the *in vivo* performance of materials, followed by larger animals as an improved model [108]. For tests with liquid materials, the main routes of administration identified are

intravenous, intramuscular, intraperitoneal and oral, while most *in vivo* studies with solid materials have been developed in femoral arteries and rat tails [102].

When graphene materials come into contact with the circulatory system of animals, they interact with different biological fluids such as plasma and serum. Consequently, they trigger different responses that depend mainly on their concentration and contact time [109]. Considering the large number of studies addressed in the literature evaluating the *in vivo* behavior of graphitic materials, **Table 1.2** lists only some of the most representative ones for this study.

Table 1.2. Summary of different i*n vivo* studies developed with graphitic materials using animal models.

Materials	**Animal model**	**Hemostatic time (s)**	**Blood loss (g)**	**Main findings**	**Ref.**
CGS	SD rats	201 ± 46	0.085 ± 0.025	CGS promoted hemostasis compared to a gauze sponge	[13]
TCGS	SD rats	100 ± 15.5	-	TCGS shortened hemostasis by 101 s compared to a CGS	[9]
DCGS	SD rats	166 ± 51.8	~ 0.05	DCGS shortened hemostasis by 35 s and reduced the blood loss by 37.5% compared to the CGS	[14]
GMCS	Rabbit femoral artery	85 ± 9	12.1 ± 2.9	Clot formation on the wound-material interface was observed, suggesting a complete hemostasis	[108]
GKCS	Rabbit femoral artery	73 ± 12	-	The incorporation of kaolin favored hemostasis of the resulting material	[7]
BGCS	SD rats	45.9 ± 4.6	0.063 ± 0.016	BCGS lengthened hemostasis by 10.3 s and increased the blood loss	[1]

				by 21% compared to a GO sponge	
DCGO	SD rats	105 ± 15	0.9 ± 0.5	DCGO shortened hemostasis by 165 s and reduced the blood loss by 77% compared to a GO sponge	[12]

Based on the above studies, it is concluded that: *(1)* crosslinked graphitic materials improve their *in vivo* hemostatic performance compared to a single crosslinked graphene sponge, *(2)* the incorporation of new functionalities into graphitic materials could promote hemostasis, *(3)* although graphitic materials have shown toxic effects with rats, regardless of the doses administered, their functionalization with biocompatible polymers allows reducing their toxicity *in vitro* and *in vivo*. These postulates will be investigated in this study.

Thesis plan

The main findings of this study will be presented in the following chapters in a format similar to that of a scientific journal since most of these results have been published or submitted in Journals. This thesis is structured as follows:

Chapter 2.This chapter presents a new synthesis method based on microwave (MW)-assisted reactions to develop GEL-GO aerogels. The influence of the GEL:GO ratio and the pH of the GO solution on the properties of the aerogels is evaluated. In addition, the use of MW as a new synthesis method to produce these aerogels is validated. This validation was conducted by comparing the properties of these aerogels with the ones of a GEL-GO aerogel developed by a traditional synthesis method. Chapter 2 responds to specific objective 1.

Chapter 3. Based on the results obtained in Chapter 2, the GEL-GO aerogel developed under alkaline pH conditions and with the lowest GEL:GO ratio is loaded with GSE to develop a new material with improved hemostatic properties. Chapter 3 presents the experimental procedure to synthesize GSE-loaded aerogels and the main results of their physicochemical properties and biological activity characterization. In addition, the results related to GSE release kinetics are included in this chapter. Chapter 3 responds to specific objective 2.

Chapter 4. This chapter presents an evaluation of the hemostatic efficacy of GEL-GO aerogels both *in vitro* and *in vivo*, based on the evaluation of their hemolytic activity, blood clotting capacity, mechanism of hemostatic action, and aerogel-blood cell interactions. The *in vivo* studies use a rat-tail amputation model to evaluate the hemostatic time and the amount of blood loss of GEL-GO aerogels. The hemostatic efficacy of GEL-GO aerogels was compared to that of commercial materials, Spongostan™ and ChitoGauze®XR, GO-CS and GO-PVA aerogels, and a control gauze sponge. Chapter 4 responds to specific objective 3.

Chapter 5. The hemostatic potential of GSE alone is investigated in *in vitro* and *in vivo* models, based on a comparison of the properties of aerogels with and without incorporated extract. Chapter 5 presents the results of the evaluation of the coagulation parameters for GSE alone and aerogels, as well as the results of the *in vivo* hemostatic efficacy of GSE-loaded aerogels, whose values were compared with those of GEL-GO aerogel, a control gauze sponge, and the commercial material Spongostan™ to elucidate the role of the extract in hemostasis. Chapter 5 responds to specific objective 4.

Chapter 2

Development of gelatin aerogels reinforced with graphene oxide by microwave-assisted synthesis: Influence of the synthesis conditions on their physicochemical properties.

The information provided in this chapter is redrafted after publishing in: Development of gelatin aerogels reinforced with graphene oxide by microwave-assisted synthesis: Influence of the synthesis conditions on their physicochemical properties. (J. Borges-Vilches, T. Figueroa, S. Guajardo, M. Meléndrez , K. Fernández, Polymer, 208, 2020, 122951).

2.1. Abstract

GEL aerogels reinforced with GO at different pH values of GO and GEL:GO ratio were developed by microwave (MW)-assisted synthesis. The chemical characterization demonstrated non-covalent and covalent interactions under acidic and alkaline conditions, respectively. The elastic modulus increased 6 times and 1.38-fold, and the swelling ratio (SR) increased 1.2-fold and 1.4 times for aerogels at acidic and alkaline pH, respectively, when the GEL content increased. The surface charge shifted from positive to negative values by increasing the pH. Additionally, a higher SR value was found for the aerogel synthesized in alkaline environment and lowest GEL:GO ratio, and its properties were compared to an aerogel synthesized by traditional processes to validate the MW as a new synthesis method to develop these aerogels. Similar physicochemical properties were identified in both aerogels, with an increase in the SR value for the MW synthetized aerogel of 1.5 times. This study provides a new synthesis method to develop GEL-GO aerogels.

2.2. Introduction

Aerogels are colloidal materials similar to gels in which the liquid component is replaced by gas. These materials have good mechanical properties, low density, and high superficial area, porosity and electrical conductivity [21,22]. Their properties have allowed them to be used in several applications and fields: as materials for energy storage and conversion [21], as absorbent materials of organic and inorganic contaminants [109] and to remove copper ions [110]. Along with these applications, the aerogels demonstrate great potential in biomedical applications, particularly in tissue engineering, as platforms of drug delivery systems and in studies of *in vitro* and *in vivo* compatibility [4,5].

Carbon-based materials have been widely used to synthesize aerogels, including the GO [1,6]. GO has a flat 2D sheet structure with a honeycomb shape, and its chemical structure presents oxygenated functional groups in its basal and edge planes [7]. The hydrophilic character of GO allows an easy exfoliation of its sheets and a later stable dispersion of its layers [8]; therefore, it is beneficial to prepare mechanically strong composites such as aerogels and hydrogels. The formation of these composites is by covalent and non-covalent interactions of GO sheets with other materials, mainly polymers [6,9,10] such as GEL.

GEL is a polymer obtained from collagen by acid or basic partial hydrolysis with differences in its isoelectric point (pI): gelatin type A pI (~6-9) and type B (pI~5) [11,12]. Structurally, the GEL has a triple-helical conformation with high contents of glycine, alanine, proline, and hydroxyproline [12]. In addition, the GEL is a biocompatible and biodegradable polymer that has amphoteric character, great affinity with proteins and low cost. These properties endorse its use as a reducing agent in the synthesis of nanomaterials, particularly with GO, to form composites such as hydrogels and aerogels [13–16].

The formation of GEL-GO aerogels has been developed by non-covalent and covalent functionalization. The non-covalent syntheses have been developed by stirring the solution for 2 minutes at 37°C, whereas that covalent syntheses require continuous heating of the GEL-GO solution for 24 h at ~90°C [39,71]. The covalent method can cause a denaturalization of GEL by a break of its polymeric chains and may also provoke the reduction of the GO as a consequence of the thermal treatment applied during the synthesis [14,15]. These drawbacks associated with structural damages in both components that affect their chemical stability and mechanical performance [113], thus restricting their applications.

To overcome these disadvantages, MW technology could be used as an alternative in the processes that require heating. To date, MW has been widely used to develop amidation reactions, polymeric synthesis, reactions on polymers [114], in the formation of nanostructures and hydrogels [18–20], and in the synthesis of nanostructured materials such as metals, carbon, and colloidals [117]. Several attributes of MW heating contribute to a greener synthesis and allow an instantaneous and rapid heating. Thus, it is possible to reduce the reaction times with a greater selectivity, yield, and speed of reaction, decrease the energy consumption, and reduce the limitations associated with secondary reactions [18]. For example, Cook *et al.* [115] developed hydrogels based on PVA by MW reactions, obtaining a yield of 20% in 20 min compared with those 10% yields in 1 h by conventional heating, which are desirable attributes to improve the synthesis performance.

The aerogels synthesis processes are influenced by several variables. Among them are the GO/polymer ratio and synthesis temperature [38], the sonication time and the oxidation degree of the GO [13,22], and as well external stimuli such as the pH [119,120] and surface properties of the matrix [102]. All these variables directly influence the crosslinking processes and, as a consequence, the physicochemical properties of these materials. For instance, Bai *et al.* [120] evaluated the influence of pH and the GO/PVA ratio on the synthesis process of composites hydrogels used as carriers for selective releasing vitamin B_{12}. Their results indicated that GO sheets are able to form pH-sensitive composite hydrogels with PVA. Similarly, Chen *et al.* [38] developed GEL-GO nanosheets at different synthesis conditions (pH, GEL/GO ratio, and temperature) for being used in drug delivery applications. Their results showed that acid synthesis conditions are more favorable for releasing methotrexate than the neutral environments, indicating a GEL-mediated sustained release process [38]. Although some studies have been conducted in this area to date, none of them included the use of MW in the synthesis of GEL-GO aerogels.

Therefore, this study aims to develop GEL aerogels reinforced with GO by MW-assisted synthesis at different GEL:GO ratios and pH values of the GO solution. The influence of both synthesis conditions on the physicochemical and mechanical performance of these aerogels were investigated. The characterization included spectroscopic analysis, elastic modulus and apparent porosity assays, surface charge determinations, and swelling ratio measurements. Finally, the performance of these aerogels was compared to an aerogel developed by the traditional synthesis process to validate the use of MW as a new synthesis method to develop GEL-GO aerogels.

2.3. Materials and Methods

2.3.1. Materials

Graphite powder (Flake, mesh 325) was purchased from Asbury Online (Asbury Carbons, NJ). Gelatin type B was purchased from Sigma-Aldrich Company, (St. Louis, MO). The other chemicals and solvents used, such as potassium permanganate powder ($KMnO_4$, 99.9%), hydrochloric acid (HCl, 10%), oxygenated water (H_2O_2, 60 vol), sulfuric acid (H_2SO_4, 98%), ethanol (C_2H_5OH, 95%), silver nitrate ($AgNO_3$) and phosphoric acid (H_3PO_4, 85%), were purchased from Merck (Darmstadt, Germany). The reagents were received and used without further purification. Fresh human blood was extracted from healthy volunteers and mixed with anticoagulant in 6.0-mL tubes. Milli-Q® and distilled water were used throughout the work.

2.3.2. GO synthesis

Graphite oxide (GpO) was prepared from natural graphite powder by the modified Hummers method [45] with subsequent purification and exfoliation at different reaction times [49]. In this synthesis, 30 mL of concentrated H_3PO_4 and 270 mL H_2SO_4 were added into a beaker in an ice bath, followed by a slow addition of 2.25 g of graphite powder and 13.5 g of $KMnO_4$. The chemicals were incorporated carefully to prevent the temperature from exceeding 45°C. Then, the mixture was kept at 35-40 °C after being stirred for 1 hour. After the reaction, 60 mL H_2O_2 was added slowly until a green-brown color was observed in the mixture. Subsequently, the oxidation product was continuously washed and centrifuged at 800 rpm for 15 min. In the first wash, the mixture was treated with Milli-Q® water (200 mL) and aqueous HCl solution (20 mL) to remove the metal ions until the suspension pH was close to 7, using the $AgNO_3$ as an indicator. Afterward, the mixture was washed with ethanol (100 mL) and four times with Milli-Q® water (200 mL in each case), eliminating the supernatant every time until obtaining a pH between 3.5 - 4. Finally, the mixture was dialyzed in dialysis membranes for 3 days to remove any remaining impurities and lyophilized for 72h (Labconco freeze-dry system, Germany) to obtain a GpO solid dispersion.

2.3.3. GEL-GO aerogels synthesis

GEL-GO aerogels were developed by a MW-assisted reactions under different synthesis conditions (**Table 2.1**). In this synthesis process, 0.1 g of GpO (2 mg/mL) was dissolved in 50 mL Milli-Q® water and sonicated for 30 min (Digital Ultrasonic cleaner model CD 4820, 42 kHz, 160 W, Shenzhen Codyson Electrical Co. Ltd., China) to avoid the formation of conglomerates in the GO solution. Then, the pH of the GO solutions was adjusted to values of 3, 7, and 11.

GEL solutions were prepared by heating a desirable amount (1 g, 1.25 g, and 1.5 g) of GEL dissolved in 150 mL of Milli-Q® water at 60°C for 15 min, adjusting the GEL:GO ratios at 10:1, 12.5:1 and 15:1 (**Table 2.1**), respectively. The GO and GEL solutions were mixed and the resulting mixture was placed in flasks and subjected to MW-assisted reaction (Microwave Somela 17L C1700N), operating at a power of 800 W for 30 min. The total reaction time (30 min) included heating and cooling intervals of 5 min each, ensuring that the temperature did not exceed 90°C to avoid denaturing and damaging the chemical structure of the GO and GEL [15,22]. Finally, the GEL-GO solutions (black color) were put in Petri dishes with cylindrical shapes and crosslinked for 12h at 4°C until obtaining GEL-GO hydrogels. These hydrogels were frozen at -86°C and lyophilized (Labconco freeze-dry system, Germany) for 72h to get a porous structure (GEL-GO aerogels) after water sublimation. The GEL-GO aerogels were

designated as $G_{\alpha}GO_{\beta}$, where α indicates the GEL content incorporated into each aerogel, and β indicates the pH value of the GO solutions.

Table 2.1. Nomenclature used to identify the GEL-GO aerogels according to the modified synthesis conditions.

Synthesis conditions		
pH of GO solutions	GEL: GO ratio	$G_{\alpha}GO_{\beta}$ aerogels
3	10:1	$G_{10}GO_3$
3	15:1	$G_{15}GO_3$
7	12.5:1	$G_{12.5}GO_7$
11	10:1	$G_{10}GO_{11}$
11	15:1	$G_{15}GO_{11}$

2.3.4. Physicochemical characterization of aerogels

The physicochemical and mechanical properties and the morphology of the GEL-GO aerogels were studied by X-ray diffraction (XRD), Attenuated total reflection Fourier Transform Infrared Spectroscopy (ATR-FTIR), Raman analysis, X-ray photoelectron spectroscopy (XPS), thermogravimetric analysis (TGA), scanning electron microscopy (SEM), uniaxial compression test, and surface charge measurements. A detailed information about these characterization techniques is included in the **Appendix A.1** of this thesis.

2.3.5. Apparent porosity measurements

The apparent porosity was evaluated using the Archimedes principle, according to reported methodologies [121]. The exterior volume (V_d) of each GEL-GO aerogel (1.0 cm^3) was measured, and the samples were immersed in a pycnometer containing a 99% ethanol solution. The actual volume (V_a) was calculated using **Equation 2.1**:

$$V_a = \left((W_W - W_O) - (W_T - W_P) \right) / 0.789 \quad (2.1)$$

where W_w is the ethanol and pycnometer weight; W_o is the dry weight of the pycnometer; W_T is the combined weight of ethanol, pycnometer and the sample of aerogel, W_p is the dry pycnometer weight and the dry sample of aerogel, and 0.789 is the ethanol's density (expressed in g/mL). The apparent porosity was calculated following **Equation 2.2**:

$$\text{Porosity} = \left((V_d - V_a) / V_a \right) * 100 \quad (2.2)$$

2.3.6. Swelling behavior of GEL-GO aerogels

The SR of the GEL-GO aerogels was determined by contacting samples with water, phosphate-buffered saline (PBS, pH=7.4), and blood with anticoagulant at room temperature for 5 s, 10 s, 15 s, 30 s, 60 s, 120 s, and 240 s. First, the dry aerogel samples were cut of equal size and shape (1.0 cm^3). Then, 3.0 mL of each liquid medium was dripped onto the surface of the aerogels. After each reaction time, the excess liquid was eliminated, and the SR of the GEL-GO aerogels was determined using **Equation 2.3**:

$$SR = \left({\left(W_{wet} - W_{dry} \right)} \Big/ {W_{dry}} \right) * 100 \quad (2.3)$$

where W_{dry} is the dry sample weight, and W_{wet} is the wet sample weight (after contact with the liquid medium).

2.3.7. Statistical analysis

Data were processed using OriginPro8.5® software and the statistical analyses were done by ANOVA test and an analysis of multiple ranges (test of Duncan) using Statgraphics Centurion XVII® software. The level of significance was determined as $p \leq 0.05$. The mean values and the error bars are reported in each figure.

2.4. Results and Discussion

2.4.1. Chemical characterization of GEL-GO aerogels

GEL-GO aerogels were developed by MW-assisted synthesis at different GEL:GO ratios and pH conditions of the GO solution. The oxidation degree and crystallinity of these materials were evaluated through the XRD patterns for GO, GEL, and GEL-GO aerogels (**Figure 2.1a**). The GO pattern shows the absence of a peak at 26.6° (associated with graphite) and the appearance of a strong peak at 10.5° attributed to the existence of oxygenated functional groups in the GO sheets [38,39,71,122]. These results confirm the successful oxidation and exfoliation of the GO sheets, allowing the separation of its layers and the subsequent crosslinking with the GEL. In the GEL pattern, two characteristic peaks at 7.6° and 21.4° are observed, which are associated to the triple-helical conformation of the GEL. The first peak corresponds to residual amino acids and the second one to the diameter of its helices [38,71,113]. In the GEL-GO aerogels, similar patterns to the GEL are observed, due possibly to the high GEL content incorporated into the aerogels (greater than 90% *w/w* in all aerogels). However, the aerogel patterns show peaks wider and less pronounced compared to the GEL pattern. This result indicates a lower crystallinity and a greater structural disorder in the GEL-GO aerogels compared to

their pure components, which could be caused by the crosslinking between GEL and GO during the aerogel formation.

The functional groups of GEL, GO, and GEL-GO aerogels were analyzed by ATR-FTIR spectroscopy (**Figure 2.1b**). The GO spectrum shows a -OH band stretching bond between 3390-3170 cm^{-1}, a peak at 1738 cm^{-1} associated with its carbonyl groups (C=O), C=C vibrations at 1630 cm^{-1}, C-OH stretching vibrations at 1405 cm^{-1}, and peaks at 1224 cm^{-1} and 1048 cm^{-1} associated with the epoxy groups and the alkoxy stretching, respectively [37,38,71,122,123]. The GEL spectrum shows peaks at 1637 cm^{-1}, 1540 cm^{-1} and 1230 cm^{-1}, which were associated with vibrations of amide I, amide II, and amide III, respectively [37,71]. In addition, peaks at 1452 cm^{-1} related to the stretching vibrations in the pyrrolic ring and a peak at 3290 cm^{-1} ascribed to the N-H vibrations of the GEL chains are also detected in the GEL spectrum [124–126].

Additionally, the aerogels spectra were compared to both GEL and GO spectra to identify functional modifications. After the functionalization, the carboxylic groups of GO became weaker with the increase in the GEL content and disappeared completely in the aerogels synthesized under acidic conditions ($G_{10}GO_3$ and $G_{15}GO_3$). This result could be due to the formation of a ammonium carboxylate complex through the protonated amino groups of GEL and the carboxylic groups of GO, increasing the electrostatic forces between GEL and GO [39,71]. Additionally, all aerogels spectra show a weak vibration of the epoxy groups, indicating a ring-opening reaction between this functional group and the amino groups of the GEL. Both reactions are corroborated by the presence of the amide I and amide II bands in the GEL-GO aerogel spectra. Similarly, the C-OH and C-O functional groups associated with the GO spectrum became weaker with the increase in the GEL content, which indicates a partial elimination of hydroxyl groups during the GEL-GO aerogel synthesis. Moreover, the N-H stretching vibration located at 3290 cm^{-1} in the GEL spectrum became broader and more intense as the GEL content increased.

In terms of pH variations, the results indicate that increasing the pH of the GO solutions increases the intensity of the vibrations of the aerogels' functional groups obtained under alkaline environments ($G_{10}GO_{11}$ and $G_{15}GO_{11}$). This outcome could be explained because an increase in the pH of the GO solution makes that the system move away from the pI of the GEL (pI~5), thus producing activation of the functional groups of both GEL and GO [127,128]. Finally, agglomeration of GO sheets is not observed when reacting with the GEL, which corroborated the lower crystallinity of the aerogels. These findings indicate that the different synthesis conditions used to produce the GEL-GO aerogels give rise to different physicochemical interactions between GEL and GO, suggesting non-covalent bonds for the

aerogels synthesized under acidic environments and covalent bonds for the aerogels developed in alkaline conditions.

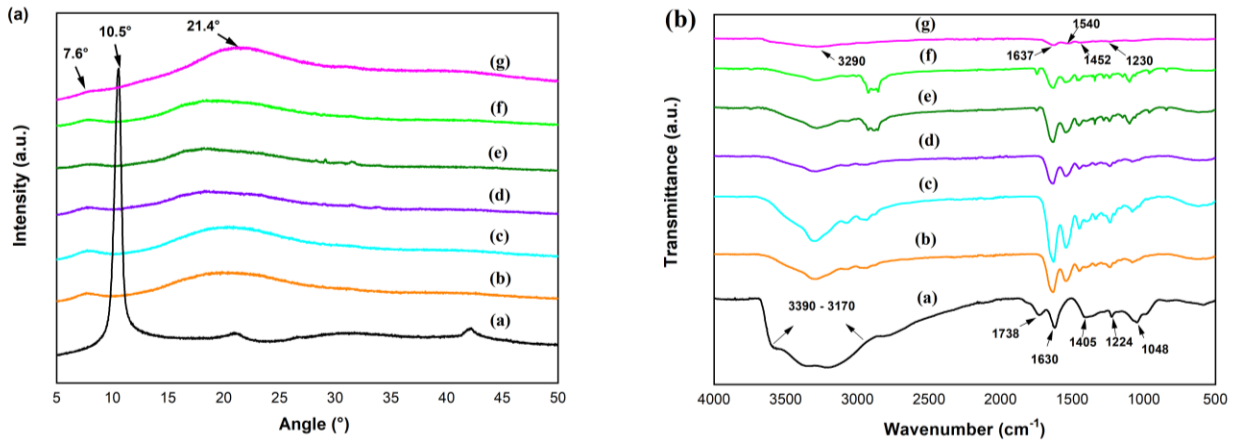

Figure 2.1. (a) XRD patterns and (b) FTIR spectra of (a) GO, (b) $G_{10}GO_3$, (c) $G_{15}GO_3$, (d) $G_{12.5}GO_7$, (e) $G_{10}GO_{11}$, (f) $G_{15}GO_{11}$ and (g) GEL.

The chemical characteristics of the GO and GEL-GO aerogels were studied by Raman spectroscopy (**Figure 2.2**). The GO Raman spectrum is characterized by a D band at ~1335 cm^{-1} associated with the formation of sp^3 defect bonds caused by the oxidation process [58] and a G band at ~1590 cm^{-1} originated from the phonon scattering of graphitic structure and is related to concentric cylinders of graphene layers (sp^2 hybridization) [71,122] (**Figure 2.2a**). As a result of the cooperation of D+G bands is originated a 2D region (located between 2445-3020 cm^{-1}), which is related to the number of layers of the material [58]. **Figure 2.2b** shows the aerogel Raman spectra, indicating the presence of a D band at ~1335 cm^{-1} and a G band at ~1605 cm^{-1}. The Raman shift of the G band in the aerogels spectra compared to the GO spectrum could be owing to the charge transfer of the branched-chain amino groups from GEL to GO sheets [39].

To evaluate the influence of the synthesis conditions on the structural properties of the GEL-GO aerogels, the relative intensity ratio (I_D/I_G) of each deconvoluted Raman spectra was determined according to the area ratio in the deconvoluted spectra. The spectra were deconvoluted by the Lorentzian function in the spectral region between 1000-1800 cm^{-1} (**Figure A.1**). As a result of the deconvolution, a new band named D** was found between 1500~1550 cm^{-1} spectral region. Some authors have associated the origin of this band with the contributions from the phonon density of states in finite-size graphitic crystals or due to C-H vibrations in hydrogenated carbons [129]. In contrast, others authors have ascribed the D** band origin to the amorphous phases present in the graphitic

materials, in which the intensity decreases when the crystallinity increases [130]. The appearance of this new band caused a decrease in the intensity of the G band; thus, the I_D/I_G ratios were quantified according to the area ratio in the deconvoluted spectra.

As a result of the I_D/I_G ratio calculated, an increase in the GEL content raised the I_D/I_G ratios from 4.1 to 4.9 in the aerogels synthesized in acidic medium ($G_{10}GO_3$ and $G_{15}GO_3$). Similarly, aerogels developed under alkaline conditions ($G_{10}GO_{11}$ and $G_{15}GO_{11}$) increased their I_D/I_G from 2.1 to 2.8 when the GEL content was increased. These variations indicate a decrease in the average size of the sp^2 carbon domains (loss of aromaticity) and a partial reduction of the GO in the presence of GEL. These structural changes could be due to the thermal treatment applied during the aerogel synthesis as a consequence of the crosslinking between GO and GEL [15,29]. The I_D/I_G ratio variations were also investigated against pH modifications. A pH increase of the GO solutions decreased the I_D/I_G ratio in aerogels developed under alkaline environments, indicating a minor number of structural defects in these materials. These results are attributed to the aerogel synthesis conditions since a higher activation of both GEL and GO functional groups improves the physicochemical interactions between both compounds [127,128]. This behavior agrees with the one reported with the ATR-FTIR analysis.

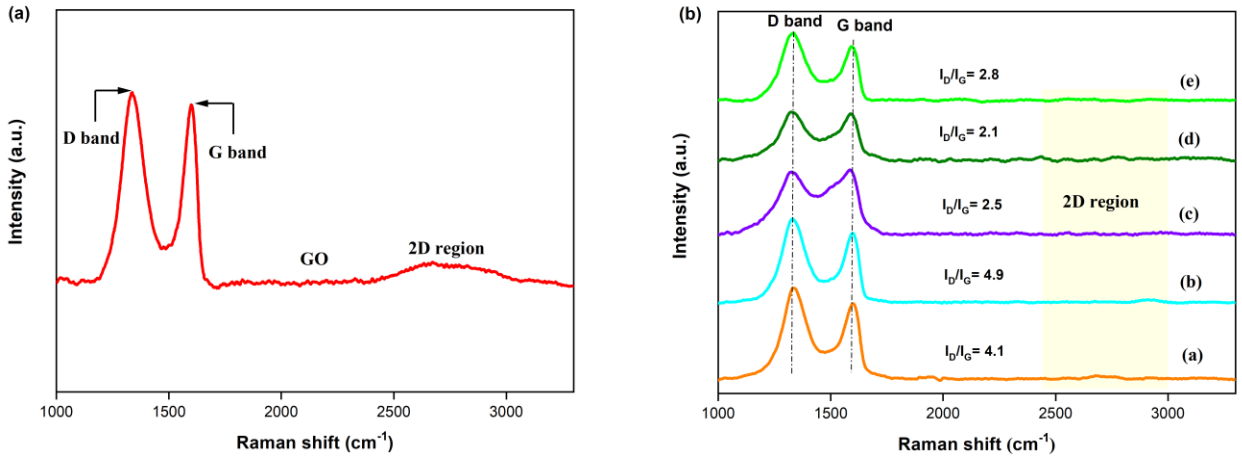

Figure 2.2. Raman spectra of (a) GO and (b) GEL-GO aerogels: (a) $G_{10}GO_3$, (b) $G_{15}GO_3$, (c) $G_{12.5}GO_7$, (d) $G_{10}GO_{11}$, (e) $G_{15}GO_{11}$.

XPS analysis was carried out on the GEL-GO aerogels to investigate their surface chemistry. **Figure 2.3** shows the XPS C1s spectra of the GO, GEL, and aerogels synthesized under acidic and alkaline conditions at the highest GEL:GO ratio ($G_{15}GO_3$ and $G_{15}GO_{11}$). The deconvoluted C1s spectra show peaks of C-C (~284.7 eV), C-N (~286.4 eV), C-O (~286.6 eV), C=O (~287 eV), and COOH/O=C-N (~288.4 eV) [122,124,131]. After the functionalization process, both aerogels show a decrease of the C-C sp^2 compared to GO and GEL spectra, which indicate a loss of aromaticity as a consequence of

the crosslinking process [124]. Additionally, the intensity peak at 288.4 eV decreased for the aerogel developed under alkaline conditions ($G_{15}GO_{11}$) compared to the $G_{15}GO_3$ aerogel, which could be due to the reaction between the carboxylic groups of the GO sheets and the amine groups of GEL chains caused by the replacement of oxygen in the oxygenated carbons by the presence of heat [71]. This result confirms the formation of a covalent bond between GEL and GO for the $G_{15}GO_{11}$ aerogel. Comparatively, the intensity of the epoxy groups in the $G_{15}GO_3$ aerogel increased compared to the GO spectrum, thus indicating the formation of physical interactions through H-bonding for aerogels developed under these synthesis conditions. Similar results have been observed by other authors for epoxy-based nanocomposites reinforced with GO and functionalized with hexamethylene-diamine [122], and polypyrrole/graphene nanocomposites [124]. Finally, the XPS results agree with the ATR-FTIR findings, indicating that the GEL was successfully grafted onto the GO surface to develop GEL-GO aerogels with a chemical nature pH-dependent of the GO solutions used.

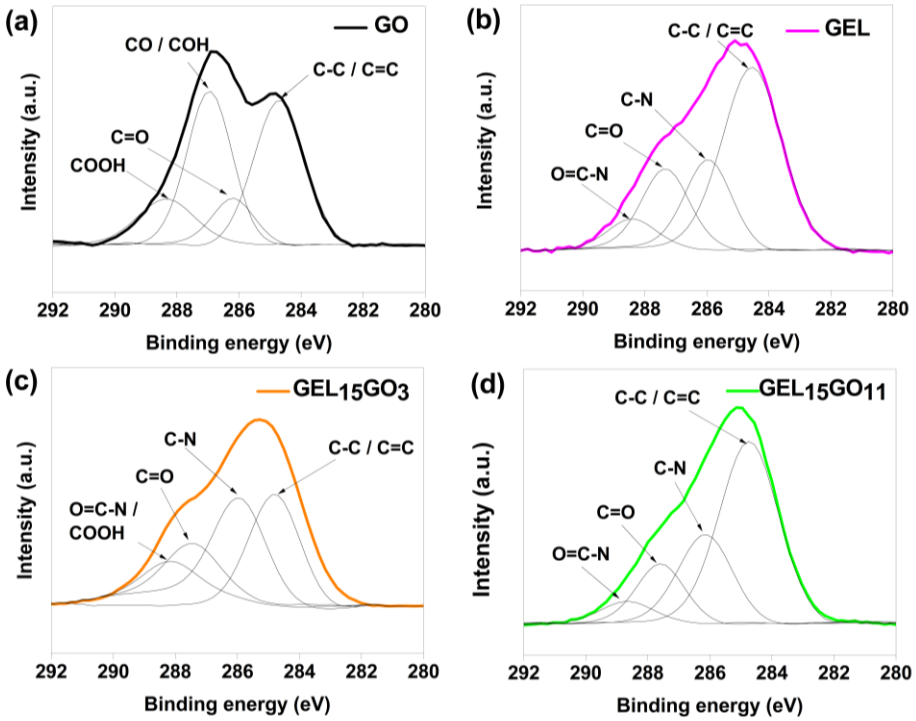

Figure 2.3. XPS C1s spectra of (a) GO, (b) GEL, (c) $G_{15}GO_3$, and (d) $G_{15}GO_{11}$.

The thermal stability of the GO, GEL, and GEL-GO aerogels was evaluated by TGA analysis (**Figure 2.4**). The thermograms show an initial GO loss mass below 100°C associated with the evaporation of absorbed water and the stabilization process [38,53]. An additional loss mass of ~20% is observed in the GO curve at ~138°C, which is attributed to the pyrolysis of its labile oxygen-containing groups,

yielding CO, CO_2, and steam [5,71]. The curve of GEL shows a weight loss of ~70% from 240°C to 500°C due to the pyrolysis of its polymeric chains. TGA curves of the GEL-GO aerogels show similar behavior to the GEL curve due possibly to the high GEL content incorporated into the aerogels. The total weight loss of the GEL-GO aerogels was close to ~65% at temperatures between 185°C and 250°C. In more detail, the aerogels developed using the highest GEL:GO ratio ($G_{15}GO_3$ and $G_{15}GO_{11}$) had a lower weight loss compared to the aerogels synthesized with the lowest GEL:GO ratio ($G_{10}GO_3$ and $G_{10}GO_{11}$). In addition, the thermal stability of the GEL-GO aerogels improved when the pH of the GO solutions increased. TGA results are consistent with those obtained by ATR-FTIR and XPS analysis, indicating that the alkaline synthesis conditions favored a higher activation of the functional groups of the GEL and GO [127,128], thus allowing greater stability for the GEL-GO aerogels compared to their pure components. Therefore, the improvement of the thermal stability of these aerogels confirms the formation of covalent and non-covalent interactions, according to the synthesis conditions used.

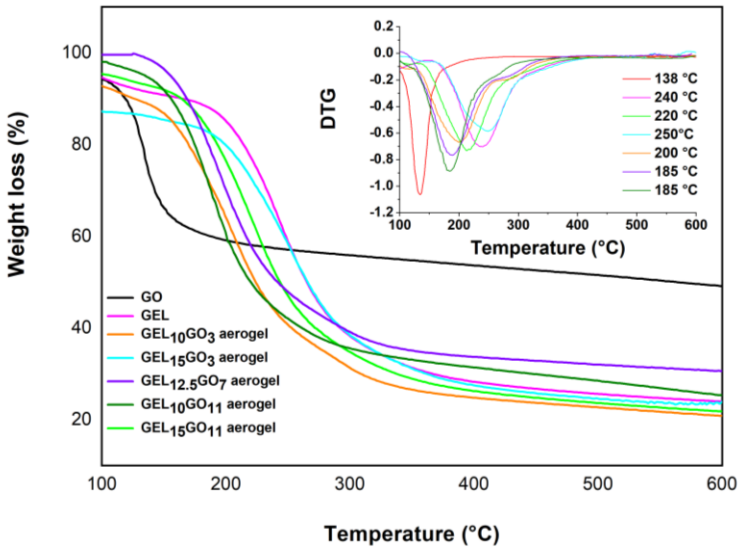

Figure 2.4. TGA curves for GO, GEL, and GEL-GO aerogels (at heating rate of 10 °C/min under nitrogen atmosphere). The inner graphic shows the DTG curves.

2.4.2. Physical characterization of GEL-GO aerogels

The morphology of GEL-GO aerogels was investigated by SEM analysis (**Figure 2.5**). All aerogels show interconnected porous structures with pore sizes between 12.3 µm and 18.6 µm (**Table 2.2**). The different synthesis conditions used to produce the GEL-GO aerogels influenced the morphological characteristics of these materials. With an increase in the GEL content, the pores become more uneven, shallower, and smaller. This result was due to the crosslinking ability of the GEL, which, when

it increases in concentration, increases the crosslink density; thus decreasing the pore size. Similar behavior was observed by Lai *et al.* [132], who demonstrated that an increase of the GEL concentration decreases the width and length of the pore for crosslinked porous GEL hydrogels. SEM analysis confirms the influence of the GEL content on the morphological features of these aerogels.

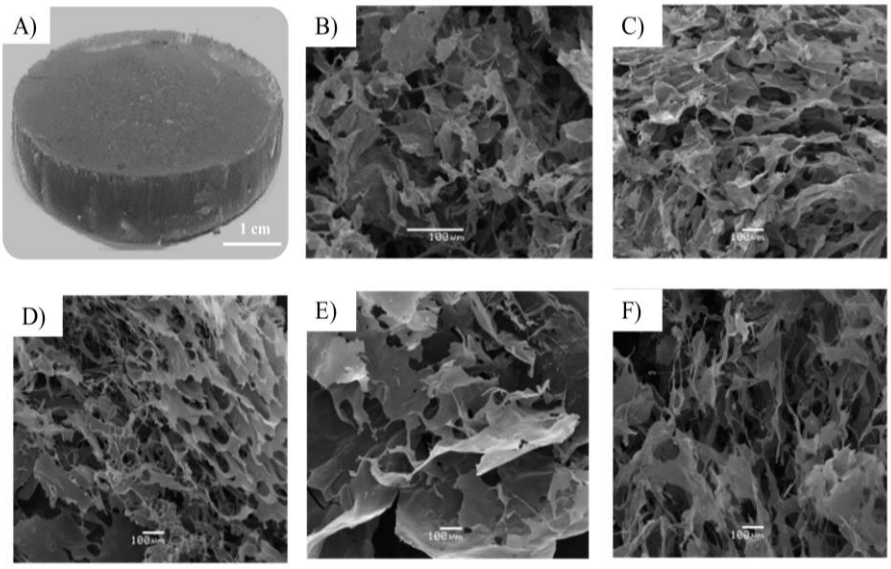

Figure 2.5. Morphology of GEL-GO aerogels by SEM images A) photograph of GEL-GO aerogel, B) $G_{10}GO_3$ aerogel, C) $G_{15}GO_3$ aerogel, D) $G_{12.5}GO_7$ aerogel, E) $G_{10}GO_{11}$ aerogel, and F) $G_{15}GO_{11}$ aerogel.

To determine the elastic modulus values of the GEL-GO aerogels, a uniaxial compression test was carried out on the samples. **Table 2.2** lists the elastic modulus values determined in the first linear region of the stress-strain curves for each aerogel (**Figure A.2**). The synthesis conditions had a significant influence on the mechanical properties of the aerogels (*p-value<0.05*). An increase of the GEL content increased 6-fold the elastic modulus values for aerogels developed at acidic pH and 1.38 times for aerogels synthesized under alkaline conditions, respectively. The highest elastic modulus value, around 4.8 ± 0.21 kPa was found for the aerogel developed under acidic pH and with the highest GEL:GO ratio ($G_{15}GO_3$), being this pH synthesis close to the pI of the GEL. However, when the system moved away from this pI, it produced electrostatic repulsions and reduction of the triple-helical conformation of the GEL chains, decreasing the elastic modulus values for the GEL-GO aerogels [133]. These results indicate that during the synthesis process, the GO sheets are functionalized with the GEL chains, acting as multifunctional cross-linkers [37], whose behavior was pH-dependent. In a related study, Liu *et al.* [134] demonstrated that the addition of 40 mg/mL and 60 mg/mL of GEL

increase in 3.4-fold the elastic moduli in hydrogels based on dextran and GEL. On a scale comparable to the results obtained in this study, Cha *et al.* [135] informed elastic modulus values of 4-5 kPa for GEL methacrylate and GO aerogels. Similarly, Lee *et al.* [136] stated elastic modulus values of 3.42 kPa for GEL-GO hydrogels. All these studies demonstrate that GO incorporated into the aerogel matrices can act as a reinforcement material for developing aerogels with improved mechanical properties, even incorporating a low GO content [28]. In addition, these results corroborate the influence of the synthesis conditions on the performance of the GEL-GO aerogels.

Table 2.2. Physical properties and elastic modulus values for GEL-GO aerogels.

$G_{\alpha}GO_{\beta}$ aerogels	Pore size (μm)	Elastic modulus (kPa)	Surface charge (mV)	Apparent porosity (%)
$G_{10}GO_3$	16.2 ± 4.5	0.8 ± 0.13	1.7 ± 0.15 [a]	90.6 ± 0.50 [a]
$G_{15}GO_3$	12.3 ± 3.7	4.8 ± 0.21	1.6 ± 0.23 [a]	97.7 ± 0.87
$G_{12.5}GO_7$	15.4 ± 3.1	1.3 ± 0.24	-8.8 ± 1.16 [b]	87.3 ± 1.12
$G_{10}GO_{11}$	18.6 ± 3.5	1.8 ± 0.16	-8.1 ± 0.57 [b]	91.8 ± 1.41 [b]
$G_{15}GO_{11}$	13.5 ± 2.6	2.5 ± 0.13	-2.5 ± 0.47	93.3 ± 0.37 [ab]
Standard aerogel	-	4.9 ± 0.18	-20.5 ± 1.07	96.2 ± 3.20

a, b homogeneous groups

The surface charge of the GEL-GO aerogels was evaluated by ζ-potential measurements (**Table 2.2**). The pH variations of the GO solutions had a significant influence on the surface charge of the aerogels (*p-value<0.05*). The oxygen-containing functional groups on the GO structure give a negative charge to the materials, and an increase of its pH allows more carboxylic and hydroxyl functional groups on its structure to be ionized, forming negatively charged radicals; as a result, the surface charge of the GO materials becomes more negative [127,128]. Conversely, the amphoteric character of the GEL modifies the ζ-potential values of these materials by a pH-effect [65,66]. As a result of the interaction between GO and GEL, the aerogels synthesized under acidic conditions have positive surface charges, whereas that aerogels developed under alkaline environments show negative surface charges. These differences can be attributed to the amphoteric property effect of the GEL on the GEL-GO aerogels. A decrease below the pI of the GEL leads to an increase of its ζ-potential, whereas that pH values above its pI leads to negative charges [65]. As a result, the combined effect of the GEL and the GO gives rise to negative and positive surface charges for the different GEL-GO aerogels. These results confirm the influence of the pH on the physical properties of these aerogels.

The apparent porosity of the GEL-GO aerogels was evaluated using the Archimedes principle (**Table 2.2**). All aerogels present apparent porosities above 85%, independent of the synthesis conditions (*p-value>0.05*). The results indicate that an increase of the GEL content slightly increases the apparent porosity of aerogels synthesized under acidic conditions. The highest porosity, around 97.7% was achieved by the $G_{15}GO_3$ aerogel. Similar behavior is observed for the aerogels developed under alkaline conditions. These results were compared to those reported by Lai *et al*. [132], who informed porosity values between 78-96% working at a GEL concentration range between 5-15% (*w/v*) for cross-linked porous GEL hydrogels. Thus, these results confirm that the porosity is a property of the materials ruled by physical interactions, as previously reported [137].

2.4.3. Swelling ratio of GEL-GO aerogels

The swelling ratio (SR) of the GEL-GO aerogels was measured in water, PBS, and anticoagulant blood at different contact times, up to 240 seconds (**Figure 2.6**). At the beginning, a high velocity of absorption is observed, until reaching equilibrium after the first 60 s (data not shown). All aerogels maintained their original shapes, and no migration of components from aerogels into liquid mediums was observed during the swelling processes.

The synthesis conditions used to produce these aerogels influenced the SR values (*p-value<0.05*). The measured SR in water was the smallest, followed by PBS, and the highest values were the measured SR in blood with anticoagulant. Among the test materials, the highest SR was found for the aerogel synthesized under alkaline conditions and with the lowest GEL:GO ratio ($G_{10}GO_{11}$), achieving SR values of 44.5 $g_{water}/g_{aerogel}$, 55 $g_{PBS}/g_{aerogel}$, and 58 $g_{blood}/g_{aerogel}$, respectively. An increase in GEL content decreases the SR values by 1.2-fold in aerogels synthesized under acidic pH and 1.4 times for aerogels synthesized under acidic and alkaline pH being in contact with water. These differences can be attributed to the fact that an increase in the polymer concentration generates an increase in the crosslink density, thus restringing the entrance of the liquids into the structure of the aerogels. In addition, all aerogels show similar SR values by contacting with PBS and anticoagulant blood. These results corroborate that the SR processes are influenced by factors such as gel composition, charge, and crosslinking density, as previously reported [134]. Therefore, the understanding of the mechanism of aerogel formation is of great interest for predicting physical properties.

The physicochemical characterization of the GEL-GO aerogels developed by MW-assisted synthesis demonstrated the influence of both synthesis conditions (GEL:GO ratio and pH of the GO solution) on the aerogels' performance. Greater activation of the functional groups of the GO sheets and the GEL chains was achieved under alkaline environments, which favored the formation of covalent interactions

between both components [127,128]. At these pH conditions, the aerogels ($G_{10}GO_{11}$ and $G_{15}GO_{11}$) show similar elastic modulus and apparent porosity values. However, their surface charges and the SR values were different, resulting in a higher SR for the aerogel developed with the lowest GEL:GO ratio at alkaline conditions ($G_{10}GO_{11}$). Considering that the SR is an important property to evaluate the material's applicability in treating different wounds, the $G_{10}GO_{11}$ aerogel was chosen to validate the use of MW as a new synthesis method to develop GEL-GO aerogels. This validation was performed by comparison of the physicochemical properties of this aerogel with those of a standard aerogel developed by the traditional process under the same synthesis conditions.

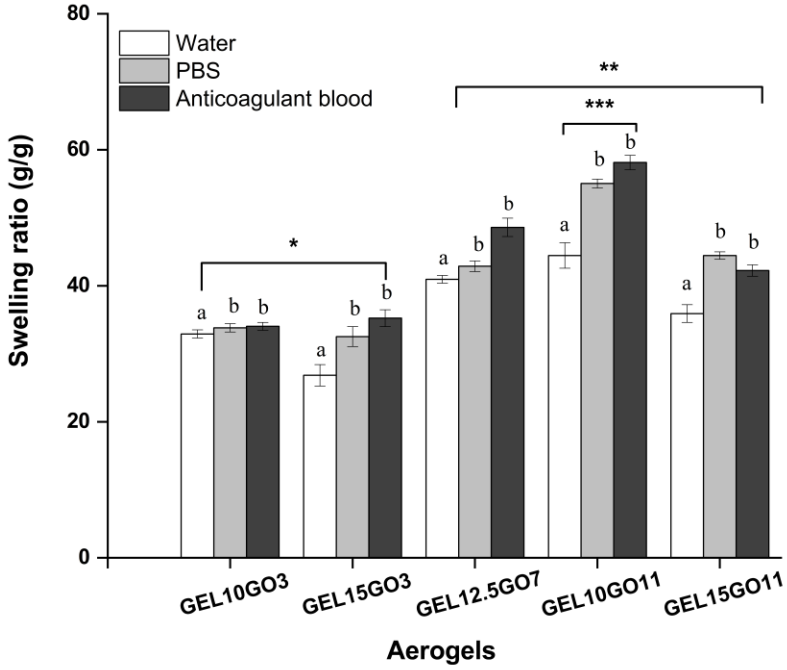

Figure 2.6. Swelling ratio values for GEL-GO aerogels at 240 *s* of contact with water, PBS, and anticoagulant blood. The values are expressed as mean ± SD (*n=3*). The * indicates significant differences between the GEL-GO aerogels (*p-value<0.05*) and the letters (a,b) indicate significant differences between the aqueous media (*p-value<0.05*).

In addition, the evaluation of the physicochemical properties of these aerogels evidenced the formation of highly porous three-dimensional structures, with the capacity to absorb up to 58 times their own weight by interacting with blood. Also, the synthesized aerogels under alkaline pH conditions showed negative surfaces charges, which suggests their affinity with blood components [14]. These results indicated that GEL-GO aerogels could be used as wound dressings to control the profuse bleeding.

2.4.4. MW-assisted synthesis validation to develop GEL-GO aerogels

MW technology is a greener synthesis method that allows an instantaneous and rapid heating at shorter reaction times, with a minimum exposure of hazardous chemicals and maximum utilization of energy [114,115,138,139]. Despite its advantages, the use of MW as *a* synthesis technology to develop GEL-GO aerogels has not been reported before. Herein, the physicochemical and mechanical properties of the $G_{10}GO_{11}$ aerogel were compared with those of a GEL-GO aerogel developed by a covalent traditional synthesis, according to the methodology proposed by Piao *et al.* [71] (described in **Appendix A.2**) to validate the MW as a new synthesis method.

It is well known that there is a strong correlation between the mechanical and physicochemical properties of these aerogels and its crosslinking process [37]. The chemical nature of both aerogels was investigated by ATR-FTIR spectroscopy (**Figure A.3**). The spectra show the functional groups of GO and GEL and similar chemical environments to those discussed in section 2.4.1. This result confirms the formation of covalent interactions in both aerogels as a consequence of the reaction between the GO carboxylic groups and the GEL amino groups. The evaluation of the measured properties in the GEL-GO aerogels show an increase in the elastic modulus and surface charge values for the standard aerogel compared to MW aerogel (**Table 2.2**). In addition, both aerogels have similar apparent porosity values over 85% (**Table 2.2**). Additionally, the SR (analyzed only in PBS medium) increased its value 1.5-fold in the MW aerogel compared to the standard aerogel (SR of 36.25 ± 3.14 $g_{PBS}/g_{aerogel}$).

The differences observed in the physical and mechanical properties of both aerogels could be caused by the synthesis method used to develop the aerogels, and even related to the synthesis process itself. Firstly, MW generates heat inside the material and then heats the entire volume [140,141], producing a deep inner heating with a homogeneous temperature to all the material compared to the conventional heat transfer mechanisms [21,49]. However, the traditional synthesis requires continuous heating at 90°C for 24h, which induces damage to the structures of the GO and GEL, causing the denaturation of the GEL chains and the GO reduction by heating, as previously reported [54,71]. Meanwhile, the MW synthesis method proposed in this study requires a total reaction time of 30 min at ~90°C, which is a feasible alternative to overcome the drawbacks above-mentioned. Therefore, the synthesis of GEL-GO aerogels with suitable and similar physicochemical properties by MW-assisted synthesis allows a reduction in the reaction time of 97% compared to the traditional processes.

2.5. Partial conclusions

- GEL-GO aerogels were successfully developed by a new synthesis method based on an MW-assisted reaction.

- The different synthesis conditions (GEL:GO ratios and pH of the GO solution) influenced the physicochemical and mechanical properties of aerogels, promoting the formation of covalent and non-covalent bonds between GEL and GO for aerogels developed under alkaline and acidic pH conditions, respectively.
- The aerogels developed under alkaline environments showed negatively charged surfaces and higher SR values than the aerogels synthesized under acidic conditions.
- The MW-assisted synthesis was validated as a new synthesis method to produce GEL-GO aerogels with suitable properties for a wide range of applications, allowing a reduction of the total reaction time of 97% compared to the traditional covalent synthesis method.
- Among the GEL-GO aerogels evaluated in this study, the material developed under alkaline conditions and with the lowest GEL:GO ratio ($G_{10}GO_{11}$) showed suitable properties for wound-dressing applications, and therefore, it was used for further studies.

Chapter 3

Evaluation of the *in vitro* hemostatic efficiency of gelatin-graphene oxide aerogels reinforced with grape skin extracts.

The information provided in this chapter is redrafted after publishing in: Improved hemocompatibility for gelatin-graphene oxide composite aerogels reinforced with proanthocyanidins for wound dressing applications. (J. Borges-Vilches, T. Figueroa, S. Guajardo, C. Aguayo, K. Fernández, Colloids and Surface B: Biointerfaces Journal 206, 2021, 111941).

3.1. Abstract

GEL-GO aerogels were synthesized by MW-assisted reactions, incorporating grape skin extracts (GSE) -high in proanthocyanidins (PAs)- to develop a hemostatic device with improved properties. The effects of incorporating PAs into the aerogels were investigated in relation to their physicochemical properties, absorption ability, clotting activity and cytotoxicity on human dermal fibroblast (HDF) cells. The aerogels showed highly resistant porous structures, capable of absorbing more than 50 times their weight when in contact with a PBS and fresh human blood. Interestingly, the PAs addition increased the negative surface charges and the blood absorption ability of the aerogels, which may make them suitable for hemostasis. The incorporation of 5% and 10% (*w/w*) of extracts into the aerogels increased the total coagulated blood content by 36.6% and 24.5% compared to GEL-GO aerogels, respectively. These improvements in the hemostatic properties of the aerogels were greater with the inclusion of 5% (*w/w*) of GSE into the aerogels. All aerogels were also able to adhere RBCs onto their surfaces, which could favor the formation of stable fibrin networks to promote hemostasis. Their clotting activity suggested the activation of alternative routes based on complement coagulation systems. Finally, the aerogels were non-toxic for HDF cells and the PAs were successfully released from their matrices. Therefore, GEL-GO aerogels loaded with PAs are promising as topical phytodrug delivery systems, with great potential as wound-dressing materials in hemostatic applications.

3.2. Introduction

One of the current challenges in modern medicine is the development of effective functional devices that act as promoters of hemostasis [142]. The most commonly used include organic and inorganic materials, as well as their composites [5,9,13,143]. The hemostatic potential of these materials is based on their capacity to quickly control blood loss, minimize collateral damage, be biocompatible,

biodegradable, non-toxic, and inexpensive [2,10]. Up to now, structures such as films, microspheres, foams, 3D porous scaffolds, fibers, hydrogels, and aerogels have been used as hemostatic platforms. We are particularly interested in aerogels, based on their physicochemical properties and their potential hemostatic applications.

Aerogels are highly porous materials, with low density, high specific surface areas, and micro and mesoporous structures [21,22]. Their ability to absorb liquids such as blood plasma makes them suitable for hemostatic applications [13]. Several materials have been used to develop these aerogels, among them being graphene-derived materials, in particular graphene oxide (GO). GO is a biocompatible and hydrophilic material widely used as a hemostatic device with great potential for the treatment of traumas [5,9,14,108]. Despite this, its cytotoxic effects and high hemolysis rate have limited its use in medical applications [1]. These disadvantages have been overcome by crosslinking or combining it with biocompatible polymers such as GEL.

GEL is a natural polymer derived from collagen that has been considered as a promising biomaterial due to its useful properties such as its capacity for potential modifications [31], amphoteric character, good affinity with proteins, biocompatible and biodegradable characteristics, and non-toxic effects [31]. Its crosslinking with GO has allowed the formation of composite materials with high structural stability for biomedical applications [37,38,71,144].

One of the most important properties of these materials to be used as hemostatic devices is the capacity for interfacial stimulation. GO-derived materials have demonstrated their capacity to activate platelets and then elicit their strong aggregate response due to the oxygenated-functional groups in their structure [12]. However, this hemostatic function of GO could be inhibited by the loss of its oxygen-containing groups [13,14]. In order to overcome this drawback, the use of natural crosslinking agents may be an effective strategy to incorporate new functionalities into these matrices. To this purpose, this study proposes the incorporation of GSE- high in PAs- into the GEL-GO composite aerogels. These extracts are obtained from the skin and seed of grapes, other fruits, and vegetables. They are polyphenolic compounds of high molecular weight (over 500 Da) formed by flavan-3-ols subunits whose chemical structure is composed by hydroxyl groups attached to a benzene ring, which provides negative surface charges to these materials [80]. Its antioxidants, antimicrobial, anti-inflammatory, and cardioprotective properties, as well as its high PAs content support the therapeutic use of this natural compound [78,145].

Therefore, this study aims to develop GEL-GO aerogels loaded with different GSE concentrations (5% and 10% *w/w*) to produce a new hemostatic device with improved hemostatic properties. The

effects of incorporating GSE into aerogels were thoroughly investigated in relation to physicochemical properties, absorption ability, clotting activity and cytotoxicity on HDF cells. The PAs' kinetic release from the aerogels was also evaluated.

3.3. Materials and Methods

3.3.1. Materials

The chemical reagents used in the GO and the aerogel syntheses were mentioned in section 2.3.1. Gelatin type B was purchased from Sigma-Aldrich Company, (St. Louis, MO). In addition, the glutaraldehyde ($C_5H_8O_2$,10%), acetone (C_3H_6O), and n-hexane (C_6H_{14}) were purchased from Merck (Darmstadt, Germany). These reagents were received and used without further purification. Other reagents such as dimethyl sulfoxide (DMSO), Dulbecco's modified Eagles medium (DMEM), 3-(4,5-dimethylthiazol-2-yl)-2,5-diphenyltetrazolium bromide (MTT) reagent, and fetal bovine serum (FBS) were purchased from Sigma Aldrich (Saint Louis, USA). The *País* grapes were collected from Quillón Valley, Bio Bio Region, Chile, and were preserved in sealed bags and frozen at -18°C. Fresh human blood was extracted from healthy volunteers, and the standard medical gauze sponges (hydrophilic, 100% cotton, aseptic, and sterile) were purchased from a commercial pharmacy. HDF cells were purchased from Sigma-Aldrich Company. Milli-Q® and distilled water were used throughout the investigation.

3.3.2. Production of *País* grape skin extracts

Natural extracts rich in PAs were extracted from the skin of *País* grapes, as described by Morales *et al.* [146]. For that purpose, the skin of 200 grapes was separated manually. The extraction was carried out in Erlenmeyer flasks of 500 mL with 250 mL of an acetone/water 2:1 (*v/v*) mixture. The mixtures were stirred for 15h at room temperature in a dark room to avoid oxidation, using a gyratory shaker (New Brunswick Scientific Co. Edison, United States). Then, the samples were vacuum filtered to recuperate the extracts, and the acetone contained was eliminated in a rotary evaporator (Bibby Sterilin Ltd., RE-100B, STONE Staffordshire, England) at reduced pressure and temperature (<35°C) until 50 mL of skin extract was obtained. The liposoluble components of the grape extracts were removed in three washing steps with 50 mL of n-hexane.

The raw extracts were purified according to the size exclusion chromatography column using Toyopearl HW-40F resin packed in an Omnifit column (420 Å~ 35 mm, 7.0 mL/min), for which the column was equilibrated with an ethanol/water mixture (55:45 *v/v*) to remove the sugars and phenolic acids present in the skin extracts. Then, the PA fraction was eluted with an acetone/water (60:40 *v/v*) mixture, and the acetone was eliminated in a rotary evaporator at reduced pressure and temperature

(one column volume). Finally, the GSE were lyophilized (Labconco freeze-dry system, Germany) for 72h and stored at 4°C.

The PAs contained in the GSE were characterized by total phenol content according to the Folin-Ciocalteu method [24]. The degree of polymerization (mDP), average molecular weight (aMW), and molar composition of these extracts were determined by HPLC detection, based on the acid-catalyzed depolymerization method (phloroglucinolysis) [25]. Their molecular weight distribution was determined by gel permeation chromatography (GPC) [25] and their functional groups were investigated by Fourier transform infrared spectroscopy (FTIR). The details of the procedures followed for these characterizations are given in **Appendix B.1**.

3.3.3. Aerogel synthesis

A GEL-GO aerogel was developed by MW-assisted synthesis at pH~11 of the GO solution and 10:1 in the GEL:GO ratio according to protocol described in section 2.3.3. After the MW reactions, the GEL-GO solution obtained was cooled up to 30°C. For the preparation of GSE-loaded aerogels, different GSE concentrations (5% and 10% *w/w*) were separately loaded into the GEL-GO solution. The solution was stirred at room temperature until homogenization. The final mixtures were poured into Petri dishes for crosslinking for 12h, followed by freezing to -86°C and lyophilization to form the aerogels. Hereafter, the aerogels will be identified as GEL-GO, GEL-GO-5%, and GEL-GO-10%, respectively.

3.3.4. Physicochemical characterization of aerogels

The chemical nature, structure, morphology, and mechanical properties of the aerogels were investigated by XRD, ATR-FTIR, Raman analysis, TGA, SEM, compression test, and surface charge measurements. These measurements were performed following the description given in **Appendix A.1**. The apparent porosity of the aerogels was measured according to procedure described in section 2.3.5. The carbon and oxygen contents of each aerogel were determined through elemental analysis. The absorption capacity of aerogels was also measured as described in **Appendix B.1**.

3.3.5. *In vitro* dynamic whole-blood clotting

The coagulation capacity of the aerogels was evaluated by coagulation time assays using human whole blood, according to reported methodologies [5,13]. The test was carried out in 24-well plates of equal size. Five test groups of equal size (1.0 cm^3), including GEL-GO, GEL-GO-5%, and GEL-GO-10% aerogels, a standard medical gauze sponge, and a human fresh blood sample were evaluated. A total volume of 500 µL of human whole blood was dropped directly into each test group for contact times of 30, 60, 120, and 240 seconds. After each reaction time, 10 mL of distilled water were added to stop the reaction and dissolve the uncoagulated RBCs. The hemoglobin content of the supernatant

was quantified by UV spectroscopy (Spectroquant Prove 600; Merck, Germany) at 540 nm. The hemoglobin content was calculated using **Equation 3.1**:

$$Hemoglobin\ content\ (\%) = \frac{I_s}{I_r} * 100 \quad (3.1)$$

where *Is* is the absorbance of the resulting samples and *Ir* is the reference absorbance (human fresh blood).

3.3.6. Blood cell adhesion onto aerogel surfaces

The blood cell retention in the aerogel matrices was investigated by SEM images. Human whole blood (50 µL) was added to the aerogel samples of 1.0 cm^3 and incubated for 5 min at 37°C [13,14]. Then, the samples were gently rinsed with a PBS (10×; pH=7.4) and immobilized with glutaraldehyde at 4°C for 2h. Blood cells were dehydrated with 50%, 60%, 70%, 80%, and 90% of ethanol for 15 min and freeze-drying for 12h before the SEM observation. The images were recorded at different resolutions using a SEM microscope (JEOL JSM-6380LV, Japan).

3.3.7. Clotting activity of aerogels

The clotting activity of the aerogels was evaluated by determinations of activated partial thromboplastin time (aPTT), prothrombin time (PT) and soluble P-selectin levels in the plasma. These determinations were done following the methodology previously described by Liu *et al.* [147] with slight modifications. In brief, fresh human blood was centrifuged for 10 min at 3000G to obtain the platelet-poor plasma (PPP). Thereafter, 500 µL volume of the PPP was added to each aerogel sample (1.0 cm^3) and incubated at 37°C for 30 min. For the aPTT measurement, 100 µL of PPP were mixed with 100 µL of aPTT reagent and incubated at 37°C for 3 min. Following incubation, 100 µL of aqueous $CaCl_2$ (0.03 M) were added to the mixture, and the coagulation time was measured in an automated blood coagulation analyzer (Rayto RT-2204C, China). Using the same method, 100 µL of PT reagent were added to 200 µL of PPP in a test tube and then the PT was evaluated in the same instrument.

The activation of platelets adhered to the aerogels was evaluated by measuring the soluble P-selectin levels in the blood plasma. For this purpose, fresh human blood was centrifugated at 2000G for 10 min to obtain the platelet-rich plasma (PRP). A 200 µL volume of PRP was added to each aerogel sample and incubated at 37°C for 30 min under static conditions. The concentration of soluble P-selectin in the plasma was quantified using an ELISA kit (Thermo Fisher, USA) as indicated by the manufacturer. Each experiment was repeated in quadruplicate with reproducible results.

3.3.8. *In vitro* cytotoxicity of aerogels

The *in vitro* cytotoxicity of each aerogel and their component materials was evaluated on HDF cells through determinations of the cell viability (*c.v.*). DMEM (1 mL) was added to 10 mg of each material and incubated for 24 h at 37°C. The supernatants were recovered and used as a complete medium by mixing with 2% (*v/v*) FBS, 1% (*v/v*) antibiotics (100 units/mL of penicillin and 100 units/mL of streptomycin) and 1% of amphotericin to avoid fungal proliferation in the cells. Subsequently, the supernatants were added to HDFs (10^4 cells/mL) in 96-well plates and were incubated for 48h at 37°C in a humidified air condition of 5% (*v/v*) of CO_2. The cells were washed with PBS (pH=7.4), and the supernatant was removed. Then, 100 µL of fresh DMEM was added to HDFs and 5 mg/mL of MTT solution was used as the test kit. To do this, the HDFs were incubated for 4 h at 37°C with CO_2, followed by removal of 85 µL of medium and the addition of 50 µL of DMSO for 10 min. Finally, the cell viability was calculated according to **Equation 3.2:**

$$c.v.(\%) = \left({Abs_{540\ test}}/{Abs_{540\ control}}\right) * 100 \quad (3.2)$$

where *Abs* indicates the absorbance measured at 540 nm by UV-vis spectrometry (Spectroquant® Prove 600 spectrometer, Merck KGaA, Germany). The controls used in this assay were HDFs without material (positive control) and the GO (10 mg/mL) in contact with the HDFs cells was used as negative control. These assays were repeated six times with reproducible results.

3.3.9. *In vitro* PA kinetic release assay

The *in vitro* release kinetics of PAs were evaluated in PBS (pH=7.4, 37°C), which simulates blood plasma conditions. Aerogel samples of equal size and weight were used in this assay, and two PBS media with 250 mL each were prepared. One of them was used as a release medium and the second one as a fresh replacement medium to ensure a constant volume during the assay. The aerogel samples were immersed in PBS solution and capped with parafilm to avoid fluid evaporation. Solutions of 1.5 mL were extracted at different time intervals. After each extraction, the extracted volume was returned with fresh PBS solution. The release amounts *Qd (t)* were quantified based on determinations of total phenol content according to the Folin-Ciocalteu method described in **Appendix B.1**. For this purpose, the absorbances were measured by UV-vis spectroscopy at 765 nm (Spectroquant Prove 600 spectrometer; Merck, Germany) and *Qd (t)* was calculated using **Equation 3.3:**

$$Q_d\ (t) = \frac{Abs_{measured} - A_o}{Abs_{max}} \quad (3.3)$$

A blank absorbance (A_o) and the maximum absorbance (Abs_{max}) equivalent to the pure extract content incorporated in aerogel were also considered. This assay was performed in triplicate with reproducible results.

3.3.10. Statistical analysis

Data were processed using OriginPro8.5® software and the statistical analyses were done by ANOVA test and Duncan´s test using Statgraphics Centurion XVII® software. The level of significance was determined as *p-value<0.05*. ImageJ® software was used to measure the pore size of the aerogels. The mean values and the error bars are reported in each figure.

3.4. Results and Discussion

3.4.1. Physicochemical characterization of GO, GEL, GSE, and aerogels

The oxidation degree of GO and crystalline nature of GEL and aerogels were studied by XRD (**Figure 3.1a**). The XRD patterns of the GEL and GO were similar to those observed in **Figure 2.1a**, and their explanation was given in section 2.4.1. For the aerogels, similar patterns to the GEL were observed, but with wider and less pronounced peaks. This may be due to high GEL content in their structures, thus indicating a lower crystallinity and greater structural disorder in the aerogels compared to their pure components. This behavior was not modified with the inclusion of GSE.

ATR-FTIR spectroscopy was used to investigate the functional groups of the GEL, GO, and aerogels (**Figure 3.1b**). As discussed in section 2.4.1, the GO and GEL showed their characteristic functional groups, and as a consequence of their crosslinking, the covalent bond formation for aerogels under alkaline conditions and with the lowest GEL:GO ratio was suggested. When the system moves away from the pI of the GEL (pI~5) and the GO (pI~2) a greater activation of their functional groups occurs [30–32], thus causing changes in the absorbance bands. These findings have been reported by other authors for composite materials of GO and GEL [16,17].

The functional groups of the GSE were studied by FTIR as shown in **Figure B.1**. The characteristic bands of aromatic C-H extensions of aromatic rings out-of-plane bend (700-880 cm^{-1}) and in-plane bend at (950-1200 cm^{-1}), as well as bands of C-O stretch from pyran-derived ring structure (1200-1280 cm^{-1}), C=C-C aromatic ring stretch (1400-1520 cm^{-1} and 1604-1612 cm^{-1}) and hydroxyl groups -OH (3200-3400 cm^{-1}) were identified [148]. These results confirm the presence of phenolic compounds in the chemical structure of the GSE, further suggesting the formation of noncovalent bonds with the GEL-GO matrix. These interactions are due to the ability of the phenolic compounds to act as hydrogen-bond donors, forming strong bonds with molecules such as GEL [34–36].

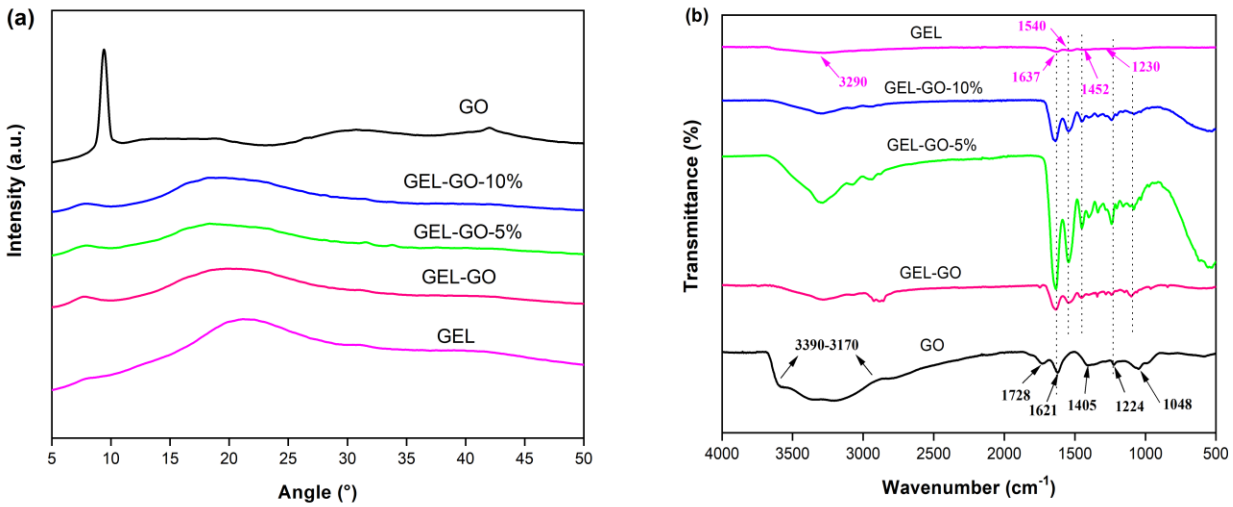

Figure 3.1. (a) XRD patterns and (b) FTIR spectra for GO, GEL and aerogels.

País grape skin extracts were also characterized by the type of flavan-3-ols subunits, aMW, mDP, molecular weight distribution, and total phenol content. **Table B.1** lists the structural composition of the GSE, in which were identified seven different phenolic compounds, with a predominance of epicatechin gallate-phloroglucinol (EC-P) and epigallocatechin- phloroglucinol (EGC-P). In addition, the mDP and aMW values were 25.5 ± 0.8 (dimensionless) and 7565 ± 221 (molecular weight units), respectively. These GSE had a molecular weight distribution from 451-25807 g/mol (**Table B.2**) and a total phenol content of 0.62 ± 0.15 (g equivalent gallic acid/g extract, for 1g/L of solution). These characterizations together with FTIR analysis confirm the functional groups and chemical features of the GSE, showing them to be complex and large molecules with the ability to interact physically with GEL-GO matrices once incorporated.

Figure 3.2a shows the Raman spectra of the aerogels in the spectral region between 1000 - 1800 cm^{-1}. Two characteristic bands of graphitic materials were identified in these spectra. A D band at ~1350 cm^{-1} was associated with structural disorders and defects in the graphitic materials (sp^3 diamond-like carbons) and the G band at ~1600 cm^{-1} due to the in-phase vibration of the graphite lattice [17,37–39]. Similarly, both bands were identified in the GO spectrum (**Figure B.2**), and additionally, a 2D region between 2475-3000 cm^{-1}, which is related to the number of layers of the material [38], was observed. In addition, the inclusion of GSE did not cause modifications in the Raman patterns of the aerogels.

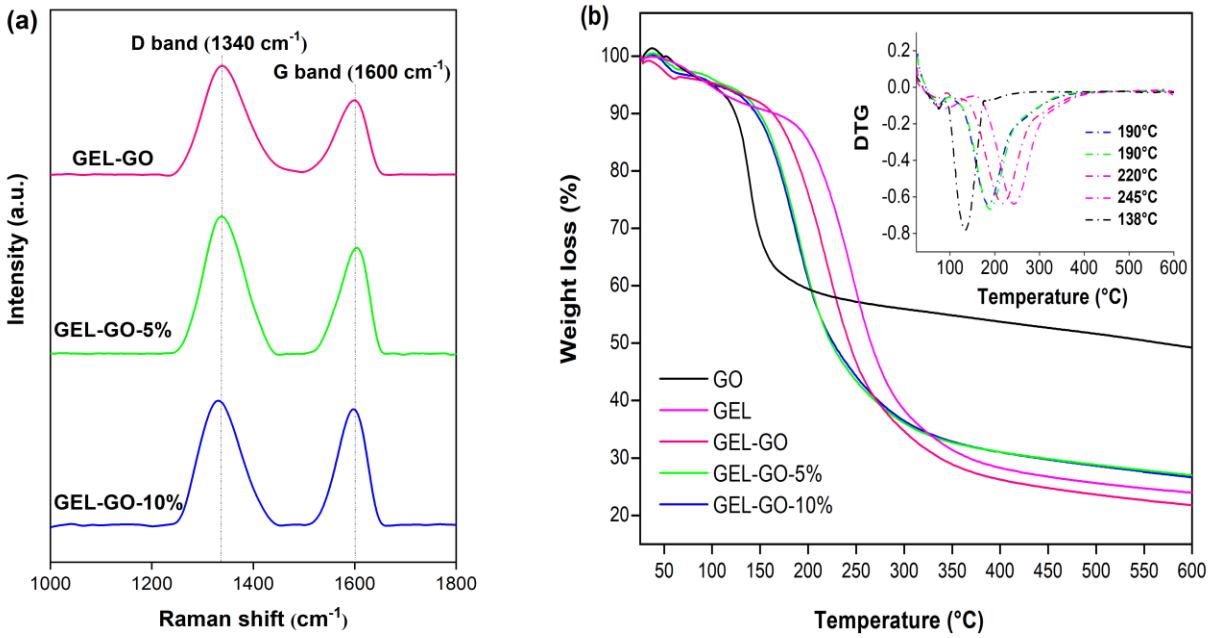

Figure 3.2. (a) Raman spectra of the aerogels and (b) TGA and DTG curves for GO, GEL, and aerogels.

The thermal stability of the aerogels and their component materials was analyzed by TGA (**Figure 3.2b**). The weight losses associated with the GO and GEL were previously discussed in section 2.4.1. For the GEL-GO aerogel, the TGA curve show a weight loss of ~50% at 220°C, achieving a total loss of 80% at the end of the analysis. The TGA curves for both GEL-GO aerogels loaded with PAs were similar to those of the GEL-GO aerogel, displaying a mass loss of 48% at ~190°C and reaching a total weight loss of 75% at 600°C. These results indicate that GSE incorporation into GEL-GO matrices improved the thermal stability of the aerogels, which could be attributed to an increase in the oxygenated functional group content in these matrices when the GSE were added.

The changes in the chemical composition of the aerogels were determined by elemental analysis (**Figure 3.3a**). The carbon content of the aerogels decreased with the addition of GSE, with values of 45.38%, 43.55%, and 42.16% for the GEL-GO, GEL-GO-5%, and GEL-GO-10% aerogels, respectively. Meanwhile, the oxygen content increased from GEL-GO (34.95%) to GEL-GO-5% and GEL-GO-10% aerogels (35.31% and 37.56%, respectively). Thus, the C/O ratio for GEL-GO was 1.3 whereas for GEL-GO-5% and GEL-GO-10% it was 1.2 and 1.1, respectively. This indicates that the inclusion of GSE provided a higher content of oxygenated functional groups in these matrices due to its chemical structure. This is in accordance with the surface charge measurements shown below.

The surface charge of GO, GSE, and aerogels were determined through ζ-potential measurements, as shown in **Figure 3.3b**. As demonstrated in section 2.4.2, the GO has a negative surface charge due to its oxygen-containing functional groups [5,127,128]. In comparison with GO, the negative charge of the GEL-GO aerogel significantly decreased. This fact is mainly due to the amphoteric character of the GEL and its high content (90% *w/w*) incorporated into the aerogel matrix. It is known that the ζ-potential of the materials is modified by the pH-effect [65,66], and, in this case, the GEL provides a negative surface charge to the material surfaces in pH conditions above its pI (pI~5). Moreover, the ζ-potential of GSE was -31.1 ± 2.7 mV, the negative character being due to the oxygenated groups present in its chemical structure. The incorporation of GSE into GEL-GO matrices allowed a lower decrease in the ζ-potential values for the aerogels compared to the GEL-GO aerogel. Although the ζ-potential values of this study are lower than those reported by other authors for graphene-based aerogels for hemostatic applications [5,12,19], the negative surface charge densities obtained suggest a good affinity of these aerogels with blood components, as previously reported [9,13,14].

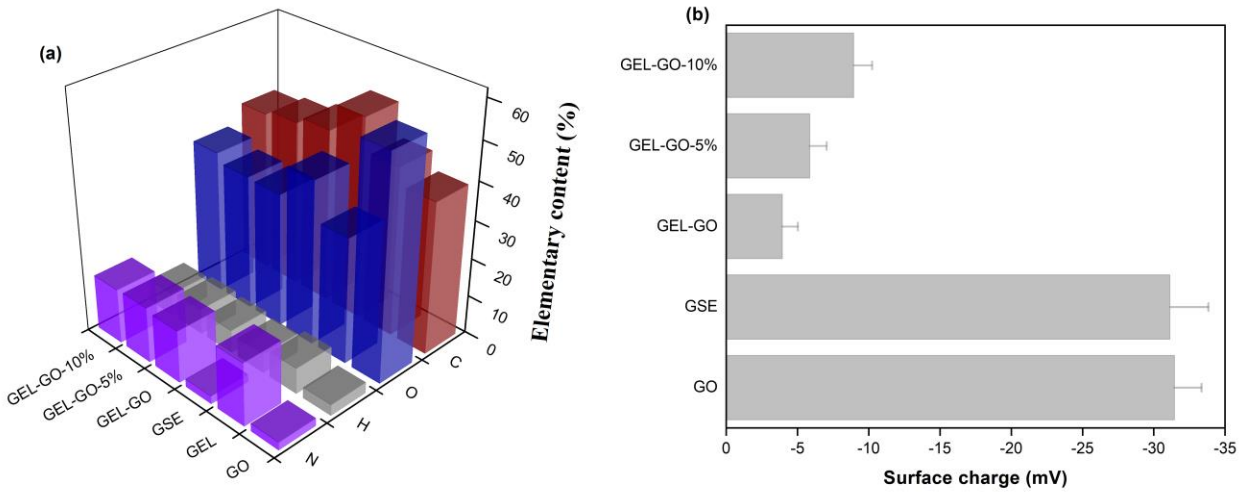

Figure 3.3. (a) Elemental analysis and (b) Surface charge values for GO, GSE, and aerogels.

The morphology of the aerogels was investigated by SEM images (**Figure 3.4**). Heterogeneous porous structures with interconnected networks of different shapes and pore sizes were observed for all aerogels. Their pore size values and distributions are presented in **Table 3.1** and **Figure B.3**, respectively. No statistical differences were observed between the pore sizes for aerogels (*p-value>0.05*), which may be due to the low percentages of GSE added to the aerogels.

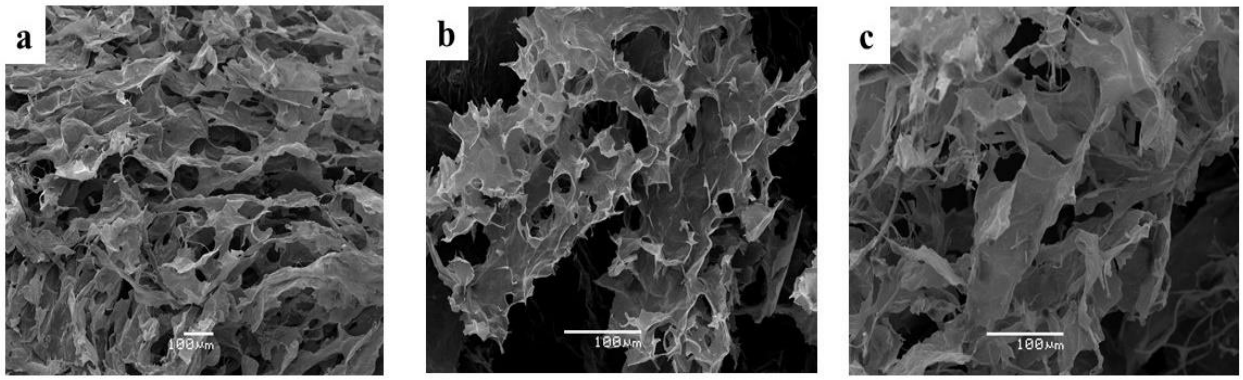

Figure 3.4. SEM images of the micromorphology of the aerogels (a) GEL-GO aerogel, (b) GEL-GO-5% aerogel, (c) GEL-GO-10% aerogel.

Table 3.1. Values of pore size, apparent porosity, absorption capacity, and elastic modulus for the aerogels.

Aerogels	Pore size (μm)	Apparent porosity (%)	Absorption capacity (g/g)		Elastic modulus (kPa)
			PBS	Blood	
GEL-GO	25.0 ± 1.9 [a]	91.8 ± 1.4 [b]	54.6 ± 3.4 [c]	52.8 ± 2.1 [d]	2.52 ± 0.6 [f]
GEL-GO-5%	24.9 ± 1.6 [a]	91.3 ± 1.2 [b]	55.4 ± 2.6 [c]	64.7 ± 4.7 [e]	2.84 ± 0.3 [f]
GEL-GO-10%	24.7 ± 1.8 [a]	90.5 ± 1.6 [b]	58.2 ± 1.1 [c]	63.2 ± 2.3 [e]	3.18 ± 1.1 [f]

The letters a,b,c,d,e and f indicate significant statistical differences for p-value<0.05.

The porosity, liquid absorption capacity, and good mechanical properties are critical for materials in wound dressing applications. They must be able to absorb large amounts of wound exudates while maintaining their integrity during use. These properties were evaluated for aerogels and the results are presented in **Table 3.1**. All the composites had apparent porosity values above 90%, which is in concordance with their porous structures observed by SEM images. The elastic modulus of each aerogel were also determined through the stress-strain curves (**Figure B.4**). The results showed no significant differences between the aerogel samples (*p-value>0.05*), indicating that the GSE amount added did not change the mechanical resistance of these materials.

The absorption ability of these aerogels was also measured in PBS (pH=7.4, 37°C) and fresh human blood (**Table 3.1**). The aerogels were able to absorb more than 50 times their weight when in contact with either of the aqueous media, showing an increase of 18% in the blood absorption with the addition of PAs (*p-value<0.05*). This behavior is in agreement with the ζ-potential values presented above, since a higher negative surface charge promotes the adsorption and activation of plasmatic proteins and

enhances the Vroman effect [94]. In turn, both effects accelerate the activation of the blood coagulation cascade.

3.4.2. *In vitro* dynamic whole-blood clotting

The hemostatic potential of the aerogels was evaluated by a dynamic whole-blood clotting test. **Figure 3.5** shows the hemoglobin content values expressed as free RBC amounts for each aerogel and also for fresh human blood and sterilized gauze used as controls. The results evidenced that the blood coagulated in the first 30 s of contact with the aerogels. Also, the inclusion of PAs into aerogels increased the total coagulated blood content by 36.6% and 24.5% for GEL-GO-5% and GEL-GO-10% aerogels, respectively. An increase in the GSE content of the aerogel did not improve the blood clotting process, the GEL-GO-5% aerogel being the one with the highest clotting performance. This may be due to the fact that a higher GSE content in the aerogel increases its crosslinking density, which makes the passage of liquids inside the matrix difficult. These findings demonstrate that loaded GSE- aerogels have a high and rapid capacity to generate blood clots, which favor the hemostatic processes.

Similar findings have been reported for other authors for GO-based aerogels with hemostatic applications. Mellado *et al.* [5] demonstrated that GO aerogels reinforced with PVA and *País* grape skin extracts (GO-PVA-SK) increased their blood coagulation time by 37% compared with GO-PVA aerogel. Similarly, Liu *et al.* [12] showed that crosslinked GO sponges with polydopamine were able to stop bleeding 96 s and 165 s faster than a crosslinked GO sponge and un-crosslinked GO aerogel, respectively. In another studies, Li *et al.* [9] and Quan *et al.* [14] evaluated the hemostatic potential of GO sponges with added thrombin or added diaminopropionic acid, respectively. They demonstrated that incorporating these materials in GO sponges increased the blood absorption capacity and improved the material/blood interactions, thus favoring hemostasis. These studies coincide in the use of molecules whose chemical functionalities and bioactive properties increase blood absorption capacity and decrease hemostatic times in GO-based materials. Taking into consideration this evidence, we suggest that the inclusion of GSE into GEL-GO matrices will favor such processes.

3.4.3. Blood cell adhesion on aerogel surfaces

The adhesion of blood cell components on the aerogel surfaces was investigated using SEM images (**Figure 3.6**). RBCs were adhered to the surfaces of all aerogels, arranged as aggregates. These RBCs maintained their original morphology in all composites, which could help to form stable fibrin networks on aerogel surfaces and favor hemostasis. Other authors have observed this phenomenon in GO-based materials [12–14], which may be due to the strong thrombus-inducing property of the GO and its affinity with plasmatic proteins, mainly fibrinogen, which is the major protein responsible for platelet

adhesion [92,101,149]. In addition, no evident changes were observed on the aerogel surfaces with the inclusion of PAs. Although platelet adhesion was not observed during aerogel mapping, its activation can occur without it being adhered to the material surface [150]. To understand whether aerogels activate the coagulation cascade, these results were complemented by studies of the clotting activity.

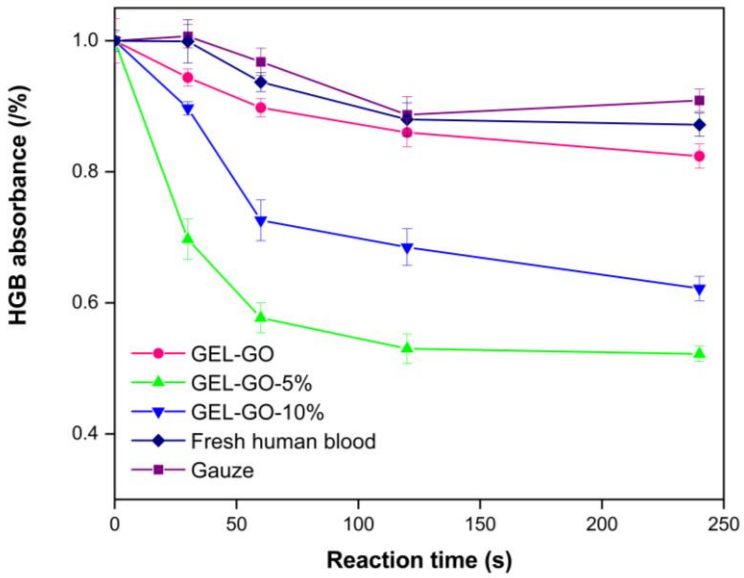

Figure 3.5. *In vitro* dynamic whole-blood evaluation for the synthesized aerogels. Standard gauze and fresh human blood are used as controls in this test. The values correspond to mean ± SD (*n=3*).

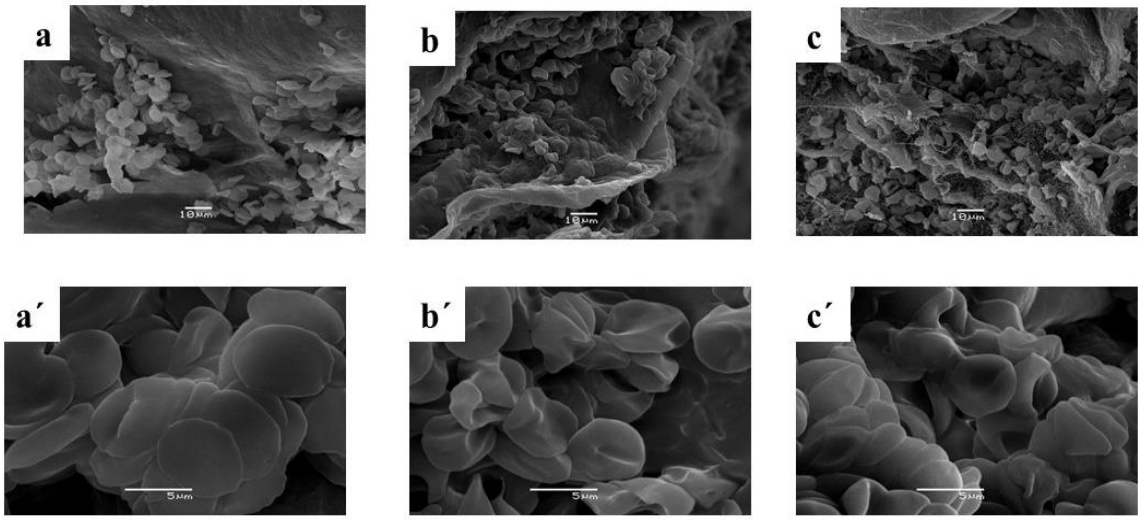

Figure 3.6. SEM images of blood cell adhesion on aerogel surfaces (a and a´) GEL-GO aerogel, (b and b´) GEL-GO-5% aerogel, and (c and c´) GEL-GO-10% aerogel.

3.4.4. Clotting activity of aerogels

Biomaterial surfaces directly influence the blood coagulation processes by modifying protein function after adsorption, as well as through the affinity with RBCs and other blood cell components on their surfaces [19,94]. These processes belong to an initiation pathway of the coagulation cascade that eventually leads to the thrombin formation [151] and involves intrinsic, extrinsic, and common coagulation paths that allow the promotion of hemostasis through different coagulation routes [147].

Therefore, the clotting activity of the aerogels was evaluated by measuring aPTT, PT, and soluble P-selectin levels in the plasma. **Table 3.2** lists the values of each clotting parameter evaluated in the aerogels, also including the values for a standard medical gauze and blood plasma used as control groups. In comparison with both control groups, the aerogels showed no statistically significant difference in the aPTT values and therefore they did not activate coagulation through the intrinsic route. The PT values of the aerogels decreased compared to both controls, being lower in the aerogels with GSE added. These results suggest that these composites did not accelerate the coagulation by the extrinsic pathway. Additionally, the soluble P-selectin levels decreased up to 4-fold in the aerogels compared to the blood plasma control, this decrease being more accentuated with the inclusion of GSE in these matrices. The sharp reduction observed in soluble P-selectin levels suggests that the aerogel´s surfaces generated inhibition of plasmatic proteins on platelets, which could be due to the formation of platelet-blood component aggregates that may suppress the levels of detected P-selectin.

Table 3.2. Values of aPTT, PT, and soluble P-selectin levels for aerogels.

Samples	aPTT (s)	PT (s)	P-selectin level (ng/mL)
GEL-GO	33.25 ± 0.75 [a]	13.24 ± 0.75 [b]	124.64 ± 3.24 [e]
GEL-GO-5%	33.87 ± 0.40 [a]	13.08 ± 0.21 [b]	92.39 ± 1.91 [f]
GEL-GO-10%	32.13 ± 1.36 [a]	12.0 ± 0.15 [c]	53.47 ± 4.28 [g]
Blood plasma	35.30 ± 1.08 [a]	13.75 ± 0.46 [bd]	216.52 ± 2.02 [h]
Gauze	33.25 ± 0.75 [a]	14.43 ± 0.49 [d]	167.39 ± 3.81 [i]

The letters a, b, c, d, e, f, g, h, and i mean significant statistical differences for p-value<0.05.

Rapid adsorption of plasma proteins onto artificial surfaces is the initiating event in thrombus formation, which is particularly evident on negatively charged hydrophilic surfaces [92]. This phenomenon allows the deposition of fibrinogen on the material´s surfaces, thus triggering the activation of platelets and factors that promote coagulation [15,92,150]. According to this study´s

results, none of the synthesized aerogels were able to promote the coagulation cascade through extrinsic or intrinsic pathways. However, it is possible to hypothesize that they promote alternative coagulation routes based on complement systems, which allow the release of reactive fragments and proteins that promote coagulation. This hypothesis is supported by the fact that the alternative coagulation pathways are relevant for surfaces with hydrophilic and amine groups -such as GEL- capable of forming covalent bonds with complement proteins such as C3b [150].

It is interesting to note that several factors are involved in the hemocompatibility of biomaterials, such as surface characteristics, hydrophilic and/or hydrophobic nature, charge surfaces of the materials, and protein adsorption during the initial response to material-blood contact [151]. This is a complex process and the combined roles of coagulation and complement activation in blood compatibility have not been well investigated [94]. Thus, further assays are needed to evaluate the contribution of the different blood components to the clotting activity of these aerogels.

3.4.5. *In vitro* cytotoxicity assay

HDF cells were used to evaluate the *in vitro* cytotoxicity of GO, GEL, GSE, and aerogels. GO and HDF cells without aerogels were used as negative and positive controls in this assay, respectively. **Figure 3.7** shows the cell viability values obtained for each material and control groups. GO showed slight toxic effects (cell viability less than 80%) at the study concentration. On the contrary, the GEL induced cell proliferation on HDFs (cell viability greater than 100%) due to the presence of collagen in its structure, which acts as a potent protagonist of fibroblast survival, migration, and metabolism [33]. The GSE had a cell viability of 94.2 ± 10.8%, indicating their non-cytotoxic effects on HDF cells. This behavior has been associated with the presence of PAs in these extracts, which help to improve the activity of fibroblast cells [41]. The cell viability values for all the aerogels were above 80%, indicating their non-toxic effects on HDF cells. In addition, the loaded GSE-aerogels showed statistically significant differences compared to the GEL-GO aerogel that could be attributed to the presence of PAs as explained above. Thus, these findings suggest the promising effect of PAs loaded on GEL-GO aerogels on the growth of fibroblast cells and demonstrate that the functionalization of graphitic materials with other molecules, mainly polymers, decreases the toxic effects of these materials, which has been described in the literature [26,43,54].

3.4.6. *In vitro* PA release from aerogels

Aerogel-based biomaterials are considered promising candidates for drug loading and delivery due to their porous structures with high surface areas. They can increase the bioavailability of poorly soluble drugs and improve both the stability and release kinetics of drugs due to their surface areas [19,41]. In

this regard, the *in vitro* release of PAs from GEL-GO aerogels was studied, using PBS (pH=7.4, 37°C) at physiological conditions to simulate the wound environment as release medium. The release profiles over time for the aerogels to both PA concentrations are shown in **Figure 3.8**. Herein, two phases can be well established: an initial step where there was a quick release of PAs in the first 10 min of the assay, and the second one where the extract release was slow until a plateau was achieved at 60 min. At this time, both aerogels reached their highest release percentages, being 7.5% and 16.6% for GEL-GO-5% and GEL-GO-10% aerogels, respectively. These percentages coincided with those calculated from the phenol content loaded in each aerogel (**Table B.3**), showing that the amount of PA released from the aerogels was proportional to the extract contained in the GEL-GO matrices. The maximum amounts of extract released were similar to those reported by Mellado *et al.* [5] for GO-PVA aerogels loaded with grape skin and seed extracts, achieving release percentages of 14% and 20%, respectively. Similarly, Figueroa *et al.* [15] reported that maximum release percentages of PAs loaded into GO-CS aerogels were between 14% and 24%. In this context, it is worth mentioning that the drug release processes are influenced by several variables such as the physicochemical properties of GO, including its size, shape, and oxidation levels, as well as experimental conditions to perform the loading and/or release of compounds, among others [5,145]. Taking into consideration these factors, in addition to the high affinity of polyphenolic compounds with molecules such as GEL [85,90], it is possible to understand the lower percentages of released PAs from the aerogels.

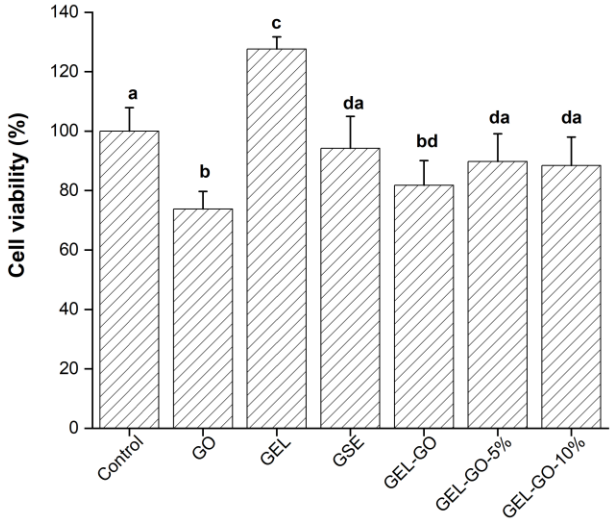

Figure 3.7. Cell viability values for GO, GEL, GSE, and aerogels evaluated HDF cells. GO and HDF cells without aerogels were used as negative and positive controls in this assay, respectively. Data correspond to mean ± SD (*n=7, p-value<0.05*).

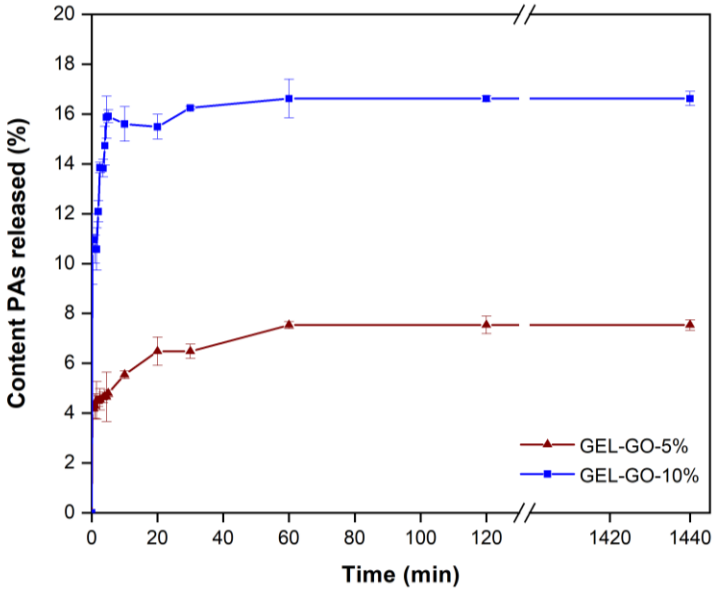

Figure 3.8. *In vitro* release profiles of PAs from GEL-GO aerogels at different times.

Aerogel-based biomaterials for wound dressings are expected to absorb exudate and toxic substances, allow gas exchange, and prevent the invasion of microorganisms [19]. Their highly porous structures with large surface areas make them capable of absorbing a large quantity of aqueous fluids and of providing an adequate moisture balance and pH in the wound site. Traditional materials such as standard medical gauzes and cotton do not actively participate in the wound healing processes and tend to become attached to the wound scab, thus weakening their hemostatic efficiency [7]. In addition, advanced materials have advantages that foment improvements in their hemostatic performance and minimize their shortcomings in wound dressing applications. These materials are designed to have biological activity on their own or to include compounds with bioactive properties that help to promote hemostasis. In this regard, polyphenol compounds have shown beneficial effects on health, with physiological properties [5,41,78] and wound healing activities [5,40] that favor the hemostatic processes. Also, they contribute to decreasing the pH in wounds, which favors healing [50]. Thus, their incorporation into GEL-GO aerogels could lead to the development of aerogels with improved hemostatic properties.

3.5. Partial conclusions

- GEL-GO aerogels loaded with different GSE concentrations (5% and 10% *w/w*) showed themselves to be highly resistant porous materials, non-toxic, and capable of absorbing more than 50 times their own weight when in contact with liquid media under physiological conditions.

- GEL-GO aerogels loaded with GSE exhibited increased negative surface charge, blood absorption capacity, and total coagulated blood content compared to the GEL-GO aerogel, being these improvements greater with the inclusion of 5% (*w/w*) of GSE into the aerogels.
- The RBCs were successfully adhered onto the aerogels' surfaces, which could favor hemostasis by promoting coagulation alternative routes.
- All aerogels showed a synergic action to interact with blood cells and release natural compounds from these matrices, which justify their possible use as a topical drug delivery system with potential use for wound dressing applications.

Chapter 4

Study of the hemostatic performance *in vitro* and *in vivo* of graphene oxide-based aerogels.

The information provided in this chapter is redrafted after submitting in: Novel and effective hemostatic materials based on graphene oxide-polymer aerogels: In vitro and in vivo evaluations (J. Borges, T. Figueroa, S. Guajardo, S. Carmona, C. Mellado, M. Meléndrez, C. Aguayo, K. Fernández, Biomaterials Journal).

4.1. Abstract

In this study, GO-based aerogels cross-linked with CS, GEL, and PVA were characterized and their hemostatic efficiencies both *in vitro* and *in vivo* were investigated and compared to commercial materials (ChitoGauze®XR and Spongostan™). All aerogels exhibited highly porous structures, with negative surface charge densities, blood coagulation capacities above 60%, and a high hemocompatibility. Among them, the GO-CS aerogel being the one with the highest blood clotting and the GO-GEL aerogel exhibited the lowest hemolytic activity. According to their blood clotting activity, aerogels did not promote coagulation through extrinsic and intrinsic pathways. However, their surfaces are suitable for accelerating hemostasis by promoting alternative routes. All aerogels adhered platelets and gathered RBCs on their surfaces, and in addition the GO-CS aerogel surface also promoted the formation of filamentous fibrin networks adhered on its structure. Furthermore, *in vivo* evaluations revealed that all aerogels significantly shortened the hemostatic times and reduced the blood loss amounts compared both to the Spongostan™ and ChitoGauze®XR commercial materials and to the gauze sponge (control group). The hemostatic performance *in vitro* and *in vivo* of these aerogels suggest that they could be used as hemostats for controlling profuse bleedings.

4.2. Introduction

Uncontrolled bleeding is a significant cause of death in medical operations, traffic accidents, on battlefields, and in emergencies [1–5]. Consequently, developing effective hemostatic materials that can control bleeding and minimize collateral damage remains a crucial challenge for saving lives [9,12,152]. To date, many new hemostatic agents or modifications of the existing ones have been developed based on inorganic or organic materials, or a combination of both [2,7,9]. The combined material solution has been further studied as an alternative to developing hemostats with improved

hemostatic and biological performance compared to a single hemostat [4,18]. Accordingly, new types of hemostatic materials such as sponges, powders, hydrogels, foams, scaffolds, fibers, aerogels, and so on have been designed and evaluated for hemostasis [1,5,12–18].

GO-based materials have shown remarkable potential in bleeding control due to their ability to absorb plasma, adhere to and accumulate blood cells on their surfaces, and promote blood coagulation [1,5,9,14–18]. Singh *et al.* [23] reported for the first time that GO sheets elicited a strong aggregatory response in platelets, because of the presence of oxygenated-functional groups in their structure [12,24,25]. However, GO has also shown some shortcomings as a hemostat in relation to its high hemolysis rate, cytotoxicity, and potential thrombosis, limiting its use in hemostatic applications [1]. An effective strategy to overcome these drawbacks has been to crosslink the GO with other materials, mainly polymers, to provide new functionalities [27,28,144].

To date, numerous materials have been crosslinked with GO, including CS [29], alginate [30], GEL [16], PVA [5], PEG [17], kaolin [7], thrombin [9], and others. CS is a polymer extensively used in hemostatic applications due to its biocompatibility, biodegradability, non-toxicity, and hydrophilic nature [2,15,29,69]. CS-based materials have been demonstrated to promote blood coagulation by a charge effect, in which positively-charged CS attracts negatively-charged cell membranes of erythrocytes (RBCs), thus leading to the RBCs' agglutination and the formation of a hemostatic "plug" in the wound site [13,15,29]. Another interesting polymer is GEL, a natural, hydrophilic, biocompatible, and biodegradable polymer, which is non-toxic and has a good affinity with proteins [10,31]. GEL-containing materials provide a structural composition similar to the extracellular matrix (ECM), allowing them to activate platelet aggregation [16,69]. Both the hemostatic effectiveness of GEL and its capability for potential modifications are suitable features for hemostatic applications and have been previously demonstrated [18,31]. As a synthetic polymer, PVA is also biocompatible, non-toxic, water-soluble, and has blood clotting ability [5,153]. PVA-containing materials provide a suitable environment for cell growth due to their pH stability and semi-permeability characteristics [154]. Despite their excellent properties, certain disadvantages limit the use of these polymers in hemostatic applications. For instance, CS-based materials have exhibited mechanical instability [15,155], whereas GEL-containing materials have shown poor mechanical strength [35,36]. It has been also noted that a single PVA sponge is ineffective in the control of fast-flowing blood hemorrhages and lacks cellular functionalities [156,157].

Thus, GO/polymer aerogels with improved mechanical and biological features have been developed to overcome those drawbacks [5,15,18]. The findings obtained provided evidence supporting the

suitability of these aerogels in hemostatic applications. However, it is necessary to validate their use with commercial materials and in more realistic conditions. Therefore, this study aims to compare the hemostatic efficiency both *in vitro* and *in vivo* -in a rat-tail amputation model- of the GO-GEL, GO-CS, and GO-PVA aerogels based on an evaluation of their coagulant capacity, hemolytic activity, blood clotting activity, and aerogel-blood cell interactions. The hemostatic efficiencies of these aerogels were compared to those of commercial hemostats, Spongostan™ and ChitoGauze®XR, and to a control gauze sponge.

4.3. Materials and methods

4.3.1. Materials

Graphite powder (Flake, mesh 325) was purchased from Asbury Online (Asbury Carbons, NJ). Chitosan, gelatin type B, and polyvinyl alcohol (PVA, molecular weight 85 000−124 000 and hydrolysis degree ~99%) were purchased from Sigma- Aldrich Company, (St. Louis, MO). Ethanol (C_2H_5OH, 95%), glutaraldehyde ($C_5H_8O_2$, 2.5%), acetic acid (CH_3COOH), sodium chloride (NaCl), and PBS were purchased from Merck (Darmstadt, Germany). Sprague-Dawley (SD) rats were purchased from the Institute of Nutrition and Food Technology, Chile. Fresh human blood was extracted from healthy volunteers and used for assays. Two commercial products, ChitoGauze®XR and Spongostan™, composed of chitosan and gelatin, were purchased from their suppliers and used in the *in vivo* assay. A standard medical gauze (hydrophilic, 100% cotton, aseptic, and sterile) was purchased from a commercial pharmacy. Milli-Q®, distilled, and deionized water (DW), was used throughout the investigation.

4.3.2. Synthesis of GO-based aerogels

GO-based aerogels cross-linked with CS, GEL, and PVA were developed according to the synthesis protocols described in our previous studies [5,15,18]. GO was produced from natural graphite powder following the procedure described by Marcano *et al.* [45] with slight modifications [49]. The synthesis of each aerogel was developed at different concentrations and pH of the GO, as briefly described below:

(a) Synthesis of GO-CS aerogels: Firstly, a GO solution (0.5 mg/mL, 600 mL) was prepared by stirring for 30 min. Then a CS solution (1 mg/mL, pH=2) was prepared using 30 mL of Milli-Q® water and ~10 mL of acetic acid to improve the CS´s solubility. This CS solution was slowly dripped onto the previously prepared GO solution. The resulting mixture was stirred for 30 min to achieve homogenization and its pH was adjusted to 10 using NaCl as an indicator. Subsequently, the mixture was stirred for another 30 min and centrifugated (3000 x g, 3 min). After centrifugation, the supernatant was removed and the

precipitate solution was washed with Milli-Q® water (three times) followed by centrifugation (three times). The final solution was lyophilized to obtain the GO-CS aerogel [15].

(b) Synthesis of GO-GEL aerogels: Firstly, a GO suspension (2 mg/mL, 50 mL) was prepared by sonication for 30 min and its pH was adjusted to 11 using NaCl as an indicator. Then, a GEL solution (1g, 150 mL) was prepared by stirring at 60°C for 15 min until homogenization. This solution was mixed with the above GO solution and the resulting mixture was reacted by a microwave-assisted reaction (800 W, 30 min total reaction time). Finally, the mixture was cross-linked at 4°C for 12 h, then frozen to -86°C, and lyophilized for 72 h to form the GO-GEL aerogel [18,144].

(c) Synthesis of GO-PVA aerogels: Firstly, a PVA solution (10 mg/mL) was prepared by sonication and stirring at 50°C until its complete dissolution. Then, 5 mL of GO (10 mg/mL) was mixed with 2.5 mL of the above PVA solution in 15mL falcon tubes. The solution was vigorously stirred for 20 s to form the hydrogel. Finally, the mixture was ultrasonicated for 10 min, followed by freezing at -15°C for 48 h, and lyophilization for 36 h to obtain the GO-PVA aerogel [5].

4.3.3. GO-based aerogel characterizations

A Scanning Electron Microscope (SEM) was used to examine the morphology of the GO-CS, GO-GEL, and GO-PVA aerogels. The aerogel samples were coated using a gold sputter coater and their surfaces were observed at different resolutions using a TESCAN microscope (VEGA3 EASYPROBE SBU model). The average pore size of each aerogel was measured in the ImageJ software using a total of 50 random pores obtained from SEM images.

The apparent porosity of the GO-CS, GO-GEL, and GO-PVA aerogels was evaluated based on a pycnometer analysis according to protocol described in section 2.3.5. The surface charge of the GO-CS, GO-GEL, and GO-PVA aerogels was determined through ζ-potential measurements using the Dynamic Light Scattering principle (Nano particle analyzer SZ-100 Horiba Scientific, Japan). Briefly, aerogel samples of 1.0 cm^3 volume were dissolved in a PBS solution (1x, pH=7.4, 37°C) by stirring and subsequent sonication for 20 min before the measurement. Then, the surface charge of each material was measured.

4.3.4. Hemostatic performance of aerogels

4.3.4.1. *In vitro* dynamic whole-blood clotting assay

An *in vitro* dynamic whole-blood clotting assay was conducted with the aerogels to evaluate their hemostatic performance. A total volume of 50 µL of fresh human blood was directly dropped on aerogel samples of equal size (1.0 cm^3). Each group was allowed to interact for 30, 60, 120, and 240 s at room temperature. After each reaction time, 10 mL of distilled water were added to each sample to stop the

coagulation process and dissolve the uncoagulated RBCs. The hemoglobin content in the supernatant was quantified by UV-VIS spectroscopy (Spectroquant Prove 600; Merck, Germany) at 540 nm. Then, 50 µL of fresh human blood in 10 mL Milli-Q® water (blank) were measured as a reference value. A standard gauze sponge was used as a control in this assay. The hemoglobin content was quantified using **Equation 4.1**:

$$Hemoglobin\ content\ (\%) = \frac{I_s}{I_r} * 100 \quad (4.1)$$

where I_s is the sample absorbance and I_r is the reference absorbance.

4.3.4.2. Hemolysis assay *in vitro*

A hemolysis assay *in vitro* was performed with the aerogels following the protocol described by Yang *et al*. [158] with slight modifications. Briefly, 1 mL of citrated fresh human blood was collected and diluted with 5 mL of PBS (1x, pH=7.4, 37°C). Aerogel samples (20 mg) were incubated with the diluted blood at 37°C for 1h. Then the samples were centrifuged at 3000 rpm for 10 min and the supernatants were recovered. The absorbance of each supernatant was measured at 540 nm using a microplate reader (Synergy 2 Multi-Detection Microplate Reader, BioTek Instruments, Inc.). PBS and DW were used in this assay as negative and positive controls, respectively. The hemolysis rate for each sample was calculated using **Equation 4.2**:

$$Hemolysis\ rate\ (\%) = \frac{Abs_{sample} - Abs_{negative\ control}}{Abs_{positive\ control} - Abs_{negative\ control}} * 100 \quad (4.2)$$

4.3.4.3. Hemostatic mechanism of aerogels

The hemostatic mechanism of the GO-CS, GO-GEL, and GO-PVA aerogels was investigated by determining the PT and the aPTT. These measurements were made using previously-reported methodologies [18,147] with slight modifications. Briefly, fresh human blood was centrifuged at 3000 x g for 10 min to obtain platelet-poor plasma (PPP). Then, PPP (500 µL volume) was added to each aerogel sample (1.0 cm^3) and incubated at 37°C for 30 min. For the PT measurements, 200 µL of Thromborel® S reagent were added to 100 µL of PPP in a test tube, and then the coagulation time was measured in an automated blood coagulation analyzer (Rayto RT-2204C, China). For the aPTT measurements, 100 µL of PPP were mixed with 100 µL of Actin® FS reagent and incubated at 37°C for 3 min. Then, 100 µL of aqueous $CaCl_2$ (0.025 mol/L) were added to the mixture, and the aPTT time was measured in the same instrument.

4.3.4.4. Interaction with RBCs and platelets

The selective adhesion of RBCs and platelets onto the aerogel surfaces was investigated through SEM images. The platelet adhesion test was conducted following the protocol described by Li *et al.* [9] with slight modifications. Briefly, aerogel samples of equal size (1.0 cm^3) were equilibrated with 2 mL of PBS (1x, pH=7.4, 37°C) for 2 h. Then, 2 mL of platelet-rich plasma (PRP) were obtained by centrifugation at 1350 x g at 4°C for 20 min from a fresh human blood sample. This PRP was added to each aerogel sample, subsequently incubated at 37°C for 1h to ensure complete contact. Subsequently, the samples were slightly washed with PBS to remove the unattached blood cells from the material.

To evaluate the RBCs' selective adhesion, the aerogel samples of 1.0 cm^3 were equilibrated with 2 mL of PBS (1x, pH=7.4, 37°C) for 2 h. Then, 1 mL of anticoagulant fresh human blood was added to each sample and incubated at 37°C for 1 h. Two washes with PBS followed, to remove the unattached RBCs from the material. Finally, the samples were immobilized with 2.5% glutaraldehyde, immersed in a graded ethanol series (50%, 60%, 70%, 80%, and 90%), and freeze-dried for 12h before the SEM analysis.

4.3.5. *In vivo* hemostatic testing

The *in vivo* evaluation was conducted through a rat-tail cutting experiment according to previously-described methodologies [1,7,11,12] with slight modifications. All animal experiments in this study were approved and carried out in accordance with the Animal Ethics, Bioethics and Biosafety Committee of Universidad de Concepción. Healthy SD rats (weight of 262 ± 12 g, 14 weeks old) were received and treated in strict accordance with the protocols established by this committee for the care and use of laboratory animals. The rats were initially separated into cages and quarantined under a standard environment to ensure a healthy physiological condition. For this assay, each aerogel was synthesized with the shape and dimensions of a 12-well plate. Meanwhile, both commercial materials (Spongostan™ and ChitoGauze®XR) and a gauze sponge (used as a negative control) were cut to the same size. Each material sample was previously prepared and sterilized using UV radiation for 1h. For testing, the rats were divided into six groups of 5 animals each and anesthetized with a ketamine (80-110mg/kg) / xylazine (5-10mg/kg) solution before surgery. Then, the rat tail, measuring approximately 16 cm in length, was cut at midpoint using a sharp knife. After cutting, the rat tail was placed in the air for 15 s to ensure normal blood flow. Then, each material sample was immediately put in contact with the wound section, using slight pressure to control the bleeding. In this assay, the hemostatic time was recorded based on the criteria of no visible blood and no active bleeding on the wound section. Also,

the blood loss amount was determined by the weight difference of the material before and after the assay.

4.3.6. Statistical analysis

Data analysis was performed using OriginPro8.5® software. The average pore size of each aerogel was measured using ImageJ software. The data statistical analyses were done with Statgraphics Centurion XVII® software using ANOVA and Duncan's multiple range test. The significance levels were determined as $p<0.05$, $p<0.01$, and $p<0.001$. Data are presented as the mean ± SD and the error bars are shown in each figure.

4.4. Results and Discussion

4.4.1. Aerogel characterization

The morphology of the GO-CS, GO-GEL, and GO-PVA aerogels was analyzed by SEM images (**Figure 4.1**). All aerogels show the formation of interconnected porous and heterogeneous structures on the surface. These morphological features may favor both the aerogel´s absorption capacity and blood coagulation [29]. The aerogel's average pore sizes were between 32.4 and 36.8 µm, no statistical differences among them being shown (**Table 4.1**).

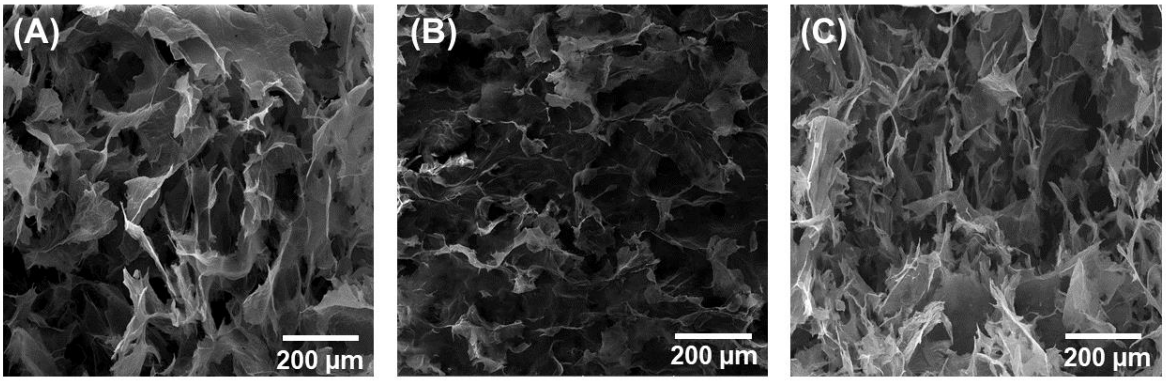

Figure 4.1. SEM images of the morphology of the (A) GO-CS aerogel, (B) GO-GEL aerogel, and (C) GO-PVA aerogel.

Porosity is one of the most important parameters to evaluate in wound-dressing materials, since it is directly related to their absorption capacity [19,108,158]. All aerogels achieved apparent porosities above 85% (**Table 4.1**), which agrees with their porous structures observed in SEM images. The highest porosity was around 99% for the GO-CS aerogel, followed by the GO-GEL and GO-PVA aerogels with porosities of 91.8% and 85.7%, respectively. The statistical differences observed between the porosity values could be ascribed, in part, to the different GO:polymer ratios used in the aerogel syntheses, generating different crosslinking densities and thus, different porosity values. The

aerogel preparation used GO:polymer ratios of around 9:1 for the GO-CS aerogel (90% *w/w* GO), 1:1 for the GO-PVA aerogel (50% *w/w* GO), and 1:9 for the GO-GEL aerogel (10% *w/w* GO). Also, the different intermolecular interactions between the polymer and the GO,- which acts as a large multifunctional crosslinker- may also influence the apparent porosity of aerogels [30].

The porosity of GO-based materials has been widely assessed by other authors, since aerogel-based biomaterials are characterized by their high porosity [19]. In a related study, Zhang *et al.* [29] reported that increasing the GO content in ACGS by 20% *w/w* increased the sponge porosity from 61.84% to 75.82%. Similarly, Chen *et al.* [1] reported that a BGCS has a porosity of 95.3%, while the porosity of a GO sponge is 96.5%, further revealing that the porosity of both materials exceeds 90%, which favors the fluid absorption capacity of the materials. Coinciding with these studies, our materials are in the superior range of porosity reported.

Table 4.1 lists the surface charge values measured for each aerogel. A negative surface charge density was observed for all aerogels, due mainly to the presence of GO in their structures. The highest surface charge was obtained, around -12 ± 0.1 mV, for the GO-PVA aerogel, which was reduced by 54% for GO-CS aerogel and by 68% for GO-GEL aerogel. The statistical differences observed between the aerogel´s surface charges could be mainly attributable to the nature of each polymer and the different GO contents incorporated into the aerogels, as was previously mentioned. The GO provides a negative surface charge to the materials due to the presence of oxygenated functional groups in its chemical structure [5,13,16,127,128,144], and its crosslinking with polymers of a different nature could modify the surface charge of the resulting material. In this context, CS is a polymer with a positive surface charge [159], while PVA is negatively charged [5]. Therefore, an increase is expected in the ζ-potential value for the GO-PVA aerogel compared to the GO-CS aerogel due to a charge effect. On the other hand, GEL is an amphoteric polymer whose surface charge is modified by the pH effect [18,65]. In the present study, GEL provides a negative surface charge to the GO-GEL aerogel because this synthesis process was developed at pH conditions above the GEL isoelectric point (pI~5) [18]. Thus, GO-GEL aerogel had a negative surface charge, but lower than that of the other aerogels. According to the literature, materials with negatively-charged surfaces are beneficial to the activation of coagulation factors, promoting the adsorption and activation of plasma proteins, and enhancing the Vroman effect [14,94]. Therefore, these aerogels could accelerate blood coagulation through a charge effect.

A large number of studies have been conducted on GO-based materials and their surface charges have been assessed [1,9,12–14]. Quan *et al.* [14] informed a negative electrical potential of -24.2 ± 1.3

mV for a diaminopropionic acid crosslinked GO sponge (DCGS), whereas Chen *et al.* [1] reported that a BGCS has a surface charge of -27.3 ± 0.9 mV. In another study, Li *et al*. [12] developed a polydopamine-reinforced GO sponge (DCGO) with a surface charge of -31.3 ± 0.3 mV. Although the surface charges of our aerogels are lower than those reported by these authors, their negative nature could improve the clotting potential of these materials and their interaction with blood cells, thus favoring hemostasis.

Table 4.1. Average pore size, apparent porosity, and surface charge of the GO-CS, GO-GEL, and GO-PVA aerogels.

Aerogels	Average pore size (μm)	Apparent porosity (%)	Surface charge (mV)
GO-CS	32.4 ± 9.7 ^{a}	~ 99.0 ^{a}	-5.5 ± 0.1 ^{a}
GO-GEL	36.8 ± 8.2 ^{a}	91.8 ± 1.4 ^{b}	-3.9 ± 1.1 ^{b}
GO-PVA	33.3 ± 9.0 ^{a}	85.7 ± 1.8 ^{c}	-12.0 ± 0.1 ^{c}

The a, b, and c letters refer to significant statistical differences between aerogel samples for p-value<0.05.

4.4.2. Hemostatic evaluation *in vitro* of GO-based aerogels

Blood clotting assays are commonly used to evaluate in *vitro* hemostatic performance of materials for wound dressing applications. The coagulant capacity of each aerogel was studied through an *in vitro* dynamic whole-blood clotting assay (**Figure 4.2a**). The highest blood coagulation capacity was around 95% for the GO-CS aerogel, followed by the GO-GEL aerogel with a clotting ability of 82%, and finally by the GO-PVA aerogel with 62% of its blood content coagulated. These values were significantly greater than the blood amounts coagulated by the gauze sponge (10%) and the fresh human blood (15%), both used as control groups in this assay. The statistical differences between the coagulation capacity values of each aerogel could be due to the different GO contents incorporated into their structure (as mentioned in section 4.4.1) and also to the nature of each polymer.

The use of various polymers with different hemostatic activities might also influence the aerogel's clotting performance. In this context, CS has a hemostatic activity related to the electrostatic interactions between its positive surface charge and the negatively-charged erythrocyte membranes [3,15]. Alternatively, the hemostatic activity of the GEL has been attributable to its active role in platelet activation [34]. Although PVA itself does not have a specific hemostatic function, it causes physical hemostasis through local compression [157]. Consequently, the combined action of both factors (GO

content and polymer nature) would produce significant differences in the aerogel's blood clotting capacity. Thus, the aerogels' clotting performance was GO-CS >GO-GEL>GO-PVA.

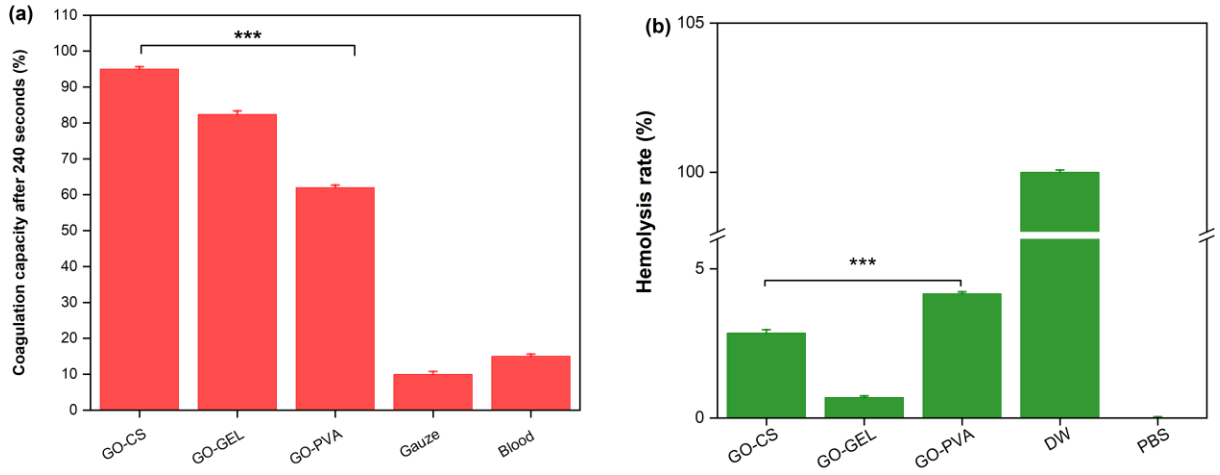

Figure 4.2. (a) *In vitro* dynamic whole-blood clotting evaluation measured after 240 s of the assay in the GO-CS, GO-GEL, and GO-PVA aerogels, gauze sponge, and a fresh human blood sample (control groups), (b) Hemolytic activity evaluation of the GO-CS, GO-GEL, and GO-PVA aerogels, and the control groups (PBS and DW). The measurements were done in triplicate (*n=3, *** p<0.001*).

The hemolysis assay *in vitro* is a universal method to assess the hemocompatibility of materials [30,158]. **Figure 4.2b** shows the hemolysis rates obtained for each aerogel, including the PBS and the DW as control groups. All aerogels achieved hemolysis rates lower than 5%, which is within the acceptable range for biomaterials [30,158]. Therefore, none of these aerogels would be expected to induce severe hemolysis, which could be due to the biocompatible and hydrophilic nature of the CS, GEL, and PVA polymers. Comparing aerogels, the lowest hemolytic activity was found for the GO-GEL aerogel (0.68%), followed by the GO-CS and GO-PVA aerogels with hemolytic rates of 2.84% and 4.16%, respectively. The abrupt reduction in the GO-GEL aerogel's hemolytic activity compared to the other materials could be caused by both the low GO content (10% *w/w*) and the high GEL amount (90% *w/w*) incorporated into this aerogel. It is well known that GO induces hemolysis in the materials [1,25], whereas GEL-containing materials provide a structural composition similar to the ECM that favors the interaction with blood cells [16,69], thus decreasing this material's hemolytic activity. In similar studies, Zhang *et al.* [29] stated that ACGS achieved hemolytic activities lower than 1%, whereas Ma *et al.* [30] demonstrated that sodium alginate/GO/PVA sponges decreased their hemolytic activity from 1.22% to 0.26% when GO content increased, indicating that GO had a positive effect on the hemolysis inhibition of those sponges. Both studies conclude that materials with hemolysis rates

less than 5% are suitable for wound dressing applications, which is in agreement with our hemolysis results.

To further clarify the hemostatic mechanism of the aerogels, the PT and the aPTT were assessed. These measurements are generally considered to be an effective method for evaluating the extrinsic and intrinsic coagulation pathways, respectively [147,160]. In **Figure 4.3**, the PT times of the GO-CS, GO-GEL, and GO-PVA aerogels were 13.1 ± 0.6 s, 13 ± 0.9 s, and 15.1 ± 1.7 s, respectively. No statistical differences were observed for the PT results, indicating that no observable coagulation effects through the extrinsic pathway were triggered. In a similar analysis, the aPTT times of the GO-CS, GO-GEL, and GO-PVA aerogels were 33.5 ± 1.0 s, 33.8 ± 0.7 s, and 35.6 ± 2.8 s, respectively. These results are significantly different from the control plasma sample with an aPTT time of 27.5 ± 0.4 s, in which the aPTT times were lengthened in the presence of all aerogels, suggesting that they do not promote coagulation by the intrinsic route either.

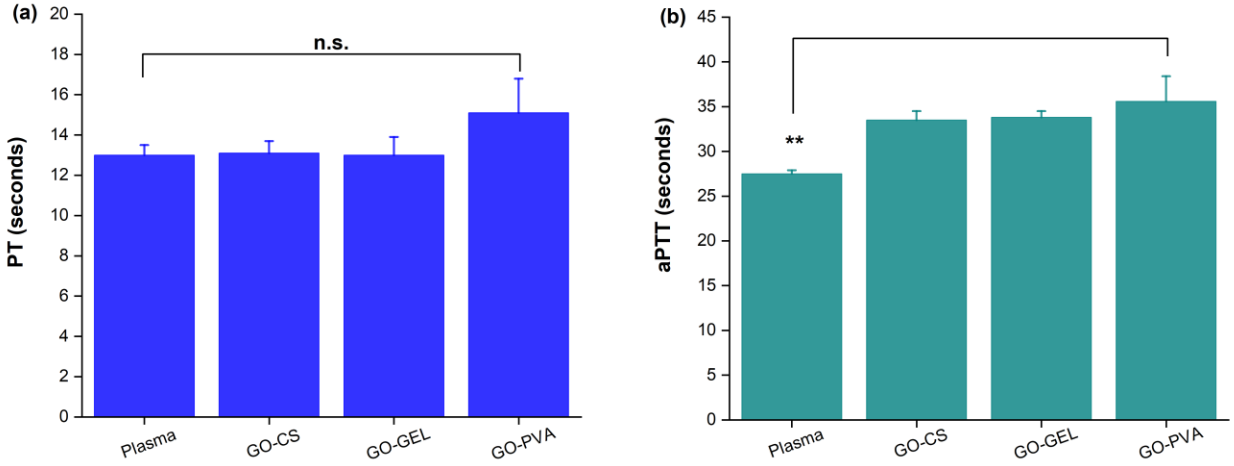

Figure 4.3. (a) PT and (b) aPTT measurements for the GO-CS, GO-GEL, and GO-PVA aerogels, and a control plasma sample. Data are expressed as the mean ± SD (*n=4*, ** *p<0.01,* n.s.: not significant).

The aerogel-blood cell interactions were also investigated through selective adhesion assays to determine whether the aerogels' surfaces could gather and/or stimulate platelets/RBCs. **Figure 4.4** shows the SEM images obtained from the platelet selective adhesion assay. When the aerogels were incubated with PRP, platelets adhered onto their surfaces, modifying their original shape and showing a pseudopodia-like morphology (marked with yellow arrows). These results are encouraging in terms of the aerogel-platelet interactions, because platelet activation could support the thrombin formation

that triggers the fibrinogen formation and the creation of a stable fibrin clot, thus accelerating hemostasis [12].

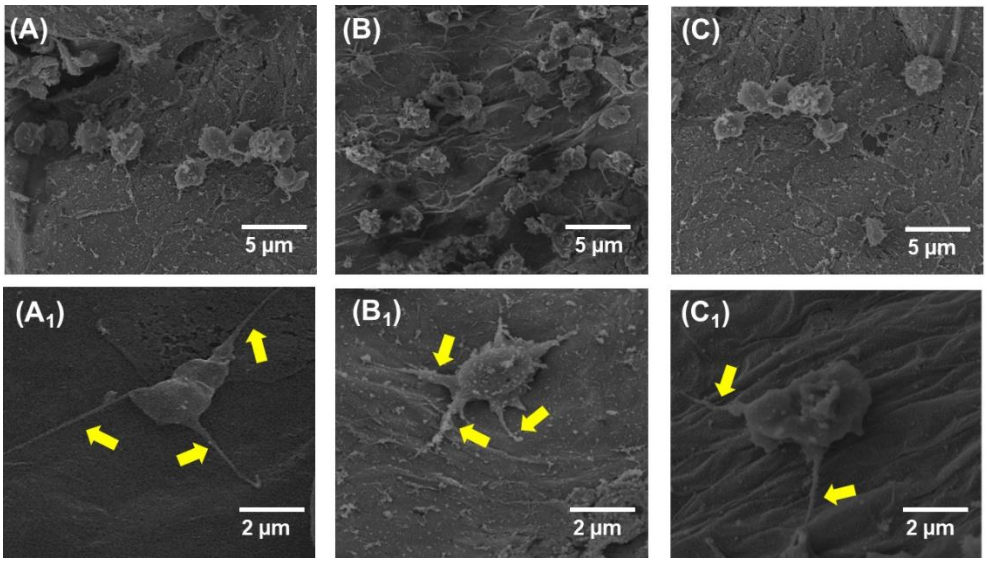

Figure 4.4. SEM images show the platelet adhesion and activation as a consequence of the aerogel-platelet interactions. The yellow arrows show the active platelets on the surfaces of the (A) and (A_1) GO-CS aerogel, (B) and (B_1) GO-GEL aerogel, and (C) and (C_1) GO-PVA aerogel, respectively.

The selective adhesion of RBCs onto the aerogel surfaces was also examined by SEM images using both a fresh human blood sample (**Figure 4.5**) and a SD rat whole blood sample obtained from the *in vivo* assay (**Figure 4.6**). In both cases the presence was observed of many RBCs adhered onto all the aerogels' surfaces, without affecting the original morphology and physiological status of the RBCs, which maintained their normal shape. **Figure 4.6** also shows the formation of filamentous fibrin meshes that trapped the RBCs adhered to the GO-CS aerogel´s surface. Considering the remarkable potential of GO to promote coagulation, this result could be explained by the fact that this aerogel has the highest GO content among the test materials. In agreement with our results, several authors evaluating the interaction of GO-containing materials with blood cell components have demonstrated that these materials can promote the gathering of RBCs, adhere to and activate platelets on their surfaces, and also develop filamentous fibrin meshes that trap RBCs and platelets [9,12–14,29]. Thus, it is expected that our aerogels' surfaces would accelerate blood coagulation.

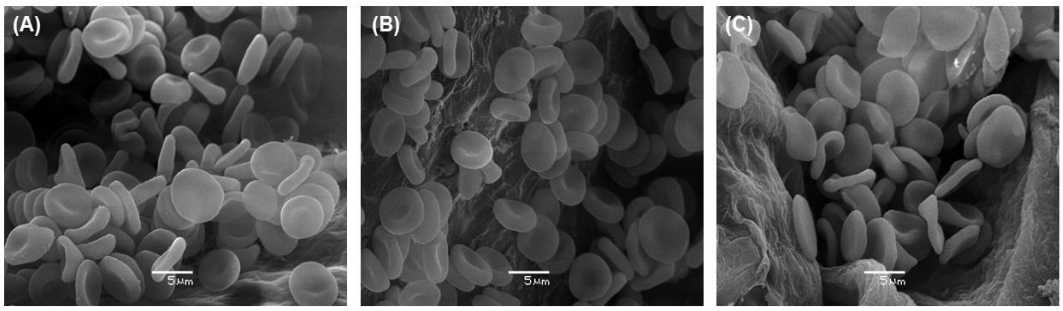

Figure 4.5. SEM images show the presence of RBCs belonging to a fresh human blood sample adhered to the surfaces of (A) GO-CS aerogel, (B) GO-GEL aerogel, and (C) GO-PVA aerogel. The scale bar of the SEM images is 5 µm.

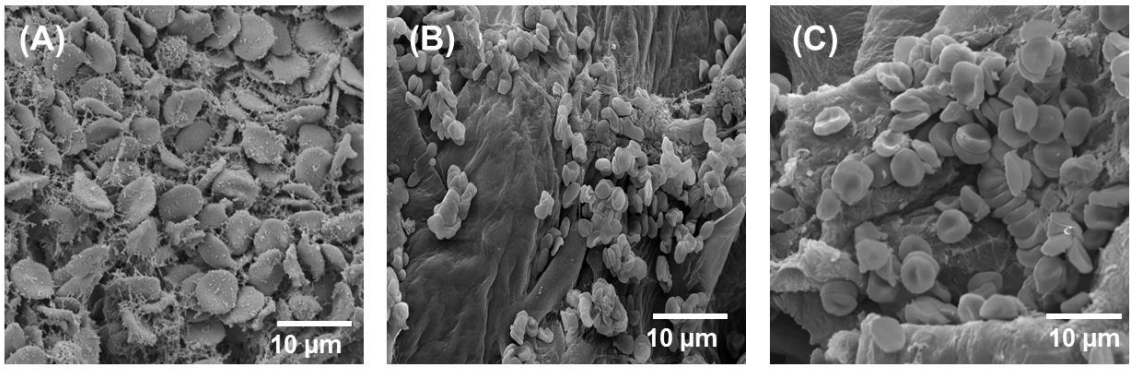

Figure 4.6. SEM images showing the aerogel-blood cell interactions using a SD rat whole blood sample in contact with the (A) GO-CS aerogel, (B) GO-GEL aerogel, and (C) GO-PVA aerogel.

4.4.3. *In vivo* hemostatic testing

Rat tail cutting models are commonly used to assess the hemostatic efficiency of trauma hemostatic materials [12]. Therefore, this animal model was used to evaluate the *in vivo* hemostatic performance of the GO-CS, GO-GEL, and GO-PVA aerogels. The hemostatic time and the blood loss amount of each aerogel were measured and compared to both commercial products and to a gauze sponge (used as a negative control). **Figure 4.7a** shows photographs of the rat tail after bleeding stopped, with the formation of a hemostatic “plug” to control bleeding as a result of the aerogel-rat tail interaction. This phenomenon might be explained by the presence of GO in the aerogel´s structure, which has shown remarkable hemostatic potential in bleeding control [1,9]. In contrast, neither the commercial materials nor the control group promoted the formation of blood clots in the wound section.

In terms of hemostatic time (**Figure 4.7b**), the GO-CS aerogel showed the highest efficiency with only 129 ± 49 s to achieve hemostasis, which indicates a 46% time reduction compared to the GO-GEL

aerogel (237 ± 13 s) and 59% compared to the GO-PVA aerogel (318 ± 52 s), respectively. In contrast, both commercial materials and the control achieved hemostasis only after 500 s bleeding, with the gauze sponge showing the longest time (748 ± 82 s). These results corroborate the fact that neither the commercial materials nor the control promoted blood coagulation, and even after 500 s, the bleeding could only be stopped by pressing hard on the wound area. When using the GO-CS aerogel to prevent bleeding from the rat tail, only 0.26 ± 0.1 g of blood loss was measured (**Figure 4.7c**). This value is significantly lower than the blood loss with the GO-GEL and GO-PVA aerogels, which was 82 ± 0.3 g and 0.94 ± 0.2 g, respectively. The blood losses measured for the ChitoGauze®XR, Spongostan™ and the gauze sponge were 1.84 ± 0.2 g, 0.8 ± 0.2 g, and 1.8 ± 0.3 g, respectively. According to these results, the blood loss of the GO-GEL aerogel was similar to that of the Spongostan™, due possibly to the high GEL content in both materials. The statistical differences observed in both *in vivo* results could be attributed to the different GO content incorporated into aerogels, the polymer nature, and other factors, as explained below.

GO has exhibited notable hemostatic potential in gathering hemocytes and platelet activation and aggregation [1,12–14]; therefore, increasing its content in the aerogels improves the hemostatic performance *in vivo* of these materials, as with GO-CS aerogel. In addition, the use of different polymers could also influence the hemostatic performance *in vivo* of aerogels, causing different hemostatic activities. As mentioned in section 4.4.2, the hemostatic activities of CS and GEL are related to a charge effect and the platelet activation, respectively, whereas PVA does not have a specific hemostatic activity. Thus, the different polymers' hemostatic activities will trigger distinct hemostatic mechanisms by which the aerogels interact with a bleeding wound and promote coagulation. Additionally, external factors such as temperature, pH, surface properties of the matrix, kind of GO/polymer interactions also influence the aerogels' properties and, therefore, should be considered in evaluating their hemostasis performance *in vivo* [38,119,144]. According to these results, our aerogels possess an outstanding hemostatic performance *in vivo,* the GO-CS aerogel being the one with the best biocompatibility *in vivo*.

The *in vivo* hemostatic efficiency of GO-based materials has also been investigated by other authors using rat-tail amputation experimental models. Quan *et al.* [14] reported a hemostatic time of 166 ± 51.8 s for a DCGS, which was a reduction of 35 s compared to a crosslinked graphene sponge (CGS) with a hemostasis time of 201 ± 46 s. Similarly, Li *et al.* [9] showed that a thrombin/crosslinked graphene sponge achieves hemostasis after 100 ± 15.5 s, which was 100 s shorter than the CGS. In another study, Chen *et al.* [1] reported a hemostasis time of 45.9 ± 4.6 and a blood loss amount of

0.063 ± 0.016 g for a BGCS. In addition, Li *et al*. [12] demonstrated that a DCGO stops bleeding within 105 ± 15 s, which was 165 s faster than the un-crosslinked GO sponge and 96 s faster than that of a CGS, respectively. In agreement with our findings, these studies reveal that crosslinking GO-based materials could be an effective strategy to improve the hemostatic efficiency of materials. In addition, the values reported in these studies are similar to our *in vivo* results.

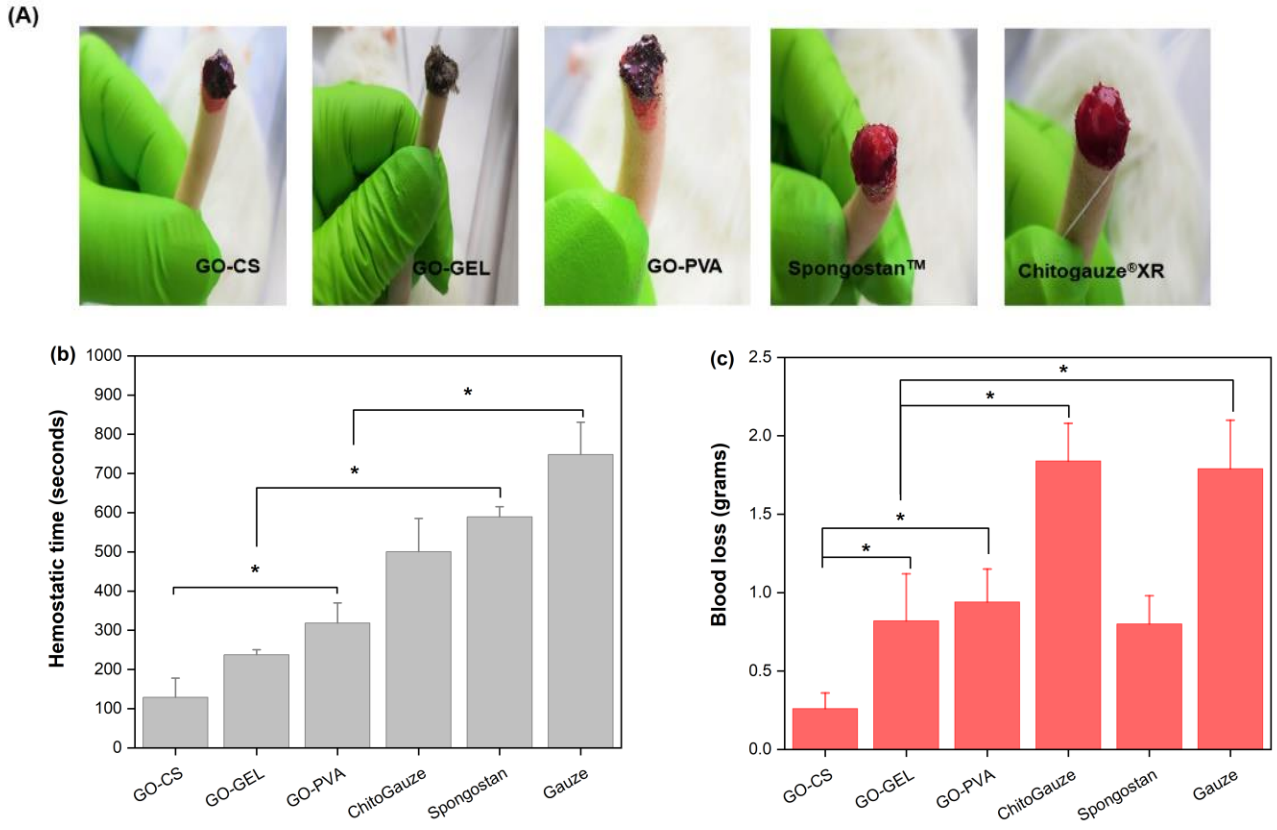

Figure 4.7. *In vivo* rat-tail cutting assay results. (A) Photographs of wound section in the rat tail after contact with different materials, (B) Hemostatic time, (C) Blood loss amounts. The test materials include the GO-CS, GO-GEL, and GO-PVA aerogels, ChitoGauze®XR, Spongostan™, and a gauze sponge. Data are expressed as the mean ± SD (*n=5, * p-value<0.05*).

4.4.4. Synergic mechanism

Based on the above-mentioned results, it was not possible to exactly define the hemostatic action mechanism of these new aerogels. However, several interpretations could be suggested: *(1)* The highly porous and interconnected structures of all aerogels could function as a support to provide a large surface area for blood coagulation and facilitate growth and cell migration that accelerate wound healing, *(2)* Because of the negative charge density and the low hemolytic activity of these aerogels,

they are expected to quickly absorb large amounts of blood and gather RBCs/platelets on their surfaces. Both phenomena will accelerate blood clot formation and therefore the blood coagulation cascade, *(3)* Based on the hemostatic efficiency *in vivo* results, these aerogels are expected to promote hemostasis through an alternative coagulation pathway. This alternative route is particularly relevant for hydrophilic surfaces with nucleophile groups such as hydroxyls and amine (OH, NH_2) capable of covalent binding of the complement protein C3b [150].

4.5. Partial conclusions

- The GO-based aerogels cross-linked with CS, GEL, and PVA were successfully developed through different synthesis processes, showing negatively charged surfaces, blood absorption capacities above 60%, and hemolysis rates lower than 5%, which is favorable to hemostasis.
- The aerogels' surfaces gathered RBCs, adhered to and activated platelets on their surfaces, and even promoted the formation of filamentous fibrin meshes that trapped the RBCs adhered to the GO-CS aerogel´s surface.
- All aerogels significantly reduced the hemostatic time and the blood loss compared to both the ChitoGauze®XR and Spongostan™ commercial materials and to the control gauze sponge, indicating their remarkable hemostatic performance *in vivo*.
- All aerogels exhibited outstanding hemostatic performance both *in vitro* and *in vivo*, validating their use as safe and quick hemostats for controlling profuse bleeding.
- These findings suggest that our aerogels could promote hemostasis due to their composition and surface charge, which favor the accumulation of RBCs and platelets on the wound surface, thus participating in the coagulation process.

Chapter 5

Evaluation of the hemostatic potential *in vitro* and *in vivo* of grape skin extracts.

5.1. Abstract

The use of polyphenolic compounds combined with engineered biomaterials has been continuously growing. Research has focused on counteracting the drawbacks of these compounds, such as volatility, high sensitivity to environmental factors and low stability, in addition to investigating their bioactivities. Among these compounds, the grape skin extracts (GSE) have shown interesting antioxidant, anti-inflammatory, and cardioprotective properties, which support their use in biomedical applications. However, the hemostatic potential of the GSE alone has not been investigated before. This justifies the growing interest in the search for new uses for this natural compound, also seeking to give it a new added value. Therefore, this study aims to investigate the hemostatic potential both *in vitro* and *in vivo* of GSE alone, based on the comparison of the physicomechanical properties, coagulant capacity, clotting activity, and cell viability of the GEL-GO-5% aerogels with the ones of the GEL-GO aerogels.

5.2. Experimental section

GEL-GO aerogels loaded with GSE were developed according to the experimental procedure described in section 3.3.3. The properties of porosity, elastic modulus, surface charge, and elemental content of the aerogels were determined. The *in vitro* performance of these aerogels was investigated by measurements of their coagulant capacity, coagulation activity, and cell viability on HDF cells. These evaluations were performed according to the protocols described in the Materials and Methods section of Chapter 3. Finally, the *in vivo* hemostatic performance of the aerogels was evaluated using a rat-tail amputation model, as described in section 4.3.5. The hemostatic time and the amount of blood loss of these aerogels were quantified and compared with a commercial hemostat (Spongostan^{TM}) and with a control gauze sponge.

5.3. Evaluation of GSE-loaded aerogel properties

The effects of adding GSE into GEL-GO aerogels were evaluated on their apparent porosity and elastic modulus (**Table 5.1**). The GSE incorporation had no significant effect on any of the parameters

evaluated (*p-value>0.05),* indicating that GSE did not modify the physical and mechanical properties of the aerogels.

The absorption capacity is another relevant property for wound-dressing materials since it determines the liquid volume absorbed by the material. **Table 5.1** lists the blood absorption capacity values for both aerogels, indicating an 18% increase in the blood absorption capacity of the aerogels after loading GSE. This result could be attributed to the chemical composition of this natural extract, which contains abundant phenolic groups that could act as donors in hydrogen bonding to interact with blood cells. Similarly, the oxygenated functional groups of these extracts could instantly stimulate RBCs and platelets through electrostatic interactions [85]. Both interactions are favorable to improve the interactions between aerogels and blood cells, which could allow a higher accumulation of RBCs on the surface of GSE-loaded aerogels compared to the GEL-GO aerogels.

Table 5.1. Values of porosity, elastic modulus, and blood absorption capacity for the aerogels.

Aerogels	Porosity (%)	Elastic modulus (kPa)	Blood absorption capacity (g/g)
GEL-GO	91.8 ± 1.4 [a]	2.52 ± 0.6 [a]	52.8 ± 2.1 [a]
GEL-GO-5%	91.3 ± 1.2 [a]	2.84 ± 0.3 [a]	64.7 ± 4.7 [b]

The letters a *and* b *indicate significant statistical differences between aerogels for p-value < 0.05*

The chemical composition of the aerogels was investigated by measurements of their contents of carbon and oxygen. **Table 5.2** lists the C/O ratios for both aerogels, indicating a slight decrease of this parameter for the GSE-loaded aerogels compared to the GEL-GO aerogels. This result confirms that GSE-loaded aerogels have a higher content of oxygenated functional groups than the aerogels without extract. This result was also corroborated by the ζ-potential measurements (**Table 5.2**), showing that the addition of GSE slightly increased the negative surface charge density of aerogels compared to the GEL-GO aerogels, which is mainly due to the increased oxygen content in the GSE-loaded aerogels.

The modification of the physicochemical and structural properties of materials due to the incorporation of new functionalities of molecules is essential for hemostatic materials. These changes could allow *(1)* the improvement of current hemostatic materials and *(2)* the induction of new hemostatic properties to materials, regardless of their hemostatic background [161]. Several authors have demonstrated that interfacial stimulation of materials can be used as an effective strategy to improve the material-blood cell interactions [9,13,14] and thus the hemostatic function of materials. Surface charges, both negative and positive, play a key role in these interactions. Negative charges are beneficial for the adsorption of platelets and RBCs on the materials' surfaces, while positively-

charged surfaces can interact with plasma and increase plasma coagulation through the intrinsic coagulation pathway [99,100]. According to the results of this study, the incorporation of GSE into GEL-GO aerogels could improve the aerogel-blood cell interactions, mainly due to a charge-effect.

The blood clotting ability of both aerogels was also measured by a dynamic *in vitro* whole-blood clotting assay (**Table 5.2**). The GSE-loaded aerogels showed a higher clotting capacity compared to the GEL-GO aerogels, with a 63% increase in this parameter. This result is favorable for hemostasis since the increase in the amount of blood absorbed and coagulated by the aerogels could increase the accumulation of blood cells on their surfaces.

Table 5.2. Values of C/O ratios, surface charge, and blood coagulation capacity of the aerogels.

Aerogels	C/O ratio	Surface charge (mV)	Blood clotting capacity (%)
GEL-GO	1.3	-3.9 ± 1.1 [a]	17.6 ± 1.8 [a]
GEL-GO-5%	1.2	-5.9 ± 1.2 [a]	47.8 ± 1.2 [b]

The letters a *and* b *indicate significant statistical differences between aerogels for p-value<0.05*

To further investigate the *in vitro* hemostatic efficiency of the GSE, the clotting activity of both aerogels and the GSE alone were assessed by determinations of the PT, aPTT, and the P-selectin levels in the plasma (**Table 5.3**). No coagulation effects were observed through the extrinsic and intrinsic pathways when the aerogels came into contact with blood. In addition, both aerogels inhibited platelets and plasmatic proteins on their surface, which was confirmed by the increased levels of P-selectin detected in this assay in comparison with the control plasma. Furthermore, the GSE-loaded aerogels increased this inhibitory effect compared to the GEL-GO aerogels. Although these findings are not encouraging in terms of the clotting activity of the aerogels, some authors have shown that materials with negatively-charged surfaces can interact with blood cells to promote hemostasis by alternative coagulation routes [94]. These pathways have shown to be relevant for materials with hydrophilic surfaces and with the presence of amine groups in their chemical composition, such as GEL [150]. These characteristics are present in both aerogels, suggesting that they could promote alternative coagulation routes to accelerate hemostasis. Considering these results, further studies should be conducted in this area to evaluate other coagulation parameters and to verify the aerogels' clotting activity.

In addition, the hemostatic potential of the GSE alone was investigated through aPTT and PT measurements. The aPTT values were 31 ± 0.5 s and 40.2 ± 0.8 s for control plasma and GSE, respectively. Similarly, their PT values were 11.9 ± 0.5 s and 13.1 ± 0.6 s, respectively. Both coagulation parameters were lengthened in the presence of the GSE compared to the control plasma, indicating that GSE alone do not promote either the intrinsic or extrinsic coagulation pathway. Although

the GSE have shown interesting therapeutic properties, their role in blood clotting is yet contradictory. Some authors have claimed that GSE help coagulation, but others do not agree [162–164]. The multifactorial nature of the coagulation process could explain these controversial results.

Blood clotting is a multifactorial process that requires the activation of distinct processes, which are influenced by factors such as the hydrophilic and/or hydrophobic nature of the materials and surface properties [151,165]. Regarding the properties of these extracts, they have hydrophilic chain portions in their structures providing hydrophilicity and a negative surface charge density. Some authors have shown that both properties are favorable for interfacial stimulation of erythrocytes and platelets during material-blood cell interactions [12,14]. In addition, some studies have shown that the GSE promote cell migration, reduce inflammation, and accelerate wound healing, in which blood clotting processes are also involved [41,166].

The *in vitro* cytotoxicity of the GSE and the aerogels was investigated by cell viability assays on HDF cells. The GSE alone had a cell viability of around 94% (data shown in Figure 3.6), indicating their non-toxic effects. This result could be due to ascribed to the presence of PAs in the chemical composition of the GSE. PAs loaded into different matrices have shown favorable effects on fibroblast cell activity [41]. In addition to this, the non-toxic effects of the GSE have been previously demonstrated by other authors [78,81,86,167,168]. Furthermore, the GSE-loaded aerogels showed a slight increase in cell viability compared to the GEL-GO aerogels, although no statistically significant differences were observed (**Table 5.3**).

Table 5.3. Evaluation of hemostatic parameters and the *in vitro* cytotoxicity of aerogels.

Aerogels	aPTT (s)	PT (s)	P-selectin level (ng/mL)	Cell viability (%)
GEL-GO	33.3 ± 0.8 [a]	13.2 ± 0.8 [a]	124.6 ± 3.2 [a]	81.8 ± 8.3 [a]
GEL-GO-5%	33.9 ± 0.4 [a]	13.1 ± 0.2 [a]	92.4 ± 1.9 [b]	89.8 ± 9.2 [a]
Plasma	35.3 ± 1.1 [a]	13.8 ± 0.5 [b]	216.5 ± 2.0 [c]	-

The letters a, b*, and* c *indicate significant statistical differences between aerogels for p-value < 0.05*

Finally, the *in vivo* hemostatic performance of the GSE was investigated by a hemostatic assay using an SD rat-tail amputation model. **Figure 5.1** and **Figure 5.2** show the hemostatic time and the blood loss values for each test material. Both parameters were compared to a commercial hemostat (Spongostan™) composed mainly of GEL and to a control gauze sponge. When comparing the aerogels, no significant differences were observed in any of the hemostatic parameters. However, both aerogels shortened the hemostatic time and reduced the amount of blood loss compared to Spongostan™ and control gauze. These results were visually corroborated because when the aerogels

came in contact with the rat wound, blood clots were observed to form on the wound surface, which is favorable for hemostasis. These results confirm that the gauze sponge is only able to control natural bleeding, but without promoting hemostasis in the wound section. Additionally, both aerogels showed a better hemostatic potential than Spongostan™, which is a material currently used as a reabsorbable hemostat in dental settings.

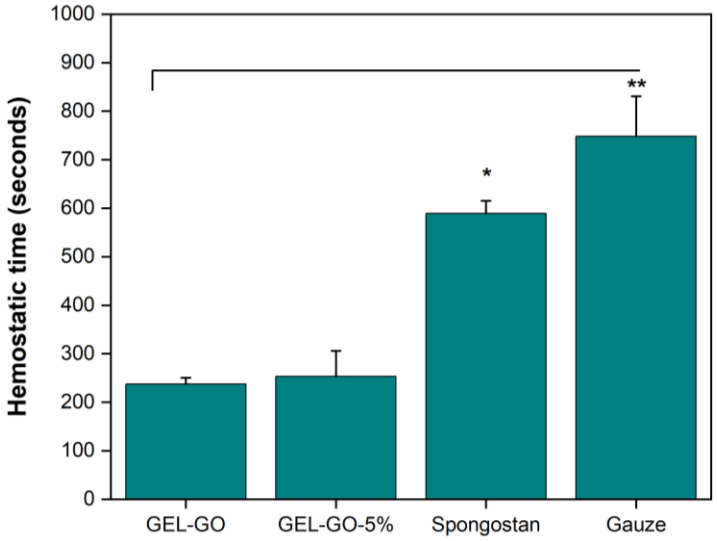

Figure 5.1. Hemostatic times measured during the *in vivo* assay for the GEL-GO, GEL-GO-5% aerogels, Spongostan™, and the control gauze sponge.

Other authors have investigated the *in vivo* performance of grape extracts for many applications. For instance, Ozkan *et al.* [169] evaluated the potential of grape seed proanthocyanidin extracts (GSPE) to prevent contrast-induced nephropathy (CIN) using SD rats. Their study demonstrated for the first time that GSPE provided biochemical and histopathological improvement in CIN. In another study, Zhao *et al.* [170] evaluated the protective effects of grape seed extracts against colonic injury induced by short-term exposure to PhIP using Wistar rats as an *in vivo* model. They demonstrated that grape extracts can be used as an effective dietary supplement to prevent PhIP damage *in vivo*. Similarly, other authors have demonstrated the potential effects *in vivo* of grape extracts in protecting different injuries, such as neuronal loss [171] and amiodarone-induced kidney injuries in rats [172].

According to the results of this study, the incorporation of GSE into GEL-GO aerogels improved relevant properties for hemostasis, such as their blood absorption capacity, total coagulated blood content, negative surface charge, and as well their *in vitro* cell viability compared to the GEL-GO aerogels. In addition, we observed a slight reduction of the PT values in GSE-loaded aerogels compared to aerogels without extracts, which suggests that GSE might favor blood clotting. Although

the GSE by themselves do not promote blood coagulation through the extrinsic and intrinsic pathways, their incorporation into GEL-GO aerogels could accelerate hemostasis by alternative coagulation pathways due to the synergistic action of all component materials.

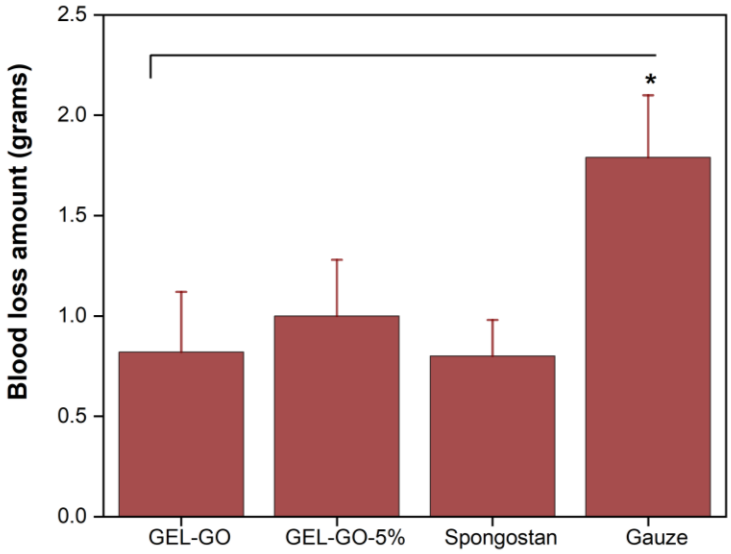

Figure 5.2. Blood loss amounts measured during the *in vivo* assay for the GEL-GO, GEL-GO-5% aerogels, Spongostan™, and the control gauze sponge.

5.3. Partial conclusions

- Both aerogels showed high porosity and favorable mechanical resistance for use as wound-dressing materials in hemostatic settings.
- GSE-loaded aerogels showed higher surface charge, blood absorption ability, clotting capacity, and *in vitro* cell viability compared to GEL-GO aerogels. These improvements were mainly associated with the presence of PAs in the composition of these extracts and with a charge-effect due to the increased content of oxygenated groups after loading GSE.
- GSE by themselves did not show remarkable effects to promote hemostasis; however, their incorporation into GEL-GO aerogels favor hemostasis.

Conclusions

In this study, GEL-GO aerogels were developed by a new microwave-assisted synthesis method for use as wound dressing materials in hemostatic applications. These aerogels showed resistant and highly porous structures, capable of rapidly absorbing liquid media such as water, PBS, and fresh human blood. They also showed a negative surface charge, high hemocompatibility and high coagulant capacity, which is favorable for their interaction with blood cells. Loading the GEL-GO aerogels with different concentrations of GSE resulted in increased blood coagulation capacity, clotting activity, and negative surface charge density. These modifications were favorable for hemostasis since a greater number of blood cells could be accumulated and activated on the aerogel surface. GSE-loaded aerogels also enhanced the *in vitro* cell viability on HDF cells compared to GEL-GO aerogels, which was mainly attributed to the high PA content present in the GSE composition. In addition, the hemostatic action mechanism of both aerogels was investigated. Although none of the aerogels promoted hemostasis through the extrinsic and intrinsic pathways, their surfaces showed suitable characteristics to promote alternative coagulation pathways. In terms of their *in vivo* hemostatic performance, the surfaces of both aerogels promoted a rapid blood clot formation in the rat-tail wound, thus allowing a quick accumulation and activation of RBCs and platelets on the injury site. Furthermore, *in vivo* studies showed that the GEL-GO aerogels shortened the hemostatic time and reduced the amount of blood loss compared to the two commercial hemostats evaluated (Spongostan™ and ChitoGauze®XR) and the control gauze sponge. However, these aerogels showed lower *in vivo* hemostatic efficiency compared to the GO-CS aerogel, which could be mainly attributed to the different GO contents incorporated in their structures. The hemostatic potential *in vitro* and *in vivo* of the GSE was also investigated. Although the GSE alone did not promote blood coagulation, their incorporation into GEL-GO aerogels improved the hemostatic performance of the resulting materials. These findings demonstrate that when our aerogels act on the wound surface, their composition and surface charge favor the accumulation of RBCs and platelets on the damaged surface to participate in the coagulation system. Consequently, the results of this study support the applicability of these aerogels as safe and effective materials for the control of profuse bleeding.

Scope of future work

This research leads to interesting conclusions that support the use of these aerogels in hemostatic settings. However, further studies are needed to validate their final application. These studies involve the evaluation of other coagulation parameters related to alternative coagulation pathways promoted by aerogels. In addition, the *in vivo* hemostatic efficacy of these aerogels should be evaluated in bigger animals as an upgraded model before testing them in humans. Furthermore, the effects of loading higher concentrations of GSE into the aerogels on their *in vitro* and *in vivo* hemostatic performance should be investigated. It is also interesting to investigate new biomedical applications for these aerogels based on their properties, such as wound healing and tissue engineering.

Appendixes

Appendix A: Supporting Information for Chapter 2

A.1. Material characterization techniques

X-ray diffraction (XRD). The XRD was used to evaluate the oxidation degree of GO and the crystallinity of GEL-GO aerogels. The measurements were performed on the X-ray diffractometer (Bruke Axs, D4 Endeavor, USA) with reference target: Cu Kα radiation (λ=1,541841 Å; 2,2 kW), voltage: 40 kV, and current: 20mA. The samples were measured from 2 to 50° during 141 s with steps of 0.02°.

Attenuated total reflection Fourier Transform Infrared Spectroscopy (ATR-FTIR). The ATR-FTIR was used to investigate the chemical nature of interaction of GEL-GO aerogels. The spectra were recorded in the Perkin Elmer UATR Two FTIR Spectrometer. The wavenumber range analyzed was 4000-500 cm^{-1} and a total of 40 accumulated scans were acquired.

Raman analysis. The Raman was used to identify the spectra features and structural properties of GO and GEL-GO aerogels. The data were acquired by high-resolution confocal (LabRamHR Evolution Horiba Jobin Yvon microscope, Japan) at 633 nm of wavenumber in the excitation laser line, a power of 13.3 mW and 1.96 eV. The laser spot was focused on the samples using an optic Objective Olympus 100x VIS and a NUV camera (B/S UV 50/50+ Lens F125 D25). The measurements were performed in quadruplicate at room temperature, and with a laser intensity constant to avoid damaging on the samples. In addition, for the calculation of either the intensity and the area of the D and G bands were applied a Lorentzian function in the spectral region 1000-1800 cm^{-1}.

X-ray photoelectron spectroscopy (XPS). XPS technique was used to quantitatively identify the surface chemistry of GEL-GO aerogels. The measurements were carried out in a Surface Analysis Station 1 (STAIB model RQ300/2, USA) at ultravacuum conditions (< 10^{-9} bar) equipped with a hemispherical electron analyzer (SPEC PHOIBOS 100, Germany). The photoelectrons were excited with non-monochromatic radiation Mg Kα (1486.6 eV) and analyzed with a constant energy step of 1 eV. The X-ray source was used with a strength of 300 W.

Thermogravimetric analysis (TGA). TGA technique was used to evaluate the thermal stability of GEL, GO, and GEL-GO aerogels. The measurements were carried out in a Cahn-Versatherm thermogravimetric analyzer with sensitivity of 0.1 μg, heating rate of 10°C/min under nitrogen atmosphere (100 mL/min) and a temperature range from 30°C to 800°C.

Scanning electron microscopy (SEM). The SEM analysis was used to investigate the micromorphology of GEL-GO aerogels. SEM images were recorded using a JEOL JSM-6380LV, Japan model microscope at 10 kV. The aerogels were coated using a gold sputter coater and their surfaces were observed at different resolutions. In addition, the average pore size of each GEL-GO aerogel was calculated through measurements of 50 random pores obtained from the SEM images using ImageJ software.

Compression test. The mechanical properties of GEL-GO aerogels were evaluated by an uniaxial compression test. Samples of thickness 1.3 cm and diameter 5 cm were compressed until 480 kN (compressive stress) in a universal testing system (Instron Model 4468, USA) with a load capacity of 0.001 ~ 500 to kN and a load speed of 1 mm/min. The stress-strain curves were obtained, and the elastic modulus was determined as the slope of the first linear region, 10-40%, of the strain axis.

Surface charge measurements. The surface charge of GEL-GO aerogels was determined through ζ-potential measurements using the Dynamic Light Scattering principle (SZ-100 Nano particle analyzer, Horiba Scientific, Japan). The measurements were conducted for the GO and GEL-GO aerogels. Samples 1.0 cm^3 in volume were dissolved in Milli-Q® water, shaken and sonicated for 20 min to achieve homogeneity. Finally, the samples were measured in triplicate.

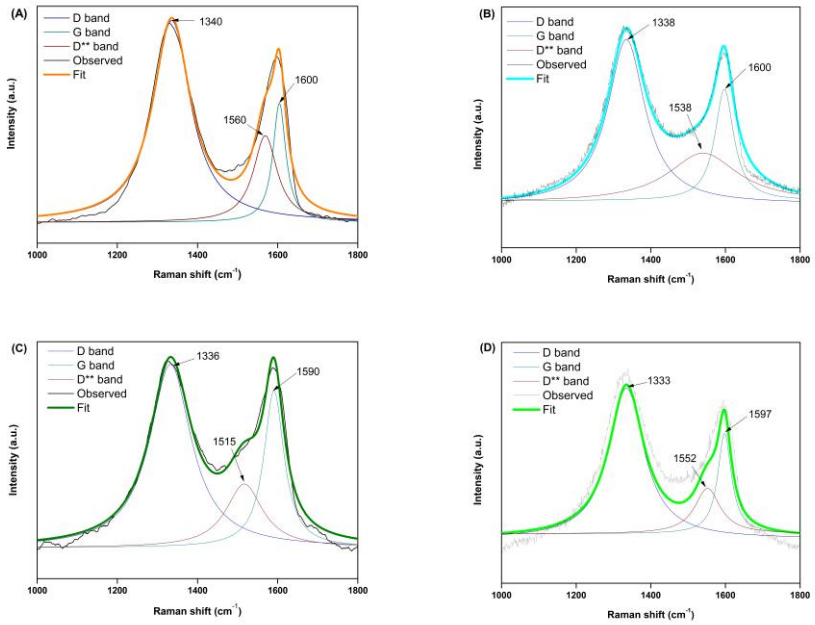

Figure A.1. Deconvoluted Raman spectra for graphitic materials (A) $G_{10}GO_3$ aerogel, (B) $G_{15}GO_3$ aerogel, (C) $G_{10}GO_{11}$ aerogel, (D) $G_{15}GO_{11}$ aerogel.

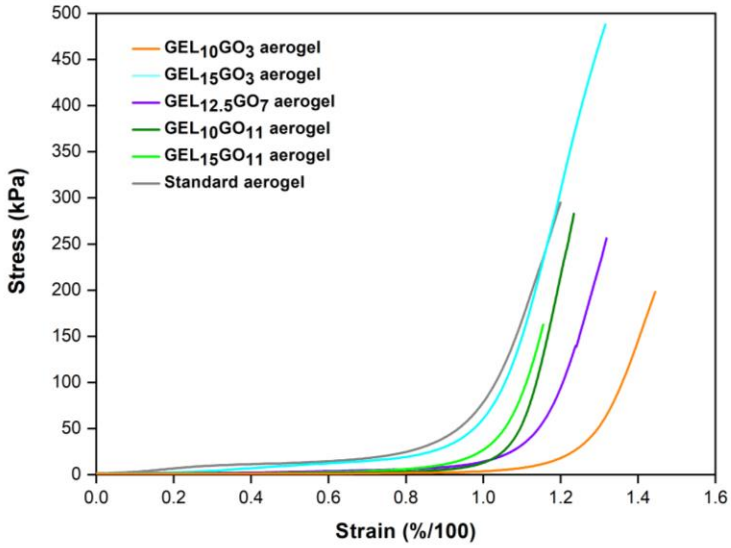

Figure A.2. Stress-strain curves for GEL-GO aerogels.

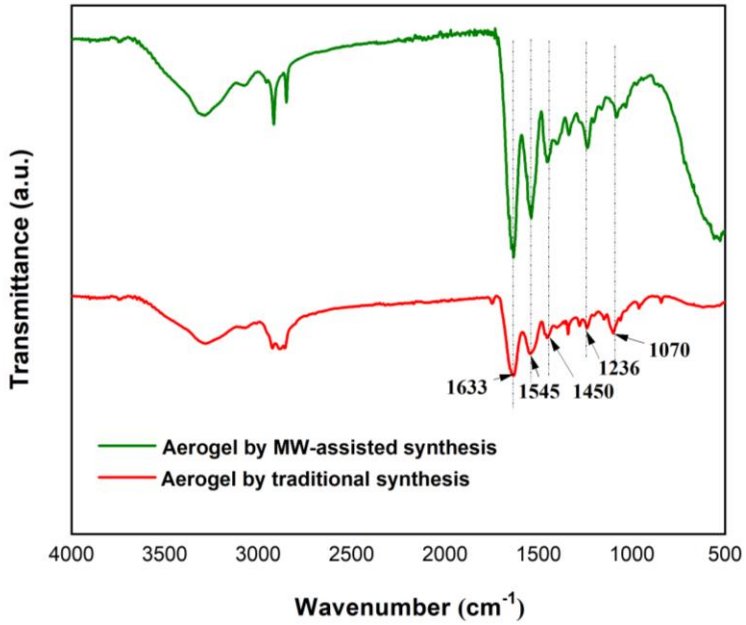

Figure A.3. ATR-FTIR spectra of aerogels synthesized by MW-assisted synthesis and a covalent traditional synthesis.

A.2. Covalent traditional synthesis method

A GEL-GO aerogel was developed according to the methodology proposed by Piao *et al.* [71], under alkaline pH conditions of the GO solutions and with a GEL:GO ratio of 10:1. The synthesis was carried out mixing GEL and GO solutions in the desired amount, at ~90°C with continuous heating for 24h.

Then, the mixtures were stored for 12h at 4°C and subsequently frozen at -86°C, then lyophilized (Labconco freeze-dry system, Germany) for 72h until to obtain the aerogels.

Appendix B: Supporting Information for Chapter 3

B.1. PAs characterization techniques

Total phenol concentration (TPC). The TPC present in the aerogels was determined according to the Folin-Ciocalteu method [173]. First, 2.5 mL of Folin-Ciocalteu reagent were dissolved with 2.0 mL of sodium carbonate solution (7.5% (w/v) and 0.5 mL of the aerogel sample. Next, this solution was heated for 15 min at 45°C and then, the absorbance was measured at 765 nm (Spectroquant® Prove 600 spectrometer; Merck KGaA, Germany). The total phenol content was calculated using the **Equation B.1:**

$$F_t = f_c * A_{bs} * D_i \quad (B.1)$$

where F_t is the total phenol content (gram equivalent gallic acid per gram of extract), f_c is an equivalence factor (0.0116 L solution/mg eq. gallic acid), A_{bs} is the absorbance of the sample (nm), and D_i is the sample dissolution. The results are expressed in units of milligram equivalent gallic acid per milligram of extract.

Phloroglucinolysis. The determination of the mDP, aMW, and molar composition of the grape skin extracts were determined by phloroglucinolysis method [174]. A solution of 0.1 moleq./HCl in methanol containing 50 g/L of phloroglucinol was reacted with 5.0 g/L of skin extracts for 20 min at 50°C. The final mixture was combined with 5 volumes of aqueous sodium acetate 40 mM to stop the reaction, and the compounds were detected with an HPLC at 280 nm (Merck-Hitachi chromatograph LaChrom L7000Series, with a gradient pump L-7100, Autosampler L-7200, UV detector L-4250) and two Chromolith Performance Series RP- 18e columns (Merck, Darmstadt, Germany). The mobile phases consisted of Milli-Q® water with 1% *v/v* aqueous acetic acid (for mobile phase A) and acetonitrile with 1% *v/v* acetic acid (for mobile phase B) and elution was performed with 3% B for 4 min. The linear gradients used in the experiment were set at 3-18% B for 14 min and 80% B for 2 min at a flow rate of 3 mL/min and 30°C. The column was washed with 3% B for 2 min before the next injection was performed. An external standard of catechin (100 mg of C/L) was used to quantify the sample. This procedure was performed in duplicate for each sample.

Gel permeation chromatography [175]**.** The samples (50 mg) were acetylated with pyridine and acetic anhydride (2.0 mL, 1:1, *v/v*) overnight at room temperature. The solvents were evaporated and the acetylated extracts were dissolved in tetrahydrofuran THF (10–15 mg/mL). The molecular weight distribution of the skin extracts was determined with the HPLC (ACME 9000, Young Lin Instrument Co. Ltd., Anyang, Korea), which was equipped with a UV/VIS detector and two PSS SDV gel columns (5

μm, 100 and 500 Å) of 30 cm and a PSS SDV gel precolumn (5 μm) equilibrated at 23°C. Analytes were detected at 254 nm using a flow rate of 1.0 mL/min for the mobile phase (THF) and an injection volume of 20 μL. Ten standards of polystyrenes with different molecular weights (Mw 162–19,950 Da) were used.

Absorption capacity of the aerogels. The absorption capacity of the aerogels was evaluated in a phosphate saline solution (PBS, pH=7.4, 37°C) and fresh human blood. To do this, PBS (50 μL) were continuously dropped on each aerogel sample (1.0 cm^3) until saturation. A similar procedure was performed with the fresh human blood. Next, the liquid supernatants were removed with a filter paper and the absorption capacity was calculated according to **Equation B.2**:

$$Absorption\ capacity\ (g/g) = \frac{W_{wet} - W_{dry}}{W_{dry}} \quad (B.2)$$

where W_{wet} is the wet sample weight (after contact with the liquid medium) and W_{dry} is the dry sample weight. Finally, the absorption capacities were expressed as grams of liquid per gram of aerogel (g/g) and the measurements were performed in quadruplicate.

Pore size measurements. The pore size measurements were performed using ImagesJ® software. A total of 100 random pore sizes for each aerogel were measured from SEM images. The frequency histograms of each aerogel were built for estimating their pore size distributions. The central limit theorem was applied to approximate the original distributions of each sample to a normally distributed one. These calculations were performed using a MATLAB algorithm where the original data were separated into sets of 40 random data each using a “sampling without replacement method” so that each sampling unit of the population was selected only once in the sample. The generated total data for plotting each histogram were 500000.

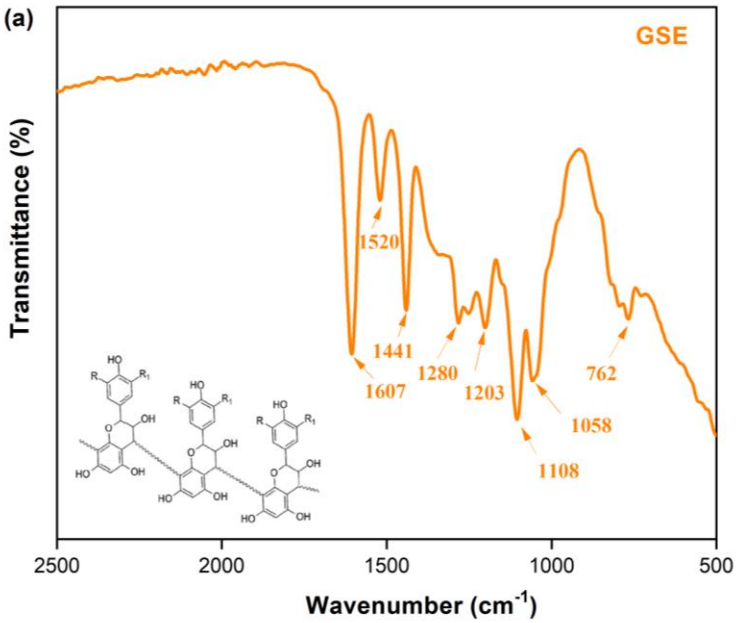

Figure B.1. ATR-FTIR spectrum of grape skin extracts.

Table B.1. Structural composition of grape skin extracts.

Compounds [a]	Content (µM)
C	156 ± 22
EC	nd
ECG	nd
C-P	92 ± 5
EC-P	2900 ± 152
ECG-P	267 ± 15
EGC-P	574 ± 46

[a]: flavan-3-ol subunits expressed in units of micromolar (µM) of (+)-catechin equivalents. C: (+)-catechin, EC: (-)-epicatechin, ECG: epigallocatechin, C-P: (+)-catechin-phloroglucinol, EC-P: (-)-epicatechin-phloroglucinol, ECG-P: epicatechin gallate-phloroglucinol, EGC-P: epigallocatechin-phloroglucinol, nd: not detected. The values are expressed as mean ± standard deviation (*n=2*).

Table B.2. Molecular weight distribution of grape skin extracts.

Molecules percentage (%)	Molecular weight (g/mol)
10.5	25807 – 14149
22.7	14149 – 8866
55.9	8866 – 1582

3.8	1582 – 1156
3.9	1156 – 791
3.1	791 - 451

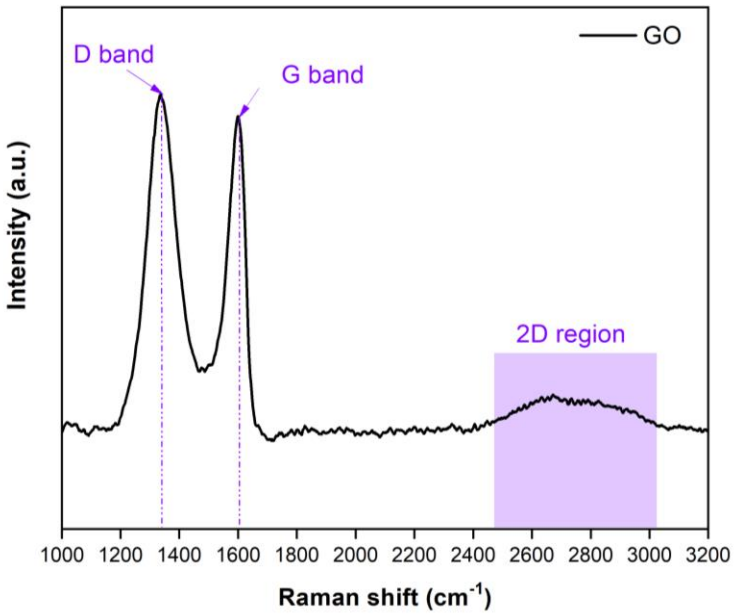

Figure B.2. Raman spectrum of GO.

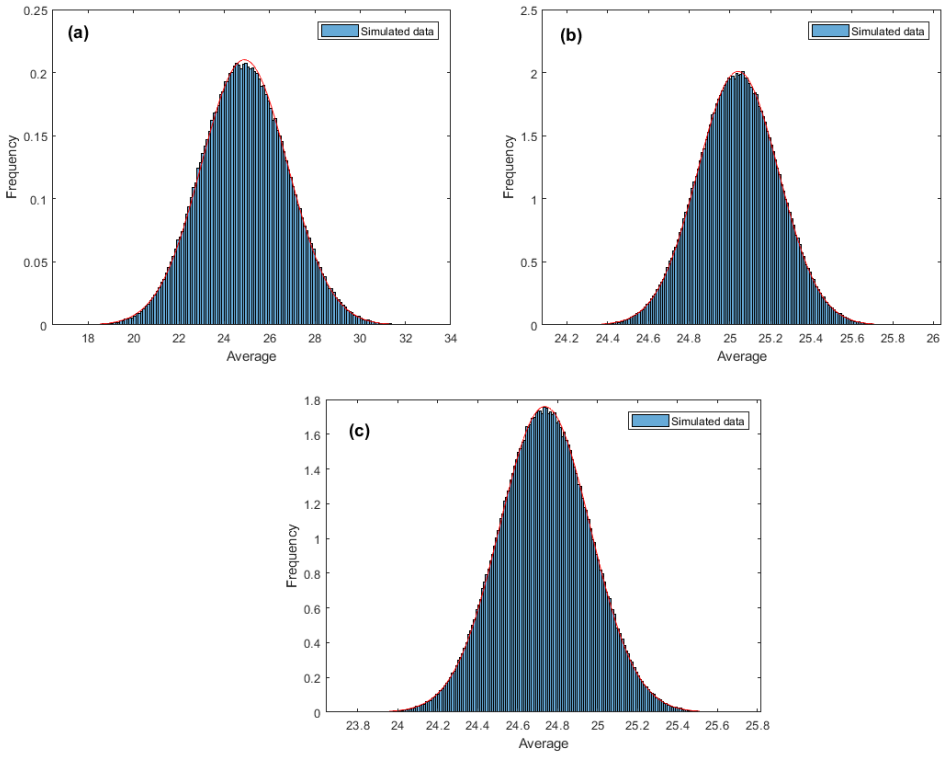

Figure B.3. Pore size distributions for (a) GEL-GO aerogel, (b) GEL-GO-5% aerogel, and (c) GEL-GO-10% aerogel, respectively.

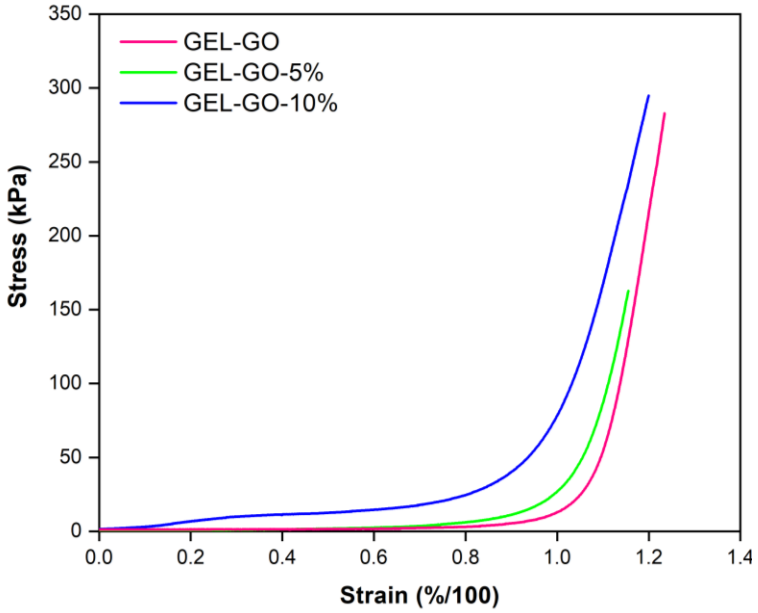

Figure B.4. Stress-strain curves for aerogels.

Table B.3. Phenol concentration values contained in each aerogel sample before and after the release test.

Before release test		
Aerogel code	Absorbance (nm)	Phenol concentration (mg eq. gallic acid /L)
GEL-GO-5%	0.072 ± 0.025	6.12 ± 2.155
GEL-GO-10%	0.132 ± 0.019	11.3 ± 1.638
After release test		
Aerogel code	Absorbance (nm)	Phenol concentration (mg eq. gallic acid /L)
GEL-GO-5%	0.053 ± 0.002	0.45 ± 0.172
GEL-GO-10%	0.023 ± 0.003	1.9 ± 0.259

The reported values are means ± SD

Appendix C: Main results obtained during the internship

As part of my internship at the Institute of Biomaterials at FAU University Erlangen-Nuremberg, Germany, I worked on the development of new biomaterials using GEL and poly(ε-Caprolactone) as starting polymers to produce nanofibrous materials loaded with *Pinus radiata* bark extracts for wound healing applications. The results obtained in this research are currently submitted to a scientific journal but are not published. Therefore, only the main results of this research will be briefly described below:

Abstract

In this study, poly (ε-Caprolactone) (PCL)/Gelatin (GEL) electrospun nanofibers loaded with two different concentrations of *Pinus radiata* bark extracts (PE) were fabricated via electrospinning for wound healing applications. The effects of incorporating PE into PCL/GEL electrospun nanofibers were investigated in terms of their physicochemical properties and *in vitro* biocompatibility. All electrospun nanofibers showed smooth, uniform, and bead-free surfaces. PE addition had no significant effect on the average fiber diameter. The electrospun nanofiber´s functional groups were detected by ATR-FTIR and their total phenol content was measured by a Folin-Ciocalteu assay. PE-loaded PCL/GEL electrospun nanofibers exhibited increased their wettability and decreased tensile stress values compared to PCL/GEL nanofibers. *In vitro* degradation studies showed a greater degradation rate over time for PE-loaded electrospun nanofibers than for the PCL/GEL nanofiber. *In vitro* release profiles evidenced an increase of PE content released over time for both PE-loaded electrospun nanofibers. The antibacterial studies demonstrated a slight bacteria viability reduction after 24h incubation in both bacteria strains, although no evident bacteriostatic and bactericidal effects were observed for both PE-loaded PCL/GEL electrospun nanofibers due to the samples' limited PE concentration. *In vitro* cell studies demonstrated that PE-loaded PCL/GEL electrospun nanofibers enhanced HaCaT cell growth, attachment, and proliferation. Similarly, PE-loaded electrospun nanofibers favored HaCaT cell migration towards the scratch area in the wound-healing assay, thus allowing a complete wound closure after 72h treatment. These findings provide evidence supporting that PE-loaded PCL/GEL electrospun nanofibers are promising candidates for wound healing usage, enlarging the family of phytotherapeutic agents containing fibers for such application.

References

[1] J. Chen, L. Lv, Y. Li, X. Ren, H. Luo, Y. Gao, H. Yan, Y. Li, Y. Qu, L. Yang, X. Li, R. Zeng, Preparation and evaluation of Bletilla striata polysaccharide/graphene oxide composite hemostatic sponge, International Journal of Biological Macromolecules. 130 (2019) 827–835. https://doi.org/10.1016/j.ijbiomac.2019.02.137.

[2] C. Feng, J. Li, G.S. Wu, Y.Z. Mu, M. Kong, C.Q. Jiang, X.J. Cheng, Y. Liu, X.G. Chen, Chitosan-Coated Diatom Silica as Hemostatic Agent for Hemorrhage Control, ACS Appl. Mater. Interfaces. 8 (2016) 34234–34243. https://doi.org/10.1021/acsami.6b12317.

[3] L. Wang, X. You, C. Dai, T. Tong, J. Wu, Hemostatic nanotechnologies for external and internal hemorrhage management, Biomaterials Science. 8 (2020) 4396–4412. https://doi.org/10.1039/D0BM00781A.

[4] B. Wu, F. Du, A. Wenjing, G. Li, X. Wang, Graphene-based hemostatic sponge, Chinese Chemical Letters. (2021). https://doi.org/10.1016/j.cclet.2021.06.029.

[5] C. Mellado, T. Figueroa, R. Baez, R. Castillo, M. Melendrez, B. Schulz, K. Fernandez, Development of Graphene Oxide Composite Aerogel with Proanthocyanidins with Hemostatic Properties As a Delivery System, ACS Appl. Mater. Interfaces. 10 (2018) 7717–7729. https://doi.org/10.1021/acsami.7b16084.

[6] D.S. Kauvar, R. Lefering, C.E. Wade, Impact of Hemorrhage on Trauma Outcome: An Overview of Epidemiology, Clinical Presentations, and Therapeutic Considerations, Journal of Trauma and Acute Care Surgery. 60 (2006) S3. https://doi.org/10.1097/01.ta.0000199961.02677.19.

[7] Y. Liang, C. Xu, G. Li, T. Liu, J.F. Liang, X. Wang, Graphene-kaolin composite sponge for rapid and riskless hemostasis, Colloids and Surfaces B: Biointerfaces. 169 (2018) 168–175. https://doi.org/10.1016/j.colsurfb.2018.05.016.

[8] J. Cabral, A.E. Ryan, M.D. Griffin, T. Ritter, Extracellular vesicles as modulators of wound healing, Advanced Drug Delivery Reviews. 129 (2018) 394–406. https://doi.org/10.1016/j.addr.2018.01.018.

[9] G. Li, K. Quan, C. Xu, B. Deng, X. Wang, Synergy in thrombin-graphene sponge for improved hemostatic efficacy and facile utilization, Colloids and Surfaces B: Biointerfaces. 161 (2018) 27–34. https://doi.org/10.1016/j.colsurfb.2017.10.021.

[10] U.A. Sezer, Z. Kocer, B. Aru, G.Y. Demirel, M. Gulmez, A. Aktekin, S. Ozkara, S. Sezer, Combination of gelatin and tranexamic acid offers improved haemostasis and safe use on

internal hemorrhage control, RSC Adv. 6 (2016) 95189–95198. https://doi.org/10.1039/C6RA16790J.

[11] R. Ma, Y. Wang, H. Qi, C. Shi, G. Wei, L. Xiao, Z. Huang, S. Liu, H. Yu, C. Teng, H. Liu, V. Murugadoss, J. Zhang, Y. Wang, Z. Guo, Nanocomposite sponges of sodium alginate/graphene oxide/polyvinyl alcohol as potential wound dressing: In vitro and in vivo evaluation, Composites Part B: Engineering. 167 (2019) 396–405. https://doi.org/10.1016/j.compositesb.2019.03.006.

[12] G. Li, Y. Liang, C. Xu, H. Sun, L. Tao, Y. Wei, X. Wang, Polydopamine reinforced hemostasis of a graphene oxide sponge via enhanced platelet stimulation, Colloids and Surfaces B: Biointerfaces. 174 (2019) 35–41. https://doi.org/10.1016/j.colsurfb.2018.10.074.

[13] K. Quan, G. Li, D. Luan, Q. Yuan, L. Tao, X. Wang, Black hemostatic sponge based on facile prepared cross-linked graphene, Colloids and Surfaces B: Biointerfaces. 132 (2015) 27–33. https://doi.org/10.1016/j.colsurfb.2015.04.067.

[14] K. Quan, G. Li, L. Tao, Q. Xie, Q. Yuan, X. Wang, Diaminopropionic Acid Reinforced Graphene Sponge and Its Use for Hemostasis, ACS Appl. Mater. Interfaces. 8 (2016) 7666–7673. https://doi.org/10.1021/acsami.5b12715.

[15] T. Figueroa, S. Carmona, S. Guajardo, J. Borges, C. Aguayo, K. Fernández, Synthesis and characterization of graphene oxide chitosan aerogels reinforced with flavan-3-ols as hemostatic agents, Colloids and Surfaces B: Biointerfaces. 197 (2021) 111398. https://doi.org/10.1016/j.colsurfb.2020.111398.

[16] S. Guajardo, T. Figueroa, J. Borges, C. Aguayo, K. Fernández, Graphene oxide-gelatin aerogels as wound dressings with improved hemostatic properties, Materials Today Chemistry. 20 (2021) 100418. https://doi.org/10.1016/j.mtchem.2020.100418.

[17] J. Borges-Vilches, J. Poblete, F. Gajardo, C. Aguayo, K. Fernández, Graphene oxide/polyethylene glycol aerogel reinforced with grape seed extracts as wound dressing, J Mater Sci. 56 (2021) 16082–16096. https://doi.org/10.1007/s10853-021-06297-z.

[18] J. Borges-Vilches, T. Figueroa, S. Guajardo, C. Aguayo, K. Fernández, Improved hemocompatibility for gelatin-graphene oxide composite aerogels reinforced with proanthocyanidins for wound dressing applications, Colloids and Surfaces B: Biointerfaces. 206 (2021) 111941. https://doi.org/10.1016/j.colsurfb.2021.111941.

[19] L. Zheng, S. Zhang, Z. Ying, J. Liu, Y. Zhou, F. Chen, Engineering of Aerogel-Based Biomaterials for Biomedical Applications, Int J Nanomedicine. 15 (2020) 2363–2378. https://doi.org/10.2147/IJN.S238005.

[20] A. Du, B. Zhou, Z. Zhang, J. Shen, A Special Material or a New State of Matter: A Review and Reconsideration of the Aerogel, Materials. 6 (2013) 941–968. https://doi.org/10.3390/ma6030941.

[21] Y. Ma, Y. Chen, Three-dimensional graphene networks: synthesis, properties and applications, Natl. Sci. Rev. 2 (2015) 40–53. https://doi.org/10.1093/nsr/nwu072.

[22] H. Maleki, S. Montes, N. Hayati-Roodbari, F. Putz, N. Huesing, Compressible, Thermally Insulating, and Fire Retardant Aerogels through Self-Assembling Silk Fibroin Biopolymers Inside a Silica Structure—An Approach towards 3D Printing of Aerogels, ACS Appl. Mater. Interfaces. 10 (2018) 22718–22730. https://doi.org/10.1021/acsami.8b05856.

[23] S.K. Singh, M.K. Singh, M.K. Nayak, S. Kumari, S. Shrivastava, J.J.A. Grácio, D. Dash, Thrombus Inducing Property of Atomically Thin Graphene Oxide Sheets, ACS Nano. 5 (2011) 4987–4996. https://doi.org/10.1021/nn201092p.

[24] R. Feng, Y. Yu, C. Shen, Y. Jiao, C. Zhou, Impact of graphene oxide on the structure and function of important multiple blood components by a dose-dependent pattern, Journal of Biomedical Materials Research Part A. 103 (2015) 2006–2014. https://doi.org/10.1002/jbm.a.35341.

[25] B. Cai, K. Hu, C. Li, J. Jin, Y. Hu, Bovine serum albumin bioconjugated graphene oxide: Red blood cell adhesion and hemolysis studied by QCM-D, Applied Surface Science. 356 (2015) 844–851. https://doi.org/10.1016/j.apsusc.2015.08.178.

[26] K.-H. Liao, Y.-S. Lin, C.W. Macosko, C.L. Haynes, Cytotoxicity of Graphene Oxide and Graphene in Human Erythrocytes and Skin Fibroblasts, ACS Appl. Mater. Interfaces. 3 (2011) 2607–2615. https://doi.org/10.1021/am200428v.

[27] R.K. Layek, A.K. Nandi, A review on synthesis and properties of polymer functionalized graphene, Polymer. 54 (2013) 5087–5103. https://doi.org/10.1016/j.polymer.2013.06.027.

[28] D. Ege, A.R. Kamali, A.R. Boccaccini, Graphene Oxide/Polymer-Based Biomaterials, Adv. Eng. Mater. 19 (2017) 1700627. https://doi.org/10.1002/adem.201700627.

[29] Y. Zhang, J. Guan, J. Wu, S. Ding, J. Yang, J. Zhang, A. Dong, L. Deng, N-alkylated chitosan/graphene oxide porous sponge for rapid and effective hemostasis in emergency situations, Carbohydrate Polymers. 219 (2019) 405–413. https://doi.org/10.1016/j.carbpol.2019.05.028.

[30] R. Ma, Y. Wang, H. Qi, C. Shi, G. Wei, L. Xiao, Z. Huang, S. Liu, H. Yu, C. Teng, H. Liu, V. Murugadoss, J. Zhang, Y. Wang, Z. Guo, Nanocomposite sponges of sodium alginate/graphene

oxide/polyvinyl alcohol as potential wound dressing: In vitro and in vivo evaluation, Composites Part B: Engineering. 167 (2019) 396–405. https://doi.org/10.1016/j.compositesb.2019.03.006.

[31] A.H.Z. Kalkhoran, S.M. Naghib, O. Vahidi, M. Rahmanian, Synthesis and characterization of graphene-grafted gelatin nanocomposite hydrogels as emerging drug delivery systems, Biomed. Phys. Eng. Express. 4 (2018) 055017. https://doi.org/10.1088/2057-1976/aad745.

[32] I. Unalan, S.J. Endlein, B. Slavik, A. Buettner, W.H. Goldmann, R. Detsch, A.R. Boccaccini, Evaluation of Electrospun Poly(ε-Caprolactone)/Gelatin Nanofiber Mats Containing Clove Essential Oil for Antibacterial Wound Dressing, Pharmaceutics. 11 (2019) 570. https://doi.org/10.3390/pharmaceutics11110570.

[33] T. E, M. A, CatersonE.J, Extracellular Matrix and Dermal Fibroblast Function in the Healing Wound, Advances in Wound Care. (2016). https://doi.org/10.1089/wound.2014.0561.

[34] T. Manon-Jensen, N.G. Kjeld, M.A. Karsdal, Collagen-mediated hemostasis, Journal of Thrombosis and Haemostasis. 14 (2016) 438–448. https://doi.org/10.1111/jth.13249.

[35] R. Ramalingam, C. Dhand, C.M. Leung, H. Ezhilarasu, P. Prasannan, S.T. Ong, S. Subramanian, M. Kamruddin, R. Lakshminarayanan, S. Ramakrishna, N.K. Verma, K.D. Arunachalam, Poly-ε-Caprolactone/Gelatin Hybrid Electrospun Composite Nanofibrous Mats Containing Ultrasound Assisted Herbal Extract: Antimicrobial and Cell Proliferation Study, Nanomaterials. 9 (2019) 462. https://doi.org/10.3390/nano9030462.

[36] P.S. Mohamadi, A. Hivechi, H. Bahrami, N. hemmatinegad, P.B. Milan, Antibacterial and biological properties of coconut oil loaded poly(ε-caprolactone)/gelatin electrospun membranes, Journal of Industrial Textiles. (2021) 1528083721991595. https://doi.org/10.1177/1528083721991595.

[37] Y. Piao, B. Chen, Synthesis and mechanical properties of double cross-linked gelatin-graphene oxide hydrogels, International Journal of Biological Macromolecules. 101 (2017) 791–798. https://doi.org/10.1016/j.ijbiomac.2017.03.155.

[38] G. Chen, C. Qiao, Y. Wang, J. Yao, Synthesis of Biocompatible Gelatin-functionalised Graphene Nanosheets For Drug Delivery Applications, Aust. J. Chem. 67 (2014) 1532–1537. https://doi.org/10.1071/CH13678.

[39] Y. Piao, B. Chen, Self-assembled graphene oxide–gelatin nanocomposite hydrogels: Characterization, formation mechanisms, and pH-sensitive drug release behavior, Journal of Polymer Science Part B: Polymer Physics. 53 (2015) 356–367. https://doi.org/10.1002/polb.23636.

[40] V. Georgiev, A. Ananga, V. Tsolova, Recent Advances and Uses of Grape Flavonoids as Nutraceuticals, Nutrients. 6 (2014) 391–415. https://doi.org/10.3390/nu6010391.

[41] D.A. Locilento, L.A. Mercante, R.S. Andre, L.H.C. Mattoso, G.L.F. Luna, P. Brassolatti, F. de F. Anibal, D.S. Correa, Biocompatible and Biodegradable Electrospun Nanofibrous Membranes Loaded with Grape Seed Extract for Wound Dressing Application, Journal of Nanomaterials. 2019 (2019) e2472964. https://doi.org/10.1155/2019/2472964.

[42] I. Unalan, B. Slavik, A. Buettner, W.H. Goldmann, G. Frank, A.R. Boccaccini, Physical and Antibacterial Properties of Peppermint Essential Oil Loaded Poly (ε-caprolactone) (PCL) Electrospun Fiber Mats for Wound Healing, Front Bioeng Biotechnol. 7 (2019). https://doi.org/10.3389/fbioe.2019.00346.

[43] D.R. Dreyer, S. Park, C.W. Bielawski, R.S. Ruoff, The chemistry of graphene oxide, Chem. Soc. Rev. 39 (2010) 228–240. https://doi.org/10.1039/b917103g.

[44] S. Das, S. Singh, V. Singh, D. Joung, J.M. Dowding, D. Reid, J. Anderson, L. Zhai, S.I. Khondaker, W.T. Self, S. Seal, Oxygenated Functional Group Density on Graphene Oxide: Its Effect on Cell Toxicity, Particle & Particle Systems Characterization. 30 (2013) 148–157. https://doi.org/10.1002/ppsc.201200066.

[45] D.C. Marcano, D.V. Kosynkin, J.M. Berlin, A. Sinitskii, Z. Sun, A. Slesarev, L.B. Alemany, W. Lu, J.M. Tour, Improved Synthesis of Graphene Oxide, ACS Nano. 4 (2010) 4806–4814. https://doi.org/10.1021/nn1006368.

[46] B.C. Brodie, XIII. On the atomic weight of graphite, Philosophical Transactions of the Royal Society of London. 149 (1859) 249–259. https://doi.org/10.1098/rstl.1859.0013.

[47] J. Chen, B. Yao, C. Li, G. Shi, An improved Hummers method for eco-friendly synthesis of graphene oxide, Carbon. 64 (2013) 225–229. https://doi.org/10.1016/j.carbon.2013.07.055.

[48] W.S.H. Jr, R.E. Offeman, Preparation of Graphitic Oxide, ACS Publications. (2002). https://doi.org/10.1021/ja01539a017.

[49] S. Wang, F. Tristan, D. Minami, T. Fujimori, R. Cruz-Silva, M. Terrones, K. Takeuchi, K. Teshima, F. Rodriguez-Reinoso, M. Endo, K. Kaneko, Activation routes for high surface area graphene monoliths from graphene oxide colloids, Carbon. 76 (2014) 220–231. https://doi.org/10.1016/j.carbon.2014.04.071.

[50] D.P. Singh, C.E. Herrera, B. Singh, S. Singh, R.K. Singh, R. Kumar, Graphene oxide: An efficient material and recent approach for biotechnological and biomedical applications,

Materials Science and Engineering: C. 86 (2018) 173–197. https://doi.org/10.1016/j.msec.2018.01.004.

[51] A. Bianco, H.-M. Cheng, T. Enoki, Y. Gogotsi, R.H. Hurt, N. Koratkar, T. Kyotani, M. Monthioux, C.R. Park, J.M.D. Tascon, J. Zhang, All in the graphene family – A recommended nomenclature for two-dimensional carbon materials, Carbon. 65 (2013) 1–6. https://doi.org/10.1016/j.carbon.2013.08.038.

[52] K.-H. Liao, A. Mittal, S. Bose, C. Leighton, K.A. Mkhoyan, C.W. Macosko, Aqueous Only Route toward Graphene from Graphite Oxide, ACS Nano. 5 (2011) 1253–1258. https://doi.org/10.1021/nn1028967.

[53] D. Bitounis, H. Ali-Boucetta, B.H. Hong, D.-H. Min, K. Kostarelos, Prospects and Challenges of Graphene in Biomedical Applications, Adv. Mater. 25 (2013) 2258–2268. https://doi.org/10.1002/adma.201203700.

[54] J. An, Y. Gou, C. Yang, F. Hu, C. Wang, Synthesis of a biocompatible gelatin functionalized graphene nanosheets and its application for drug delivery, Mater. Sci. Eng. C-Mater. Biol. Appl. 33 (2013) 2827–2837. https://doi.org/10.1016/j.msec.2013.03.008.

[55] H. Shen, L. Zhang, M. Liu, Z. Zhang, Biomedical Applications of Graphene, Theranostics. 2 (2012) 283–294. https://doi.org/10.7150/thno.3642.

[56] M.K. Satapathy, Y.B. Manga, K.K. Ostrikov, W.-H. Chiang, A. Pandey, L. R, B. Nyambat, E.-Y. Chuang, C.-H. Chen, Microplasma Cross-Linked Graphene Oxide-Gelatin Hydrogel for Cartilage Reconstructive Surgery, ACS Appl. Mater. Interfaces. 12 (2020) 86–95. https://doi.org/10.1021/acsami.9b14073.

[57] O. Akhavan, E. Ghaderi, S.A. Shirazian, R. Rahighi, Rolled graphene oxide foams as three-dimensional scaffolds for growth of neural fibers using electrical stimulation of stem cells, Carbon. 97 (2016) 71–77. https://doi.org/10.1016/j.carbon.2015.06.079.

[58] O. Akhavan, E. Ghaderi, S. Aghayee, Y. Fereydooni, A. Talebi, The use of a glucose-reduced graphene oxide suspension for photothermal cancer therapy, J. Mater. Chem. 22 (2012) 13773–13781. https://doi.org/10.1039/c2jm31396k.

[59] K. Muazim, Z. Hussain, Graphene oxide A platform towards theranostics, Mater. Sci. Eng. C-Mater. Biol. Appl. 76 (2017) 1274–1288. https://doi.org/10.1016/j.msec.2017.02.121.

[60] H. Wang, X. Yuan, Y. Wu, H. Huang, X. Peng, G. Zeng, H. Zhong, J. Liang, M. Ren, Graphene-based materials: Fabrication, characterization and application for the decontamination of

wastewater and wastegas and hydrogen storage/generation, Adv. Colloid Interface Sci. 195 (2013) 19–40. https://doi.org/10.1016/j.cis.2013.03.009.

[61] S. Syama, P.V. Mohanan, Safety and biocompatibility of graphene: A new generation nanomaterial for biomedical application, Int. J. Biol. Macromol. 86 (2016) 546–555. https://doi.org/10.1016/j.ijbiomac.2016.01.116.

[62] P. Zare, M. Aleemardani, A. Seifalian, Z. Bagher, A.M. Seifalian, Graphene Oxide: Opportunities and Challenges in Biomedicine, Nanomaterials. 11 (2021) 1083. https://doi.org/10.3390/nano11051083.

[63] V. Georgakilas, J.N. Tiwari, K.C. Kemp, J.A. Perman, A.B. Bourlinos, K.S. Kim, R. Zboril, Noncovalent Functionalization of Graphene and Graphene Oxide for Energy Materials, Biosensing, Catalytic, and Biomedical Applications, Chem. Rev. 116 (2016) 5464–5519. https://doi.org/10.1021/acs.chemrev.5b00620.

[64] B. Zhang, Y. Wang, G. Zhai, Biomedical applications of the graphene-based materials, Materials Science and Engineering: C. 61 (2016) 953–964. https://doi.org/10.1016/j.msec.2015.12.073.

[65] S.M. Ahsan, C.M. Rao, The role of surface charge in the desolvation process of gelatin: implications in nanoparticle synthesis and modulation of drug release, Int. J. Nanomed. 12 (2017) 795–808. https://doi.org/10.2147/IJN.S124938.

[66] K. Hayashi, Y. Tabata, Preparation of stem cell aggregates with gelatin microspheres to enhance biological functions, Acta Biomater. 7 (2011) 2797–2803. https://doi.org/10.1016/j.actbio.2011.04.013.

[67] S. Kommareddy, D.B. Shenoy, M.M. Amiji, Gelatin Nanoparticles and Their Biofunctionalization, in: Nanotechnologies for the Life Sciences, John Wiley & Sons, Ltd, 2007. https://doi.org/10.1002/9783527610419.ntls0011.

[68] A.A. Karim, R. Bhat, Fish gelatin: properties, challenges, and prospects as an alternative to mammalian gelatins, Food Hydrocolloids. 23 (2009) 563–576. https://doi.org/10.1016/j.foodhyd.2008.07.002.

[69] T. Yan, F. Cheng, X. Wei, Y. Huang, J. He, Biodegradable collagen sponge reinforced with chitosan/calcium pyrophosphate nanoflowers for rapid hemostasis, Carbohydrate Polymers. 170 (2017) 271–280. https://doi.org/10.1016/j.carbpol.2017.04.080.

[70] X. Xiao, G. Wu, H. Zhou, K. Qian, J. Hu, Preparation and Property Evaluation of Conductive Hydrogel Using Poly (Vinyl Alcohol)/Polyethylene Glycol/Graphene Oxide for Human Electrocardiogram Acquisition, Polymers. 9 (2017) 259. https://doi.org/10.3390/polym9070259.

[71] Y. Piao, B. Chen, One-pot synthesis and characterization of reduced graphene oxide-gelatin nanocomposite hydrogels, RSC Adv. 6 (2016) 6171–6181. https://doi.org/10.1039/c5ra20674j.

[72] M. Guastaferro, E. Reverchon, L. Baldino, Polysaccharide-Based Aerogel Production for Biomedical Applications: A Comparative Review, Materials. 14 (2021) 1631. https://doi.org/10.3390/ma14071631.

[73] H.-Y. Mi, X. Jing, Z. Cai, Y. Liu, L.-S. Turng, S. Gong, Highly porous composite aerogel based triboelectric nanogenerators for high performance energy generation and versatile self-powered sensing, Nanoscale. 10 (2018) 23131–23140. https://doi.org/10.1039/C8NR05872E.

[74] L. Li, F. Lu, C. Wang, F. Zhang, W. Liang, S. Kuga, Z. Dong, Y. Zhao, Y. Huang, M. Wu, Flexible double-cross-linked cellulose-based hydrogel and aerogel membrane for supercapacitor separator, Journal of Materials Chemistry A. 6 (2018) 24468–24478. https://doi.org/10.1039/C8TA07751G.

[75] A. Deb, N.G. Andrews, V. Raghavan, Natural polymer functionalized graphene oxide for co-delivery of anticancer drugs: In-vitro and in-vivo, International Journal of Biological Macromolecules. 113 (2018) 515–525. https://doi.org/10.1016/j.ijbiomac.2018.02.153.

[76] H. Bai, C. Li, X. Wang, G. Shi, On the Gelation of Graphene Oxide, J. Phys. Chem. C. 115 (2011) 5545–5551. https://doi.org/10.1021/jp1120299.

[77] U.J. Unachukwu, S. Ahmed, A. Kavalier, J.T. Lyles, E.J. Kennelly, White and Green Teas (Camellia sinensis var. sinensis): Variation in Phenolic, Methylxanthine, and Antioxidant Profiles, Journal of Food Science. 75 (2010) C541–C548. https://doi.org/10.1111/j.1750-3841.2010.01705.x.

[78] C.G. Fraga, M. Galleano, S.V. Verstraeten, P.I. Oteiza, Basic biochemical mechanisms behind the health benefits of polyphenols, Mol. Aspects Med. 31 (2010) 435–445. https://doi.org/10.1016/j.mam.2010.09.006.

[79] K. Fernández, J. Labra, Simulated digestion of proanthocyanidins in grape skin and seed extracts and the effects of digestion on the angiotensin I-converting enzyme (ACE) inhibitory activity, Food Chemistry. 139 (2013) 196–202. https://doi.org/10.1016/j.foodchem.2013.01.021.

[80] K. Fernández, J.A. Kennedy, E. Agosin, Characterization of Vitis vinifera L. Cv. Carménère Grape and Wine Proanthocyanidins, J. Agric. Food Chem. 55 (2007) 3675–3680. https://doi.org/10.1021/jf063232b.

[81] N. Unusan, Proanthocyanidins in grape seeds: An updated review of their health benefits and potential uses in the food industry, Journal of Functional Foods. 67 (2020) 103861. https://doi.org/10.1016/j.jff.2020.103861.

[82] G. Eriz, V. Sanhueza, M. Roeckel, K. Fernández, Inhibition of the angiotensin-converting enzyme by grape seed and skin proanthocyanidins extracted from Vitis vinífera L. cv. País, LWT - Food Science and Technology. 44 (2011) 860–865. https://doi.org/10.1016/j.lwt.2010.11.034.

[83] K. Rinki, P.K. Dutta, A.J. Hunt, D.J. Macquarrie, J.H. Clark, Chitosan Aerogels Exhibiting High Surface Area for Biomedical Application: Preparation, Characterization, and Antibacterial Study, International Journal of Polymeric Materials. 60 (2011) 988–999. https://doi.org/10.1080/00914037.2011.553849.

[84] M. Bijak, J. Kolodziejczyk-Czepas, M.B. Ponczek, J. Saluk, P. Nowak, Protective effects of grape seed extract against oxidative and nitrative damage of plasma proteins, Int. J. Biol. Macromol. 51 (2012) 183–187. https://doi.org/10.1016/j.ijbiomac.2012.05.009.

[85] L.Q. Xu, K.-G. Neoh, E.-T. Kang, Natural polyphenols as versatile platforms for material engineering and surface functionalization, Progress in Polymer Science. 87 (2018) 165–196. https://doi.org/10.1016/j.progpolymsci.2018.08.005.

[86] M. Gupta, S. Dey, D. Marbaniang, P. Pal, S. Ray, B. Mazumder, Grape seed extract: having a potential health benefits, J Food Sci Technol. 57 (2020) 1205–1215. https://doi.org/10.1007/s13197-019-04113-w.

[87] Z. Ghouila, S. Laurent, S. Boutry, L.V. Elst, F. Nateche, R.N. Muller, A. Baaliouamer, Antioxidant, antibacterial and cell toxicity effects of polyphenols Fromahmeur bouamer grape seed extracts, Journal of Fundamental and Applied Sciences. 9 (2017) 392–420. https://doi.org/10.4314/jfas.v9i1.24.

[88] Y. Du, W.-Z. Qiu, Z.L. Wu, P.-F. Ren, Q. Zheng, Z.-K. Xu, Water-Triggered Self-Healing Coatings of Hydrogen-Bonded Complexes for High Binding Affinity and Antioxidative Property, Advanced Materials Interfaces. 3 (2016) 1600167. https://doi.org/10.1002/admi.201600167.

[89] Y.-N. Chen, L. Peng, T. Liu, Y. Wang, S. Shi, H. Wang, Poly(vinyl alcohol)–Tannic Acid Hydrogels with Excellent Mechanical Properties and Shape Memory Behaviors, ACS Appl. Mater. Interfaces. 8 (2016) 27199–27206. https://doi.org/10.1021/acsami.6b08374.

[90] W. Jin, W. Xu, H. Ge, Y. Li, B. Li, Polyphenol–gelatin nanoparticles as reductant and stabilizer for one-step synthesis of gold nanoparticles and their interfacial behavior, RSC Adv. 5 (2015) 26496–26503. https://doi.org/10.1039/C5RA02566D.

[91] C. Ringwald, V. Ball, Step-by-step deposition of type B gelatin and tannic acid displays a peculiar ionic strength dependence at pH 5, RSC Adv. 6 (2016) 4730–4738. https://doi.org/10.1039/C5RA24337H.

[92] I.H. Jaffer, J.I. Weitz, The blood compatibility challenge. Part 1: Blood-contacting medical devices: The scope of the problem, Acta Biomaterialia. 94 (2019) 2–10. https://doi.org/10.1016/j.actbio.2019.06.021.

[93] C. Sepúlveda, I. Palomo, E. Fuentes, Primary and secondary haemostasis changes related to aging, Mechanisms of Ageing and Development. 150 (2015) 46–54. https://doi.org/10.1016/j.mad.2015.08.006.

[94] J.L. Brash, T.A. Horbett, R.A. Latour, P. Tengvall, The blood compatibility challenge. Part 2: Protein adsorption phenomena governing blood reactivity, Acta Biomaterialia. 94 (2019) 11–24. https://doi.org/10.1016/j.actbio.2019.06.022.

[95] V.A. Terent'eva, A.N. Sveshnikova, M.A. Panteleev, Biophysical mechanisms of contact activation of blood-plasma clotting, BIOPHYSICS. 62 (2017) 742–753. https://doi.org/10.1134/S0006350917050232.

[96] C. Zheng, Q. Zeng, S. Pimpi, W. Wu, K. Han, K. Dong, T. Lu, Research status and development potential of composite hemostatic materials, J. Mater. Chem. B. 8 (2020) 5395–5410. https://doi.org/10.1039/D0TB00906G.

[97] I.S. Timan, Y. Funahara, R. Setiabudy, J. Latu, E. Silman, PF3 activity in normal subjects and beta-thalassemia trait, Southeast Asian J Trop Med Public Health. 24 Suppl 1 (1993) 216–218.

[98] Z. Li, S. Hu, K. Cheng, Platelets and their biomimetics for regenerative medicine and cancer therapies, J. Mater. Chem. B. 6 (2018) 7354–7365. https://doi.org/10.1039/C8TB02301H.

[99] J. Zhang, S. Xue, X. Zhu, Y. Zhao, Y. Chen, J. Tong, X. Shi, Y. Du, Z. Zhong, Q. Ye, Emerging chitin nanogels/rectorite nanocomposites for safe and effective hemorrhage control, J. Mater. Chem. B. 7 (2019) 5096–5103. https://doi.org/10.1039/C9TB01019J.

[100] Z. Chen, L. Han, C. Liu, Y. Du, X. Hu, G. Du, C. Shan, K. Yang, C. Wang, M. Li, F. Li, F. Tian, A rapid hemostatic sponge based on large, mesoporous silica nanoparticles and N-alkylated chitosan, Nanoscale. 10 (2018) 20234–20245. https://doi.org/10.1039/C8NR07865C.

[101] Kenry, K.P. Loh, C.T. Lim, Molecular Hemocompatibility of Graphene Oxide and Its Implication for Antithrombotic Applications, Small. 11 (2015) 5105–5117. https://doi.org/10.1002/smll.201500841.

[102] Kenry, A. Geldert, Y. Liu, K.P. Loh, C. Teck Lim, Nano-bio interactions between carbon nanomaterials and blood plasma proteins: why oxygen functionality matters, NPG Asia Materials. 9 (2017) e422. https://doi.org/10.1038/am.2017.129.

[103] O. Dangles, C. Dufour, C. Manach, C. Morand, C. Remesy, Binding of flavonoids to plasma proteins, Methods Enzymol. 335 (2001) 319–333.

[104] C. Santos-Buelga, A. Scalbert, Proanthocyanidins and tannin-like compounds - nature, occurrence, dietary intake and effects on nutrition and health, J. Sci. Food Agric. 80 (2000) 1094–1117. https://doi.org/10.1002/(SICI)1097-0010(20000515)80:7<1094::AID-JSFA569>3.0.CO;2-1.

[105] J. Liu, L. Cui, D. Losic, Graphene and graphene oxide as new nanocarriers for drug delivery applications, Acta Biomater. 9 (2013) 9243–9257. https://doi.org/10.1016/j.actbio.2013.08.016.

[106] B. Luan, T. Huynh, L. Zhao, R. Zhou, Potential Toxicity of Graphene to Cell Functions via Disrupting Protein–Protein Interactions, ACS Nano. 9 (2015) 663–669. https://doi.org/10.1021/nn506011j.

[107] M. Dallavalle, M. Calvaresi, A. Bottoni, M. Melle-Franco, F. Zerbetto, Graphene Can Wreak Havoc with Cell Membranes, ACS Appl. Mater. Interfaces. 7 (2015) 4406–4414. https://doi.org/10.1021/am508938u.

[108] G. Li, K. Quan, Y. Liang, T. Li, Q. Yuan, L. Tao, Q. Xie, X. Wang, Graphene-Montmorillonite Composite Sponge for Safe and Effective Hemostasis, ACS Appl. Mater. Interfaces. 8 (2016) 35071–35080. https://doi.org/10.1021/acsami.6b13302.

[109] X. Cao, Z. Yin, H. Zhang, Three-dimensional graphene materials: preparation, structures and application in supercapacitors, Energy & Environmental Science. 7 (2014) 1850–1865. https://doi.org/10.1039/C4EE00050A.

[110] H. Ha, K. Shanmuganathan, C.J. Ellison, Mechanically Stable Thermally Crosslinked Poly(acrylic acid)/Reduced Graphene Oxide Aerogels, ACS Appl. Mater. Interfaces. 7 (2015) 6220–6229. https://doi.org/10.1021/acsami.5b00407.

[111] R. Scaffaro, A. Maio, F. Lopresti, D. Giallombardo, L. Botta, M.L. Bondi, S. Agnello, Synthesis and self-assembly of a PEGylated-graphene aerogel, Compos. Sci. Technol. 128 (2016) 193–200. https://doi.org/10.1016/j.compscitech.2016.03.030.

[112] Y. Pan, H. Bao, L. Li, Noncovalently Functionalized Multiwalled Carbon Nanotubes by Chitosan-Grafted Reduced Graphene Oxide and Their Synergistic Reinforcing Effects in Chitosan Films, ACS Appl. Mater. Interfaces. 3 (2011) 4819–4830. https://doi.org/10.1021/am2013135.

[113] A. Bigi, S. Panzavolta, K. Rubini, Relationship between triple-helix content and mechanical properties of gelatin films, Biomaterials. 25 (2004) 5675–5680. https://doi.org/10.1016/j.biomaterials.2004.01.033.

[114] M. Bardts, N. Gonsior, H. Ritter, Polymer synthesis and modification by use of microwaves, Macromol. Chem. Phys. 209 (2008) 25–31. https://doi.org/10.1002/macp.200700443.

[115] J.P. Cook, G.W. Goodall, O.V. Khutoryanskaya, V.V. Khutoryanskiy, Microwave-Assisted Hydrogel Synthesis: A New Method for Crosslinking Polymers in Aqueous Solutions, Macromol. Rapid Commun. 33 (2012) 332–336. https://doi.org/10.1002/marc.201100742.

[116] C. Chen, J. Xi, E. Zhou, L. Peng, Z. Chen, C. Gao, Porous Graphene Microflowers for High-Performance Microwave Absorption, Nano-Micro Lett. 10 (2018) 26. https://doi.org/10.1007/s40820-017-0179-8.

[117] Y.-J. Zhu, F. Chen, Microwave-Assisted Preparation of Inorganic Nanostructures in Liquid Phase, Chem. Rev. 114 (2014) 6462–6555. https://doi.org/10.1021/cr400366s.

[118] M.S. Hoque, S. Benjakul, T. Prodpran, Effect of heat treatment of film-forming solution on the properties of film from cuttlefish (Sepia pharaonis) skin gelatin, J. Food Eng. 96 (2010) 66–73. https://doi.org/10.1016/j.jfoodeng.2009.06.046.

[119] H. Bao, Y. Pan, Y. Ping, N.G. Sahoo, T. Wu, L. Li, J. Li, L.H. Gan, Chitosan-Functionalized Graphene Oxide as a Nanocarrier for Drug and Gene Delivery, Small. 7 (2011) 1569–1578. https://doi.org/10.1002/smll.201100191.

[120] H. Bai, C. Li, X. Wang, G. Shi, A pH-sensitive graphene oxide composite hydrogel, Chem. Commun. 46 (2010) 2376–2378. https://doi.org/10.1039/c000051e.

[121] P.-L. Kang, S.J. Chang, I. Manousakas, C.W. Lee, C.-H. Yao, F.-H. Lin, S.M. Kuo, Development and assessment of hemostasis chitosan dressings, Carbohydrate Polymers. 85 (2011) 565–570. https://doi.org/10.1016/j.carbpol.2011.03.015.

[122] F.V. Ferreira, F.S. Brito, W. Franceschi, E.A.N. Simonetti, L.S. Cividanes, M. Chipara, K. Lozano, Functionalized graphene oxide as reinforcement in epoxy based nanocomposites, Surfaces and Interfaces. 10 (2018) 100–109. https://doi.org/10.1016/j.surfin.2017.12.004.

[123] F. Emadi, A. Amini, A. Gholami, Y. Ghasemi, Functionalized Graphene Oxide with Chitosan for Protein Nanocarriers to Protect against Enzymatic Cleavage and Retain Collagenase Activity, Scientific Reports. 7 (2017) 42258. https://doi.org/10.1038/srep42258.

[124] S. Bose, T. Kuila, Md.E. Uddin, N.H. Kim, A.K.T. Lau, J.H. Lee, In-situ synthesis and characterization of electrically conductive polypyrrole/graphene nanocomposites, Polymer. 51 (2010) 5921–5928. https://doi.org/10.1016/j.polymer.2010.10.014.

[125] S. Konwer, R. Boruah, S.K. Dolui, Studies on Conducting Polypyrrole/Graphene Oxide Composites as Supercapacitor Electrode, Journal of Elec Materi. 40 (2011) 2248. https://doi.org/10.1007/s11664-011-1749-z.

[126] C. Zhu, J. Zhai, D. Wen, S. Dong, Graphene oxide/polypyrrole nanocomposites: one-step electrochemical doping, coating and synergistic effect for energy storage, J. Mater. Chem. 22 (2012) 6300–6306. https://doi.org/10.1039/C2JM16699B.

[127] M. Li, C. Liu, Y. Xie, H. Cao, H. Zhao, Y. Zhang, The evolution of surface charge on graphene oxide during the reduction and its application in electroanalysis, Carbon. 66 (2014) 302–311. https://doi.org/10.1016/j.carbon.2013.09.004.

[128] D. Li, M.B. Müller, S. Gilje, R.B. Kaner, G.G. Wallace, Processable aqueous dispersions of graphene nanosheets, Nature Nanotech. 3 (2008) 101–105. https://doi.org/10.1038/nnano.2007.451.

[129] A. Kaniyoor, S. Ramaprabhu, A Raman spectroscopic investigation of graphite oxide derived graphene, AIP Advances. 2 (2012) 032183. https://doi.org/10.1063/1.4756995.

[130] D. López-Díaz, M. López Holgado, J.L. García-Fierro, M.M. Velázquez, Evolution of the Raman Spectrum with the Chemical Composition of Graphene Oxide, J. Phys. Chem. C. 121 (2017) 20489–20497. https://doi.org/10.1021/acs.jpcc.7b06236.

[131] V.H. Luan, J.S. Chung, E.J. Kim, S.H. Hur, The molecular level control of three-dimensional graphene oxide hydrogel structure by using various diamines, Chem. Eng. J. 246 (2014) 64–70. https://doi.org/10.1016/j.cej.2014.01.105.

[132] J.-Y. Lai, D.H.-K. Ma, M.-H. Lai, Y.-T. Li, R.-J. Chang, L.-M. Chen, Characterization of Cross-Linked Porous Gelatin Carriers and Their Interaction with Corneal Endothelium: Biopolymer Concentration Effect, PLOS ONE. 8 (2013) e54058. https://doi.org/10.1371/journal.pone.0054058.

[133] M. Gioffrè, P. Torricelli, S. Panzavolta, K. Rubini, A. Bigi, Role of pH on stability and mechanical properties of gelatin films, Journal of Bioactive and Compatible Polymers. 27 (2012) 67–77. https://doi.org/10.1177/0883911511431484.

[134] Y. Liu, M.B. Chan-Park, Hydrogel based on interpenetrating polymer networks of dextran and gelatin for vascular tissue engineering, Biomaterials. 30 (2009) 196–207. https://doi.org/10.1016/j.biomaterials.2008.09.041.

[135] C. Cha, S.R. Shin, X. Gao, N. Annabi, M.R. Dokmeci, X. (Shirley) Tang, A. Khademhosseini, Controlling Mechanical Properties of Cell-Laden Hydrogels by Covalent Incorporation of Graphene Oxide, Small. 10 (2014) 514–523. https://doi.org/10.1002/smll.201302182.

[136] J.H. Lee, Y. Lee, Y.C. Shin, M.J. Kim, J.H. Park, S.W. Hong, B. Kim, J.-W. Oh, K.D. Park, D.-W. Han, In situ forming gelatin/graphene oxide hydrogels for facilitated C2C12 myoblast differentiation, Applied Spectroscopy Reviews. 51 (2016) 527–539. https://doi.org/10.1080/05704928.2016.1165686.

[137] Y. Huang, D. Wu, J. Wang, S. Han, L. Lv, F. Zhang, X. Feng, Amphiphilic Polymer Promoted Assembly of Macroporous Graphene/SnO2 Frameworks with Tunable Porosity for High-Performance Lithium Storage, Small. 10 (2014) 2226–2232. https://doi.org/10.1002/smll.201303423.

[138] I.A. Perillo, M.S. Shmidt, S.C. Prieto, M.M. Blanco, Microwave-promoted synthesis of cyclic imides, Arkivoc. 2018 (2018) 319–345. https://doi.org/10.24820/ark.5550190.p010.402.

[139] H.-S. Jhuang, Y.-W. Liu, D.M. Reddy, Y.-Z. Tzeng, W.-Y. Lin, C.-F. Lee, Microwave-assisted Synthesis of Thioesters from Aldehydes and Thiols in Water, Journal of the Chinese Chemical Society. 65 (2018) 24–27. https://doi.org/10.1002/jccs.201700045.

[140] M. Oghbaei, O. Mirzaee, Microwave versus conventional sintering: A review of fundamentals, advantages and applications, Journal of Alloys and Compounds. 494 (2010) 175–189. https://doi.org/10.1016/j.jallcom.2010.01.068.

[141] M.B. Gawande, S.N. Shelke, R. Zboril, R.S. Varma, Microwave-Assisted Chemistry: Synthetic Applications for Rapid Assembly of Nanomaterials and Organics, Acc. Chem. Res. 47 (2014) 1338–1348. https://doi.org/10.1021/ar400309b.

[142] J.S. Boateng, K.H. Matthews, H.N.E. Stevens, G.M. Eccleston, Wound Healing Dressings and Drug Delivery Systems: A Review, Journal of Pharmaceutical Sciences. 97 (2008) 2892–2923. https://doi.org/10.1002/jps.21210.

[143] A. Shukla, J.C. Fang, S. Puranam, F.R. Jensen, P.T. Hammond, Hemostatic Multilayer Coatings, Advanced Materials. 24 (2012) 492–496. https://doi.org/10.1002/adma.201103794.

[144] J. Borges-Vilches, T. Figueroa, S. Guajardo, M. Meléndrez, K. Fernández, Development of gelatin aerogels reinforced with graphene oxide by microwave-assisted synthesis: Influence of

the synthesis conditions on their physicochemical properties, Polymer. 208 (2020) 122951. https://doi.org/10.1016/j.polymer.2020.122951.

[145] N. Rahmanian, H. Hamishehkar, J.E.N. Dolatabadi, N. Arsalani, Nano graphene oxide: a novel carrier for oral delivery of flavonoids, Colloids Surf B Biointerfaces. 123 (2014) 331–338. https://doi.org/10.1016/j.colsurfb.2014.09.036.

[146] C. Morales, M. Roeckel, K. Fernández, Microscopic Modeling of País Grape Seed Extract Absorption in the Small Intestine, AAPS PharmSciTech. 15 (2014) 103–110. https://doi.org/10.1208/s12249-013-0045-z.

[147] H. Liu, X. Li, X. Niu, G. Zhou, P. Li, Y. Fan, Improved Hemocompatibility and Endothelialization of Vascular Grafts by Covalent Immobilization of Sulfated Silk Fibroin on Poly(lactic-co-glycolic acid) Scaffolds, Biomacromolecules. 12 (2011) 2914–2924. https://doi.org/10.1021/bm200479f.

[148] K. Fernández, E. Agosin, Quantitative Analysis of Red Wine Tannins Using Fourier-Transform Mid-Infrared Spectrometry, J. Agric. Food Chem. 55 (2007) 7294–7300. https://doi.org/10.1021/jf071193d.

[149] Kenry, K.P. Loh, C.T. Lim, Selective concentration-dependent manipulation of intrinsic fluorescence of plasma proteins by graphene oxide nanosheets, RSC Adv. 6 (2016) 46558–46566. https://doi.org/10.1039/C6RA04978H.

[150] M. Gorbet, C. Sperling, M.F. Maitz, C.A. Siedlecki, C. Werner, M.V. Sefton, The blood compatibility challenge. Part 3: Material associated activation of blood cascades and cells, Acta Biomaterialia. 94 (2019) 25–32. https://doi.org/10.1016/j.actbio.2019.06.020.

[151] C. Sperling, M. Fischer, M.F. Maitz, C. Werner, Blood coagulation on biomaterials requires the combination of distinct activation processes, Biomaterials. 30 (2009) 4447–4456. https://doi.org/10.1016/j.biomaterials.2009.05.044.

[152] S. Liu, Z. Zheng, S. Wang, S. Chen, J. Ma, G. Liu, B. Wang, J. Li, Polydopamine-coated chitosan/calcium pyrophosphate hybrid microflowers as an effective hemostatic agent, Carbohydrate Polymers. 224 (2019) 115175. https://doi.org/10.1016/j.carbpol.2019.115175.

[153] S. Chen, H. Wang, Z. Jian, G. Fei, W. Qian, G. Luo, Z. Wang, H. Xia, Novel Poly(vinyl alcohol)/Chitosan/Modified Graphene Oxide Biocomposite for Wound Dressing Application, Macromolecular Bioscience. 20 (2020) 1900385. https://doi.org/10.1002/mabi.201900385.

[154] Q. Zhang, Q. Du, Y. Zhao, F. Chen, Z. Wang, Y. Zhang, H. Ni, H. Deng, Y. Li, Y. Chen, Graphene oxide-modified electrospun polyvinyl alcohol nanofibrous scaffolds with potential as skin wound dressings, RSC Advances. 7 (2017) 28826–28836. https://doi.org/10.1039/C7RA03997B.

[155] R. Gu, W. Sun, H. Zhou, Z. Wu, Z. Meng, X. Zhu, Q. Tang, J. Dong, G. Dou, The performance of a fly-larva shell-derived chitosan sponge as an absorbable surgical hemostatic agent, Biomaterials. 31 (2010) 1270–1277. https://doi.org/10.1016/j.biomaterials.2009.10.023.

[156] X. Yang, M. Chen, P. Li, Z. Ji, M. Wang, Y. Feng, C. Shi, Fabricating poly(vinyl alcohol)/gelatin composite sponges with high absorbency and water-triggered expansion for noncompressible hemorrhage and wound healing, J. Mater. Chem. B. 9 (2021) 1568–1582. https://doi.org/10.1039/D0TB02480E.

[157] Y.-F. Zhao, J.-Y. Zhao, W.-Z. Hu, K. Ma, Y. Chao, P.-J. Sun, X.-B. Fu, H. Zhang, Synthetic poly(vinyl alcohol)–chitosan as a new type of highly efficient hemostatic sponge with blood-triggered swelling and high biocompatibility, J. Mater. Chem. B. 7 (2019) 1855–1866. https://doi.org/10.1039/C8TB03181A.

[158] X. Yang, W. Liu, G. Xi, M. Wang, B. Liang, Y. Shi, Y. Feng, X. Ren, C. Shi, Fabricating antimicrobial peptide-immobilized starch sponges for hemorrhage control and antibacterial treatment, Carbohydrate Polymers. 222 (2019) 115012. https://doi.org/10.1016/j.carbpol.2019.115012.

[159] K. Zhang, X. Bai, Z. Yuan, X. Cao, X. Jiao, Y. Li, Y. Qin, Y. Wen, X. Zhang, Layered nanofiber sponge with an improved capacity for promoting blood coagulation and wound healing, Biomaterials. 204 (2019) 70–79. https://doi.org/10.1016/j.biomaterials.2019.03.008.

[160] X. Wei, S. Ding, S. Liu, K. Yang, J. Cai, F. Li, C. Wang, S. Lin, F. Tian, Polysaccharides-modified chitosan as improved and rapid hemostasis foam sponges, Carbohydrate Polymers. 264 (2021) 118028. https://doi.org/10.1016/j.carbpol.2021.118028.

[161] E. Mohamed, A. Fitzgerald, T. Tsuzuki, The role of nanoscale structures in the development of topical hemostatic agents, Materials Today Nano. 16 (2021) 100137. https://doi.org/10.1016/j.mtnano.2021.100137.

[162] M. Bijak, A. Sut, A. Kosiorek, J. Saluk-Bijak, J. Golanski, Dual Anticoagulant/Antiplatelet Activity of Polyphenolic Grape Seeds Extract, Nutrients. 11 (2019) 93. https://doi.org/10.3390/nu11010093.

[163] J.W. Jin, O. Inoue, K. Suzuki-Inoue, G. Nishikawa, Y. Kawakami, M. Hisamoto, T. Okuda, Y. Ozaki, Grape Seed Extracts Inhibit Platelet Aggregation by Inhibiting Protein Tyrosine Phosphatase, Clin Appl Thromb Hemost. 20 (2014) 278–284. https://doi.org/10.1177/1076029613481103.

[164] M. Bijak, M. Bobrowski, M. Borowiecka, A. Podsędek, J. Golański, P. Nowak, Anticoagulant effect of polyphenols-rich extracts from black chokeberry and grape seeds, Fitoterapia. 82 (2011) 811–817. https://doi.org/10.1016/j.fitote.2011.04.017.

[165] M.P. Mani, S.K. Jaganathan, Fabrication and characterization of electrospun polyurethane blended with dietary grapes for skin tissue engineering, Journal of Industrial Textiles. 50 (2020) 655–674. https://doi.org/10.1177/1528083719840628.

[166] R. Rajakumari, T. Volova, O.S. Oluwafemi, S. Rajeshkumar, S. Thomas, N. Kalarikkal, Nano formulated proanthocyanidins as an effective wound healing component, Materials Science and Engineering: C. 106 (2020) 110056. https://doi.org/10.1016/j.msec.2019.110056.

[167] T. Žitek, B. Dariš, M. Finšgar, Ž. Knez, D. Bjelić, M. Knez Hrnčič, The Effect of Polyphenolics in Extracts from Natural Materials on Metabolic Activity of Metastatic Melanoma WM-266-4 Cells, Applied Sciences. 10 (2020) 3499. https://doi.org/10.3390/app10103499.

[168] M. Nassiri-Asl, H. Hosseinzadeh, Review of the Pharmacological Effects of Vitis vinifera (Grape) and its Bioactive Constituents: An Update, Phytotherapy Research. 30 (2016) 1392–1403. https://doi.org/10.1002/ptr.5644.

[169] G. Ozkan, S. Ulusoy, A. Orem, S. Ersoz, M. Alkanat, F.B. Yucesan, K. Kaynar, S. Al, Protective Effect of the Grape Seed Proanthocyanidin Extract in a Rat Model of Contrast-Induced Nephropathy, Kidney Blood Press Res. 35 (2012) 445–453. https://doi.org/10.1159/000337926.

[170] X. Zhao, Y. Wu, H. Liu, N. Hu, Y. Zhang, S. Wang, Grape seed extract ameliorates PhIP-induced colonic injury by modulating gut microbiota, lipid metabolism, and NF-κB signaling pathway in rats, Journal of Functional Foods. 78 (2021) 104362. https://doi.org/10.1016/j.jff.2021.104362.

[171] S. Ben Youssef, G. Brisson, H. Doucet-Beaupré, A.-M. Castonguay, C. Gora, M. Amri, M. Lévesque, Neuroprotective benefits of grape seed and skin extract in a mouse model of Parkinson's disease, Nutritional Neuroscience. 24 (2021) 197–211. https://doi.org/10.1080/1028415X.2019.1616435.

[172] R.A. Eid, M.S.A. Zaki, M. Al-Shraim, M.A. Eldeen, M.A. Haidara, Grape seed extract protects against amiodarone - induced nephrotoxicity and ultrastructural alterations associated with the inhibition of biomarkers of inflammation and oxidative stress in rats, Ultrastructural Pathology. 45 (2021) 49–58. https://doi.org/10.1080/01913123.2020.1864076.

[173] M. Jerez, A. Selga, J. Sineiro, J.L. Torres, M.J. Núñez, A comparison between bark extracts from Pinus pinaster and Pinus radiata: Antioxidant activity and procyanidin composition, Food Chemistry. 100 (2007) 439–444. https://doi.org/10.1016/j.foodchem.2005.09.064.

[174] J.A. Kennedy, G.P. Jones, Analysis of Proanthocyanidin Cleavage Products Following Acid-Catalysis in the Presence of Excess Phloroglucinol, J. Agric. Food Chem. 49 (2001) 1740–1746. https://doi.org/10.1021/jf001030o.

[175] V.M. Williams, L.J. Porter, R.W. Hemingway, Molecular weight profiles of proanthocyanidin polymers, Phytochemistry. 22 (1983) 569–572. https://doi.org/10.1016/0031-9422(83)83048-9.